1-1-2016

Investigating the Utility of Age-Dependent Cranial Vault Thickness as an Aging Method for Juvenile Skeletal Remains on Dry Bone, Radiographic and Computed Tomography Scans

Kelly R. Kamnikar

Investigating the utility of age-dependent cranial vault thickness as an aging method for juvenile skeletal remains on dry bone, radiographic and computed tomography scans.

By

Kelly R. Kamnikar

A Thesis
Submitted to the Faculty of
Mississippi State University
in Partial Fulfillment of the Requirements
for the Degree of Master of Arts
in Applied Anthropology
in the Department of Anthropology and Middle Eastern Cultures

Mississippi State, Mississippi

May 2016

Investigating the utility of age-dependent cranial vault thickness as an aging method for juvenile skeletal remains on dry bone, radiographic and computed tomography scans.

By

Kelly R. Kamnikar

Approved:

_____

Nicholas P. Herrmann
(Major Professor)

_____

Molly K. Zuckerman
(Co-Major Professor)

_____

Toni J. Copeland
(Committee Member)

_____

David M. Hoffman
(Graduate Coordinator)

_____

R. Gregory Dunaway
Dean
College of Arts & Sciences

Name: Kelly R. Kamnikar

Date of Degree: May 7, 2016

Institution: Mississippi State University

Major Field: Applied Anthropology

Major Professor: Nicholas P. Herrmann, Molly K. Zuckerman

Title of Study: Investigating the utility of age-dependent cranial vault thickness as an aging method for juvenile skeletal remains on dry bone, radiographic and computed tomography scans.

Pages in Study 147

Candidate for Degree of Master of Arts

Age estimation, a component of the biological profile, contributes significantly to the creation of a post-mortem profile of an unknown set of human remains. This goal of this study is to: (1) refine the juvenile age estimation method of cranial vault thickness (CVT) through MARS modeling, (2) test the method on known age samples, and (3) compare CVT and dental development age estimations. Data for this study comes from computed tomography (CT) scans, radiographic images, and dry bone. CVT was measured at seven cranial landmarks (nasion, glabella, bregma, vertex, vertex radius, lambda and opisthocranion). Results indicate that CVT models vary in their predictive ability; vertex and lambda produce the best results. Predicted fit values and prediction intervals for CVT are larger, and less accurate than dental development age estimates. Aging by CVT could benefit from a larger known age sample composed of individuals older than 6 years old.

DEDICATION

I would like to dedicate this thesis to the many people who have played an important role in my personal and professional development. Mom, Dad, Jerome, Shuala, Hannah, Kate, Mark, Ale, Linda, Miri, Clari, V, Lizz, Jose, Daniel, Suz, Gina, Whit, Kel, Marcy, Porky, Conchi, Chiara, Miguel, Amber, Sherri and Megan. The journey was much easier with your love, patience and support. Thank you.

ACKNOWLEDGEMENTS

First, I would like to thank my committee, Dr. Nicholas Herrmann, Dr. Molly Zuckerman and Dr. Toni Copeland for their guidance, advice, and invaluable input on my proposal and thesis. I would also like to thank the professors and staff in the Department of Anthropology and Middle Eastern Cultures at Mississippi State University for a wonderful experience. I would like to thank Dr. Pierre Guyomarc'h for his help and guidance with TIVMI; Dr. Priscilla Bayle from the Universite de Bordeaux in Bordeaux, France; Dr. Michael Coquerelle from the University Rey Juan Carlos in Madrid, Spain; V. Dousset, C. Douws and C. Thiebaut from the Hospital Pellegrin in Bordeaux, France; and F. Brunelle, N. Boddaert, and J.M Debaets from the Hospital Necker in Paris, France for allowing me to use their CT data for this research; Dr. Kyra Stull at Idaho State University for her help with R software equations and MARS modeling; and Dr. Stephen Ousley at Mercyhurst College for access to specific images from the radiographic database.

TABLE OF CONTENTS

DEDICATION ii

ACKNOWLEDGEMENTS iii

LIST OF TABLES vii

LIST OF FIGURES ix

CHAPTER

I. INTRODUCTION 1

The Biological Profile 1
Age at death 1
Juveniles and Age-at-death estimation 3
Research Design 5

II. BACKGROUND 10

III. MATERIALS AND METHODS 19

Materials 19
CT sample 20
Radiographic sample 20
Dry bone and other samples 21
Methods 22
CVT Collection on Computed Tomography (CT) Scans 24
CVT Collection on Radiographic Images 28
CVT Collection on Dry Bone 29
Dental Age (Transition Analysis) 30
Model and PI creation and other statistical analyses 31

IV. RESULTS 34

Summary Statistics 34
CVT measurement values 35
Hypothesis One 39
Hypothesis Two 41
MARS univariate models results 41

Nasion....43
Glabella....48
Bregma....53
Vertex....56
The Vertex Radius....60
Lambda....64
Opisthocranion....69
Standard Error and Prediction Intervals....72
MARS multivariate model results....80
All seven cranial landmarks....80
Variable importance of cranial landmarks....81
The vault set of cranial landmarks....85
Radiograph Test Results....88
Hypothesis three....92
Case Studies....94
Case Study #1: An Unknown Forensic Case....95
Case Study #2: Lyon's Bluff Archaeological Crania....99
Case Study #3: Mitrou Archaeological Cranium....107

V. DISCUSSION AND CONCLUSIONS....110

Predicting age using CVT....110
Univariate and Multivariate Models....110
Nasion....110
Glabella....111
Bregma....111
Vertex....112
Vertex Radius....112
Lambda....113
Opisthocranion....113
All Seven Landmarks....113
Highest Importance....114
Vault Set....114
Radiographic Test Data....115
Case Studies....116
Conclusions of the Method....118
Limitations....119
Limitations of the Study....120
Limitations of the Method....121
Discussion....122
Conclusions....123
Future Directions....125

REFERENCES....126

APPENDIX

A. CRANIAL LANDMARK DEFINITIONS 132

Cranial Landmark Definitions 133

B. TABLES FOR AGE ESTIMATION USING CVT 134

Age Estimation Tables Using CVT 135

LIST OF TABLES

1 Shapiro-Wilkes test on non-transformed CVT measurements. 35

2 Standard error for CT measurements using TIVMI. 39

3 Summary statistics for the Earth model at nasion. 46

4 Summary statistics for the Earth model at glabella 50

5 Summary statistics for the Earth model at bregma 54

6 Summary statistics for the Earth model at vertex 58

7 Summary statistics for the Earth model at vertex radius 62

8 Summary statistics for the Earth model at lambda 66

9 Summary statistics for the Earth model at opisthocranion 70

10 Standard Error and Prediction Intervals for the univariate models.....73

11 Summary statistics for the Earth model at all seven landmarks 81

12 Multivariate model using suite of seven cranial landmarks.....82

13 Summary statistics for the multivariate model of nasion, vertex and the vertex radius. 84

14 Summary statistics for the vault set model. 87

15 Prediction intervals at the 95% and 85% PI.....89

16 Predicted CVT age (fit values) and know ages on radiographs at cranial landmarks. 90

17 CVT PIs for case MSU 2014-02 using radiographic data 95

18 CVT PIs for case MSU 2014-02 using CT data 96

19 Multivariate models using the CT data.....98

20 Predicted CVT fit compared to predicted dental fit in Lyon's Bluff.....106
21 Correlation between CVT and dental age in Lyon's Bluff.....106
22 Results for the Mitrou Cranium.....108
23 Predictive capabilities of the models.....119
24 Definition and source of cranial landmarks used in this study.....133
25 Age estimation table for CVT at nasion at the 95% PI.....135
26 Age estimation table for CVT at glabella at the 95% PI.....137
27 Age estimation table for CVT at bregma at the 95% PI.....140
28 Age estimation table for CVT at vertex at the 95% PI.....142
29 Age estimation table for CVT at vertex radius at the 95% PI.....143
30 Age estimation table for CVT at lambda at the 95% PI.....143
31 Age estimation table for CVT at opisthocranion at the 95% PI.....145

LIST OF FIGURES

1 Cranial landmarks used in this study. 23

2 Mesh creating in TIVMI. 25

3 Point placement using planes in TIVMI. 27

4 Distribution of ages in the CT sample. 34

5 QQ plot of CVT at nasion....36

6 QQ plot of CVT at glabella....37

7 QQ plot for CVT at the vertex radius. 38

8 Plotted CVT values for each cranial landmark. 40

9 Model interpretations plots for CVT at nasion 44

10 Summary statistics for the Earth model at nasion (output example). 45

11 95% prediction intervals at nasion. 47

12 Prediction bands in a residuals plot for nasion. 48

13 Model interpretation plots for CVT at glabella....49

14 95% prediction intervals at glabella. 51

15 Prediction bands in a residuals plot for glabella. 52

16 Model interpretation plots for CVT at bregma. 53

17 95% prediction intervals at bregma 55

18 Prediction bands in a residuals plot for bregma. 56

19 Model interpretation plots for vertex. 57

20 95% prediction intervals at vertex. 59

21 Prediction bands in a residuals plot for vertex. 60

22 Model interpretation plots for the vertex radius. 61

23 95% prediction intervals at the Vertex Radius 63

24 Prediction bands in a residuals plot for the vertex radius. 64

25 Model interpretation plots for lambda. 65

26 Prediction intervals at lambda....67

27 Prediction bands in a residuals plot for lambda. 68

28 Model interpretation plots for opisthocranion 69

29 95% prediction intervals at opisthocranion....71

30 Prediction bands in a residuals plot for opisthocranion. 72

31 95% prediction intervals when age is regressed on CVT for Nasion. 73

32 95% prediction intervals when age is regressed on CVT for Glabella. 74

33 95% prediction intervals when age is regressed on CVT for Bregma. 75

34 95% prediction intervals when age is regressed on CVT for Vertex. 76

35 95% prediction intervals when age is regressed on CVT for the Vertex Radius. 77

36 95% prediction intervals when age is regressed on CVT for Lambda. 78

37 95% prediction intervals when age is regressed on CVT for Opisthocranion. 79

38 Model interpretation plots for entire suite of seven cranial landmarks 80

39 Model interpretations plots for best variables set (nasion, vertex, and vertex radius) 83

40 Prediction bands in a residuals plot. 85

41 Model interpretation plots for the vault set (glabella, bregma, vertex and lambda)....86

42 Prediction bands in a residuals plot. 88

43 95% Prediction intervals for 118-00080-01-012-012. 90

44 95% Prediction intervals for 114-00030-01-007-011. 91

45 95% PIS for 118-00080-01-012-012 with dental age. 92

46 95% PIs for 114-00030-01-007-011 with dental age. 93

47 Chart showing univariate model PIs for MSU2014-02. 97

48 All models and PIs for MSU2014-02. 99

49 Dental age plotted against CVT age at nasion in the Lyon's Bluff sample. 100

50 Dental age plotted against CVT age at glabella in the Lyon's Bluff sample. 101

51 Dental age plotted against CVT age at bregma in the Lyon's Bluff sample. 102

52 Dental age plotted against CVT age at vertex in the Lyon's Bluff sample. 103

53 Dental age plotted against CVT age at lambda in the Lyon's Bluff sample. 104

54 Dental age plotted against CVT age at opisthocranion in the Lyon's Bluff sample. 105

55 Models and PIs for Mitrou cranium 108

CHAPTER I

INTRODUCTION

The Biological Profile

The first task in the anthropological analysis of human skeletal remains is to generate a biological profile of the individual. A biological profile is the combination of four trait estimates including age-at-death, sex, ancestry, and stature, as well as the assessment of pathological conditions or other anomalies on the skeleton (Cattaneo, 2007). Information generated here is important because it can be individualizing and relate to a specific set of skeletal remains. In this regard, the biological profile can be used in forensic and humanitarian situations in an effort to identify missing persons. For archaeologically derived skeletal materials, the biological profile is used to further investigate bioarchaeological or paleopathological questions of growth and development, and demographic and health studies (Hoppa and FitzGerald, 1999).

Age at death

Age-at-death determination is the estimation of the biological or developmental age in an individual. Biological age is the physiological age reflected in skeletal features or morphology, which can be used to predict chronological age (i.e., the calendric years, months, and days that passed before death) (Garvin et al, 2012). Ages are usually expressed as a range, and researchers strive to create methods that narrow the age range as much as possible. In forensic cases, precise age ranges are very useful in the

reconciliation process between missing person's data and unidentified human remains (Garvin et al, 2012). Konigsberg and colleagues (2008) emphasize that statistically sound aging methods should have correct coverage. For example, the estimated age range should include 50% of the individuals that chronologically fall into that range, while the remaining 50% should be equally distributed above and below the targeted age estimation range (Konigsberg et al., 2008). Several studies report 50%, 90% and 95% coverages.

Estimated age ranges are based on changes in skeletal morphology. Certain elements of the skeleton, like the cranium, dentition, long bones and features on the os coxae and the ribs, change throughout the course of people's lives and can be used to estimate the age at which a person died. These changes are well documented in the literature (McKern and Stewart, 1957; Scheuer and Black, 2000b; Garvin et al., 2013), Studies of skeletal samples have demonstrated that certain features of the skeleton, namely the pubic symphysis (Todd, 1920; Suchey and Katz, 1986), auricular surface (Lovejoy et al., 1985), sternal rib ends (Iscan and Loth, 1986), epiphyseal fusion of long bones (Scheuer and Black, 2000b), dental development (Moorrees et al., 1963), and diaphyseal long bone lengths (Maresh, 1955; Hoffman, 1979) give reliable age estimates. Skeletal elements that provide reliable age estimates show a sequence of change that correspond to growth and development in children or degeneration in adults. Skeletal changes that correspond to growth and development include the formation and fusion of ossification centers and an increase in bone deposition (Scheuer and Black, 2000b; Franklin, 2010). Degenerative changes corresponding to advanced age include cranial sutures closure, osteoarthritis and osteoporosis of the skeleton and dental attrition and periodontal disease in dentition (Ubelaker, 1989; Ortner, 2003; Larson, 1999). Qualitative

changes of these bony features are then used to create methods for age estimation and tested on known-age individuals. These methods have been developed using multiple historic skeletal samples (Usher, 2002), such as the Terry Collection (n=1728), with birthdates ranging from pre 1840 to post 1960 (Hunt and Albanese, 2005), and the Hamann-Todd Collection (n=>3,000), with birthdates ranging from 1825-1877 (de la Cova, 2011). However, historic skeletal collections from the 19th and mid 20th century no longer reflect worldwide growth trends in juveniles (Stull et al., 2014). Because many skeletal collections are not reflective of current growth trends (Stull et al., 2014), methods have recently been developed and updated using samples from living individuals, via radiographs (Mays, 1998; Stull et al, 2014) and computed tomography (CT) scans (Schultz et al., 2005).

Juveniles and Age-at-death estimation

Traditionally, the term 'juvenile' refers to any individual that is not yet an adult. Normal, non-pathological changes in the juvenile skeleton can be used to estimate age because the skeleton is actively maturing. In general, juveniles pass through three stages of rapid growth. The first growth spurt begins quickly after birth, slowing around 3 years of age (Lewis, 2007:60). Growth accelerates again during the second growth spurt, which occurs between 6 and 8 years of age (Scheuer and Black, 2000b). The third growth spurt begins at the onset of adolescence, and finally, growth plateaus in late adolescence (Larsen, 1997:8; Scheuer and Black, 2000b). Because growth occurs on a relatively strict time scale in juveniles, fusion of multiple bony elements or dental development can be used to establish a more accurate age estimate than estimates based upon degenerative changes in adults (Franklin, 2010).

Age estimation methods for juveniles vary in their comprehensiveness, covering specific intervals or growth trajectories of single skeletal elements. Many of these methods are complementary to each other and are used in tandem for age estimation purposes (White and Folkens, 2000). The most commonly used age estimation methods, which can be used together, include dental development, epiphyseal union and measurements of long bone lengths (Ubelaker, 1989; Cardoso et al., 2013). The study presented here investigates an alternative age estimation method in juveniles that could be used in tandem or alone. It examines the age-dependent properties of cranial vault thickness (CVT) in juveniles using CVT measurements at linear cranial landmarks on the cranial vault. Multiple studies have examined the relationship between CVT and chronological age (Hansmen, 1966; Brown et al., 1979; Garofalo et al., 2008), but a survey of published literature does not reveal the use of regression models for age estimation using CVT. Studies by Hansmen (1966), Brown and colleagues (1979) and Garofalo and colleagues (2008) found correlations between CVT and age at nasion, vertex, right euryon, left euryon (Brown et al., 1979), the midpoint between the sagittal suture and left parietal boss (Garofalo et al., 2008), bregma and lambda (Brown et al., 1979; Garofalo et al., 2008). These findings demonstrate that CVT may be positively correlated with developmental age in juvenile crania. The results also suggest that this relationship may hold true for a lengthy portion of the sub-adult period, birth to 15 years old, making CVT the basis for a potential aging method for juvenile skeletons from a range of ages. Age-at-death estimates using CVT would allow for an additional area of the cranium to be used in age estimation. This would be beneficial for highly fragmented

remains or commingled contexts, which are commonly found in both forensic and archaeological contexts, and for use in the absence of dentition.

Research Design

The overarching research question is: Can differential CVT of juvenile crania be used to estimate age-at-death? ***The aim of this study*** is to refine the CVT age estimation method for juvenile skeletal material by creating Multivariate Adaptive Regression Spline (MARS) models at select cranial landmarks. This method demonstrates that CVT measurements at select cranial landmarks can be used to estimate age within the model. This method was developed using known age Computed Tomography (CT) data. Models were created using the CT data and then tested with radiographic images of juvenile crania to assess the fit of the model. The accuracy of the method was evaluated against chronological age and dental age estimates of the CT data, radiographic images and dry bone samples. Dental age was estimated using Shackelford and colleagues' (2012) method of transition analysis applied to dental development, in which developmental scoring procedures are based on Moorrees and colleagues (1963) seminal study. The CVT method was also used to estimate age on CT scans, radiographs and dry bone samples from a forensic case and archaeological juvenile crania. Results are discussed separately as case studies. Limitations to this approach are identified and discussed in later chapters.

The method is based on the assumption that there is a positive correlation between CVT and developmental age in juveniles at eight craniometric points, nasion, bregma, lambda, vertex, right euryon, left euryon, the midpoint between sagittal suture and left parietal boss. A sample size of 60 cranial radiographs of living individuals (Brown et al.,

1979) and 28 archaeological crania (Garofalo et al., 2008) has already been used to test this assumption. This study goes beyond this, as it is based on a sample of CT images of juvenile crania (n=74) collected from living French children of mixed ancestry provided by Drs. Priscilla Bayle and Michael Coquerelle. Thickness measurements were collected at seven craniometric points (nasion, glabella, bregma, vertex, the vertex radius, lambda, and opisthocranion) that are clearly distinguishable on CT and radiographic cephalograms, or lateral, images. Statistical analyses, specifically univariate and multivariate models using loess regression, were used to detect relationships between CVT and known chronological age. These models use the standard error associated with each score to obtain a prediction interval (PI) for age ranges associated with measurements. PIs generated from the models provide a range with an associated probability where future thickness measures should fall. Once a refined method for age-estimation using CVT was developed, it was tested on radiographic images (n=2) of known age children from the online database *Patricia* (Pediatric Radiology Interactive Atlas)[1] with known chronological age from a forensic sample containing individuals from various ancestral groups in the United States (Ousley et al, 2013). This served to test whether the refined CVT method can accurately predict age and gauge the degree of precision in age estimates as they apply to different imaging techniques.

Additionally, dry bone samples from the Lyon's Bluff collection housed at Mississippi State University were used to evaluate the CVT method in relation to archaeological material. Individuals from these samples were aged using dental

[1] http://math.mercyhurst.edu/~sousley/databases/radiographic_database/

development (Moorrees et al., 1963) and transition analysis of dental development scores (Shackelford et al., 2012). Results from the dry bone samples are discussed separately because they are prehistoric and of limited size. These cases cannot significantly contribute to method development or testing until the CVT method is calibrated using dental development or long bone length as a calibration standard. Then, the CVT method can be applied to archaeological samples that are commingled, fragmented or do not include dentition.

The proposed study addresses the following ***hypotheses***: (1) CVT measurements at select cranial landmarks conform to expected growth curves using a locally smoothed (loess) fit. This would tell researchers if developmental age and increases in CVT are linked, and the degree of correlation. (2) CVT measured on radiographic images of juvenile crania will fit to age estimation models developed on CT scans. MARS models, which use loess regression, were created to illustrate the relationship between CVT and age at each landmark. Known age radiographic data was then tested against the model and the fit evaluated. Univariate and multivariate models were created using a single landmark or a combination of landmarks. (3) Hypothesis three states: CVT will compare to chronological age and age-at-death estimates using transition analysis (Shackelford et al., 2012) on dental development scores of all available teeth (Moorrees et al., 1963); however, prediction intervals will not be as narrow as those from dental age-at-death estimates. Following this hypothesis, the accuracy of the refined CVT method was evaluated to aging through transition analysis on dental development, because dental development is viewed as the most reliable and accurate age-at-death estimation method for juveniles (Hoppa and Fitzgerald, 1999). I tested the accuracy of both methods of age

estimation as compared to chronological age. The CT and radiograph samples were chosen because they are composed of many modern, known age individuals, and reflect current worldwide growth trends, which is appropriate to use when creating a forensically based age-estimation method. However, because this study compares CVT age to dental, results are applicable to bioarchaeological research.

During refinement of the CVT method, the MARS statistical modeling methodology established by Stull and colleagues (2014) was followed on the CT scans. Stull and colleagues (2014) refined methods for estimating age in juveniles using diaphyseal dimensions of the femur, tibia, fibula, humerus, radius and ulna. They used loess regression, MARS, and univariate modeling of MARS to generate PIs of measurements and their associated age ranges. These statistical tests--loess regression and MARS modeling--were used here because they are appropriate to use on non-linear data such as growth data. These specific tests also do not make assumptions about the relationship of the variables to each other and are flexible to provide the best and least biased fit when generating a model (Stull et al., 2014). PIs with known error rates accompany each CVT measurement and describe the accuracy of the fit of the data to the model by providing an interval in which a variable yet to be observed will fall.

The benefits of this method are numerous. This method provides an alternative option for age-at-death estimation for incomplete or fragmented juvenile remains recovered from archaeological sites or forensic context. For example, if taphonomic processes severely impact traditional age estimation markers (long bones, epiphyses, dentition), the crania, specifically CVT will be an alternative element for age estimation. This method could complement other aging methods by adding statistical support for a

particular estimate, increasing the accuracy of the overall estimated age. The results explain which cranial landmarks would benefit from future research using standardized data collection protocols.

CHAPTER II

BACKGROUND

Juveniles become part of the archaeological record for many different reasons. Their deaths can be attributed to disease, nutritional deficiencies, neglect, suicide, accident, abuse, murder or warfare (Lewis, 2007:1). In bioarchaeology, information from the biological profile of juveniles is important for establishing mortality profiles, estimating fertility and other population-level processes, and understanding the role that trait estimates may play in diet, nutrition, disease, and activity (Larsen, 1997). In forensics, the biological profile helps to establish the identity of skeletal remains for legal purposes and so family members can have closure. The starting point in identification involves the creation of the biological profile.

In forensics, information from the biological profile provides authorities with specific and unique information about an unidentified skeleton. This information is crucial for correlating ante- and postmortem data (Kranioti and Paine, 2011). Antemortem data is information collected from family members or friends of a missing person. It is compared to postmortem data, which is information collected from human remains during autopsy or skeletal examination. Age-estimation methods used on unidentified human remains can contribute to resolving the fate of missing persons (Inter-Parliamentary Union and International Committee of the Red Cross, 2009) or in determination of an unlawful offense. These methods can expedite the investigation

process by reducing case-by-case comparisons of ante and postmortem data (Rogers, 2009). In practice, Kimmerle and colleagues (2010) report that estimated age was a significant factor in identifying juveniles. Age estimation methods are used to determine if humanitarian laws were violated (Plattner, 1989) or as evidence for prosecution in human rights cases (Ritz-Timme et al., 2000; Kimmerle, 2004).

Because one aspect of this research contributes to the development of a method suitable for use in a forensic context where issues of legality are concerned, it is subject to the *Daubert* standards (Dirkmaat et al., 2008). These criteria are a direct result of the 1993 Supreme Court ruling in *Daubert v. Merrell Dow Pharmaceuticals, Inc*[2]*,* in which scientific evidence crucial to the case was deemed inadmissible because it did not meet the general acceptance criteria for evidence previously established. The *Daubert* standards aid trial judges in their decision to allow certain scientific testimony, such as the inclusion and validity of methods used to estimate the biological profile. The *Daubert* standard guidelines are: (1) Has the theory or technique been tested? (2) What is the known or potential error rate? (3) Do standards exist for the control of the technique's operation? (4) Has the theory or technique been peer reviewed and published? and (5) is the theory or technique generally accepted within the scientific community in which it was established? (Christiansen and Crowder, 2009). Although the *Daubert* criteria are not a requirement of methods used in forensic anthropology, researchers involved in method development should strive to meet the criteria, specifically, criteria 1-3, in case future legislation requires such standards. In accordance with the first three criteria of the

[2] 113 S. Ct. 2786 (1993)

Daubert standards, the proposed method provides error ranges through PIs so that officers of the court—judges and jury members—can understand the degree of precision of age estimation using the method, provides results from a test sample, and includes directions and procedures for other researchers to follow when using the method (Christiansen and Crowder, 2009).

Age estimation methods aim to determine the developmental age of skeletal remains, which is then used to predict the chronological age at which the individual died (Garvin et al., 2012). In most instances, age estimation methods report a numerical age range, weeks to months in fetuses and neonates and years in sub-adults and adults. A range better captures the variation in growth and degeneration of the skeleton manifested by living individuals. One method does not provide a range; rather counts of dark and light bands present in dental cementum are used to generate a direct point estimate of age (Condon et al., 1986). Skeletal elements used in determining age-at-death are different in adults than they are in juveniles. Methods for estimating age in adults are premised on maintenance and deterioration of bony features, because growth has ceased. In contrast, skeletal indicators of growth and development are the primary focus in juvenile age-at-death estimation methods. Practitioners most frequently use dental development, epiphyseal closure and long bone length, respectively, when aging juvenile skeletal remains (Hoppa and FitzGerald, 1999).

Age estimation methods based on dental development are preferred because dental development represents a reliable indicator of age (Demirjian et al., 1973) and gives the most narrow or precise age ranges. The timing of tooth growth, development and eruption into the oral cavity is under strong genetic control and is less affected by

environmental or cultural factors (Ubelaker, 1989; Moorrees et al., 1963; Scheuer and Black, 2000b, 2004). Dental remains are also less susceptible to taphonomic damage (Ubelaker, 1989) and are more likely to be recovered at excavation. Because dental age estimation methods are reliable, narrow and most likely available, the CVT method in this study will be compared to age estimation using dental development. Two fundamental studies by Gleiser and Hunt (1955) and Moorrees, Fanning and Hunt (1963) that examine dental growth in relation to age are discussed in more detail. Gleiser and Hunt (1955) examined calcification of the crown and root of the mandibular first molar as it related to growth in males and females. They divided calcification stages of the first molar into 15 stages, and found that calcification often occurs in spurts and at different time periods in both sexes, with females tending to develop more quickly (Gleiser and Hunt, 1955). In their study, Moorrees and colleagues (1963) determined that the formation and development of several permanent teeth are strong indicators of chronological age in both sexes. Using longitudinal data on American children (N=134), they created a scoring procedure from radiographic images for determining age using permanent and deciduous mandibular and maxillary teeth—maxillary and mandibular incisors and mandibular canines, premolars and molars (Moorrees et al., 1963). Stages are associated with numerical scores and are based on crown and root development and root reabsorption. This method is comprehensive, initiating during fetal development and concluding during late adolescence or adulthood (Scheuer and Black, 2000b). Even though this method is extensive, it provides better age estimates for younger individuals (Ubelaker, 1989), and is the preferred method for aging infants (Scheuer and Black, 2000b). Shackelford and colleagues (2012) further refined the ease of this method. They

developed a code to estimate age using transition analysis on dental development scores, which illustrates maximum likelihood age estimates (MLE) for available dentition.

When dentition is unavailable, anthropologists often use epiphyseal union and long bone length to estimate age (Cunha et al., 2009; Cardoso et al., 2013). Epiphyseal union is based on three phases of biological development and their processes. These phases of development are the appearance of an ossification center, followed by the morphological appearance of the center, and finally, the fusion of the center with a separate center of ossification (Scheuer and Black, 2004). This method can be used on individual elements or across multiple elements, and is best suited for estimating juvenile age between 10 and 20 years old, because age-at-death estimates from long bone lengths are of limited value for individuals older than ten years (Ubelaker, 1989). Ubelaker (1989) recommends evaluating the total pattern of epiphyseal closure in the skeleton when providing an age assessment because some elements give more reliable estimates than others when fusing, especially the proximal humerus, medial epicondyle, distal radius, femoral head, distal femur, iliac crest, medial clavicle, and segments of the sacral joints (McKern and Stewart, 1957). The third most common age estimation method uses long bone measurements. Age estimation from long bone length is achieved through measuring the maximum diaphyseal lengths of the femur, tibia, fibula, humerus, radius, ulna, ilium and clavicle (Scheuer and Black, 2000a). These measurements are then entered into regression formula based on comparative skeletal populations (Scheuer et al., 1980). This method is best suited for fetal and infant skeletons, as the standard deviation from the mean increases significantly with age. Age estimation using long bone length is not very accurate and results vary, because growth in these elements can vary across

populations and individuals (Ubelaker, 1989:65-66) and be impacted by socioeconomic factors (Rogers, 2009).

Apart from dental development, epiphyseal closure and measurements of long bone lengths, many other methods are available to estimate age in juveniles. Many of these methods focus on changes during growth that occur in the skull. These methods are based on multiple indicators, including stages of ossification of the cranial elements (Redfield, 1970; Fazekus and Kosa, 1978; Scheuer and MacLaughlin-Black, 1984; Scheuer and Black, 2000b), and geometric changes in length between specific points in the craniofacial region (Buschang et al., 1983; Braga and Treil, 2007) and mandible (Franklin et al., 2008). Ossification methods are limited to a small age group (e.g., neonates), because cranial vault ossification begins during embryonic development and completely finishes by 7 years old (Scheuer and Black, 2000b, 2004). Other methods focus on changes in linear distance measurements and geometric morphometric changes. Buschang and colleagues (1983) examined linear distances relating to facial and cranial height in juveniles to determine how the face and cranium develops with increasing age. They found that cranial base and the head height increased in linear distance based on the assessment of points on the mandible, the maxilla, and the upper face. The greatest increase in distance in the mandible, and the least increase in distance between linear points was observed in the head height. This study provides a list of mean and standard deviations for the facial proportions relative to age (Buschang et al., 1983). Braga and Treil (2007) used geometric morphometrics to determine if shape changes in the face and cranial base could be correlated with skeletal growth and chronological age. They used a sample of CT scans (n=127), ranging in age from newborns to 17.67 years old. Through

comparison of linear regression age calculations and the centroid size of the face and cranial base, they found that age estimation was more accurate in individuals older than 10 years of age. Franklin and colleagues (2008) used morphometrics on developmental markers in the mandible to estimate age. They found that mandibular centroids of size and shape are useful for predicting age in individuals aged 10-17 years old. The standard error rates for their method varied from 1 to 3 years (Franklin et al., 2008).

Despite the abundance of cranial based age estimation methods, studies examining the relationship of CVT and age in juveniles are limited. Hansmen (1966) measured thickness of juvenile males and females (n=134) at one cranial landmark, lambda. The purpose of this study was to understand cranial thickness and sinus growth with increasing age in healthy individuals to compare to children with pathological conditions. Hansmen noted that cranial thickness increased rapidly until 3 years of age, and then increased steadily into late adolescence before leveling off. Results of this study are listed as percentile standards for different age groups (Hansmen, 1966). Another, more in depth study by Brown and colleagues (1979) collected radiographic data from Australian aboriginal juveniles (n=60) aged 6-13 years through multiple, 4 to 10 observations. They found a correlation between CVT and age at six craniometric points—nasion, bregma, vertex, lambda, right euryon, left euryon—measuring the distance between the ectocranial reference point and the nearest point on the adjacent endocranial surface. They found that CVT does not differ significantly between either sexes except at the following points: nasion at 13 years of age; bregma at 12, 13, and 14 years of age; vertex at 8 and 14 years of age; and right euryon for 8 years of age. The study also showed that CVT increased steadily through time with little evidence of

growth spurts except for thickness measures at nasion. They noted that some thickness measures varied irregularly between 8 and 18 years of age, and attribute this error to small differences between mean measurements and deviations (error rates) from the mean. Nasion did exhibit a growth spurt occurring between 13 and 14 years of age, but the data was too incomplete to provide more detailed results (Brown et al., 1979). Their publication includes a table for age estimation in juveniles aged 8-18 years old at the following landmarks: nasion, bregma, vertex, lambda, right euryon, left euryon, frontal sinus height and frontal sinus depth (Brown et al., 1979). Garofalo and colleagues (2008) examined archaeological Native American juvenile crania (n=28) housed at the Smithsonian National Museum of Natural History. The sample had been previously aged by Smithsonian staff and contract osteologists using established age estimation methods, including dental eruption (Ubelaker, 1989), fusion of the speno-occipito synchondrosis (Ingervall and Thilander, 1972), fusion of the jugular plate (Maat and Mastwijk, 1995) and, when post cranial material was available, long bone length (Scheuer and Black, 2000b). Garofalo and colleagues (2008) reassessed age independently and no interobserver error was noted. Data collection methods are explained in further detail in Zuckerman et al. (2014). Garofalo and colleagues (2008) found a correlation between CVT and age at an expanded/different set of cranial landmarks—left frontal boss, bregma, midpoint between bregma and left frontal boss, apex of the parietal bone on the left side, midpoint between sagittal suture and left parietal boss, lambda, midpoint between left frontal boss and lambda, apex of the skull lateral to sagittal suture, apex of occipital boss, most superior point of lateral orbital roof and most superior point directly posterior to supraorbital notch or foramen. Their results indicate a correlation between

age at CVT at bregma, lambda—as did Brown and colleagues' (1979)—and midpoint between sagittal suture and left parietal boss, with the bregma being the most predictive of age. Because neither of these two studies developed a comprehensive method for aging the cranial vault through CVT measures, the proposed study has the potential to fill that gap. Following methodology employed by Stull and colleagues (2014), this study will create age estimation models using CVT, list prediction intervals calculated through standard error measurements to estimate where future measurements will fall, and show the error associated with the predictive ability of each cranial landmark used in modeling. This method will be tested on a sample with known chronological age and against transition analysis of the dental development age estimation method (Moorrees et al., 1963; Shackleford et al., 2012) to gauge its performance. Finally, this study will list standard protocol for collecting CVT data on CT scans and radiographic data using two software programs available online.

CHAPTER III

MATERIALS AND METHODS

Materials

To evaluate the research question for this study, a modern sample of juvenile crania with known age was used. CVT at seven, linear cranial landmarks was measured and the data was evaluated employing the statistical modeling for method creation used by Stull and colleagues (2014). This study uses a larger sample size (Brown et al., 1979; Garofalo et al., 2008) and more cranial landmarks (Hansmen, 1966; Brown et al., 1979) than previous studies that found correlations between CVT and age. Because this study aims at creating a method to be used in forensics and bioarchaeology, contemporaneous samples were used in model development. A sample that includes contemporary individuals is more likely to reflect the aging process of juveniles and provide more reliable statistics of current populations and their variation (Stull et al., 2014; Field et al., 2012). This is important for forensically based methods, as unknown individuals come from current or recent populations. Even though the method is based on a contemporaneous sample, results from this study are applicable to bioarchaeological samples. Data was collected from two different sources; CT scans and radiographic images.

CT sample

The CT sample that was used to create the models and refine the CVT method is comprised of juvenile CT scans (n=74), ranging in age from 0.08 to 16.58 years old. These scans were collected by Drs. Pricilla Bayle and Michael Coquerelle from living French children of different ethnic backgrounds who were "referred for medical care due to suspected cranial trauma, inflammation of the maxillary sinuses or neonatal distress, but did not exhibit any reportable abnormalities" (Coquerelle et al., 2011:193). No further explanation of cranial abnormalities was given. The scans come from two hospitals, one in Paris and one in Bordeaux, France (Coquerelle et al., 2011). Each scan captures data from one individual, and information with the scan includes known chronological age and biological sex. Other demographic information has been removed. The CT data was approved for research following the Comite Consultatif pour la Protection des Personnes dans la Recherche Biomedicale Bordeaux A. The current study does not meet the requirements for Human Research Protection Program (HRPP) review, as the data set exhibits non-identifiable data that had been collected prior to this study.

Radiographic sample

The radiographic sample that was used to test the method comes from *Patricia,* the online radiographic database, which is maintained at Mercyhurst University. *Patricia* is a forensic radiographic image collection consisting of radiographs of juvenile skeletons, including skulls. These images were captured during autopsy or physical examination of individuals who had died in the United States after January 1, 2000. They were collected from medical examiner and coroner's offices throughout the United States (Ousley et al., 2013). This sample comes from a modern population ranging in age from

newborns to twenty years old from different ethnic and ancestral groupings. Data on cause and manner of death is available upon request. *Patricia* was created as a data set available for research, specifically for investigation in developing juvenile age estimation methods. The collection contains over 9,709 images of varying quality that include all elements of the body in different anatomical views. I used a subset of data (n=2) from this sample to measure CVT for this study. The images are cephalograms because the cranial landmarks selected for this study are linear points, which are readily visible in a lateral view. Other non-linear points are not easily distinguishable on radiographs and if used, could be a potential source of error. The sample size was limited by three extrinsic factors: the number of cephalograms available for each age, image quality, which was either 'very good' or 'good', and scale presence. Image quality refers to a query option in *Patricia* when searching images. It corresponds to variable quality of the images based on disparities with exposure, sharpness and contrast (Ousley et al., 2013). Scale presence refers to a measurement scale in the image. Some images do not have any markers that indicate a scale or size of objects in the image. Images without scales could not be reliably used for the study. At the time of data collection and analysis, two radiographs between 0.0 and 2.9 years old with measurement scales were accessible that followed the criteria for image selection. Even though this sample is very small, it provided two test cases with known age from a modern sample that were freely available online.

Dry bone and other samples

Dry bone samples (n=22), a radiographic image (n=1) and CT scans (n=2) available through the Forensic and Bioarchaeology (FAB) Lab and the Biological Anthropology Research Laboratory (BARL) at Mississippi State University were used to

test the method. The dry bone sample comes from Lyon's Bluff, an archaeological site (c. 1200-1650 A.D.) from Oktibbeha County, MS (Peacock and Hogue, 2005). The radiographic image comes from a forensic case from the MS State Medical Examiner's Office in Jackson, MS. The CT scan comes from the Mitrou Archaeological site in Central Greece. Because the demographic information on age is unknown in these samples, each individual was aged using dental development scores (Moorrees et al., 1963; Shackelford et al., 2012), and compared to CVT estimates. This sample is discussed separately from method creation and testing, but can provide insight into future research on method performance on archaeological and dry bone samples.

Methods

Thickness measurements were collected on CT scans using Treatment and Increased Vision for Medical Imaging (TIVMI)[3] and on radiographic cephalograms using ImageJ [4] at the following cranial landmarks: nasion, glabella, bregma, vertex, vertex radius, lambda, and opisthocranion (Howell, 1973; Martin, 1928) (see Figure 1).

[3] http://www.pacea.u-bordeaux1fr/TIVMI/
[4] http://imagej.nih.gov/ij/index.html

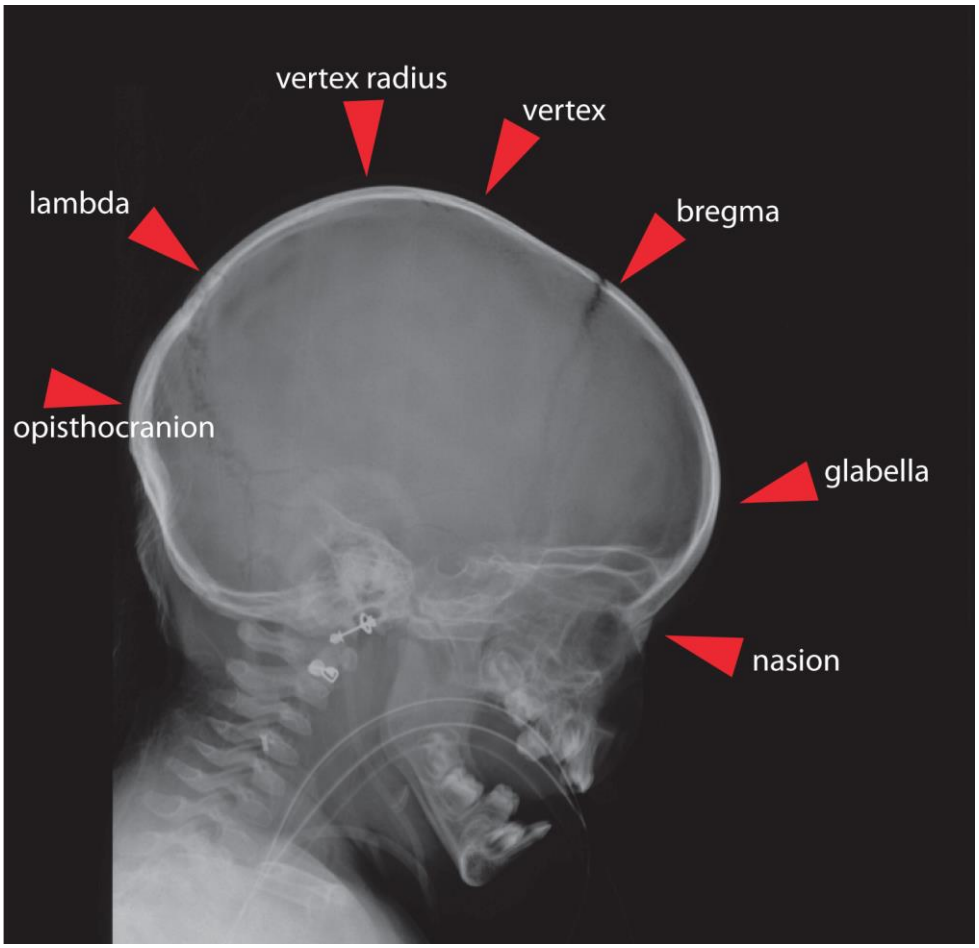

Figure 1 Cranial landmarks used in this study.

Cranial landmarks are defined as belonging to Type I, II or III (Bookstein, 1991: 63). Type I landmarks are located at sutural intersections, such as bregma, lambda, and nasion. Type II landmarks are located at the geometric maxima of bony protrusions or depressions. They are points of application of biomechanical forces. These points are opisthocranion, vertex, and glabella. The vertex radius was identified according to Howell's (1973) definition and the cranial landmark, vertex, was identified following Martin (1928). Definitions for each cranial landmark are listed in Appendix A. Some of

the cranial landmarks were chosen because they are points that have been shown to be predictive of age following previous studies on CVT and aging; namely nasion, bregma, vertex, and lambda. All seven points are visible on radiographic and CT data. CVT was reported as the smallest measure from the ectocranial to endocranial surfaces at a specific cranial landmark.

CVT Collection on Computed Tomography (CT) Scans

CVT measurements were collected on CT scans using TIVMI software developed by Guyomarc'h and colleagues (2011). TIVMI is a flexible medical imaging software used to perform various functions, including measuring, on multiple data types and files. Images were received as TSO files, which are a form of DIACOM images compatible with the TIVMI software. Threshold values were calculated to best illustrate bone and skeletal structures without including tissues, like veins, muscles, cartilage and skin or non-osseous material. A mesh, or 3D reconstruction, of each skull was created using the "Surface HMH 2" plug-in (see Figure 2). The "Surface HMH 2" plug-in reconstructs the skull using the half maximum height (HMH) protocol described by Spoor and colleagues (1993).

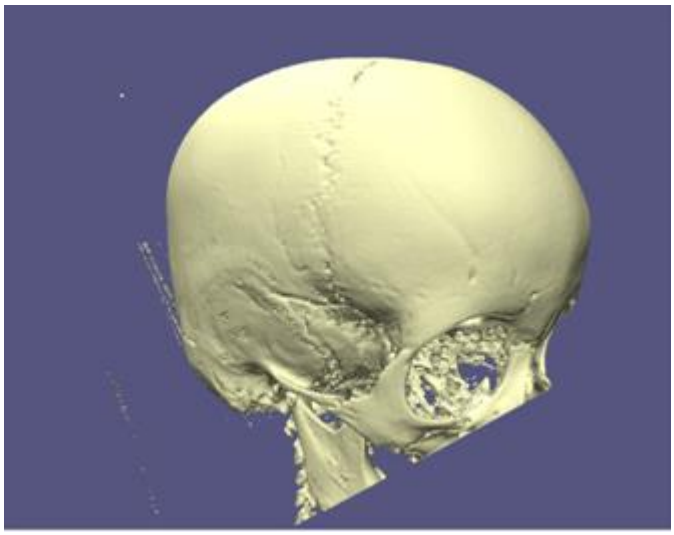

Figure 2 Mesh creating in TIVMI.

The image shows the mesh from the reconstructed CT scan using the TIVMI software. Cranial landmarks were placed on the mesh in order to reconstruct planes.

The seven cranial landmarks used in this study were marked as points on the mesh using a combination of visual placement and calculated placement through the creation of planes. The TIVMI user manual (Dutailly and Guyomarc'h, 2012) outlines the procedure for creating planes and placing Type II landmarks. Following the instructions in the manual, bregma, lambda, nasion, right and left porion, and right and left infraorbitale were visually placed on the cranium. The remaining landmarks, glabella, vertex and opisthocranion, were identified and marked using planes. The plug-in "Plane 3D" was used to create all planes. The sagittal plane was created from three placed points at nasion, bregma and lambda, or basion, if bregma was not available. Because the "Plane 3D" plug-in requires three points in the calculation of a plane, four separate planes were created to make the Frankfort Horizontal or mean transverse plane; FH1 (right porion, left porion, right infraorbitale), FH2 (right porion, left porion, left infraorbitale), FH3 (right infraorbitale, left infraorbitale, right porion) and FH4 (right infraorbitale, left

infraorbitale, left porion). FH1 and FH2 were averaged using the "Mean Plane" function to make FH5, and FH3 and FH4 were averaged to make FH6. The FH5 and FH6 planes were averaged to create the mean transverse, or Frankfort Horizontal plane. Two coronal planes were created using the "Orthogonal Plane from a Plane and 2 Points" function. The function input requires one previously created plane and two previously created points to create a new plane. The first orthogonal plane, C1, was created using the mean transverse plane, right, and left porion as the inputs. The second plane, C2, was created using the mean transverse plane, right and left infraorbitale as the inputs. C1 and C2 were averaged, using the "medium plane" as function to create the mean coronal plane.

After Type I cranial landmark placement was complete, each image was resliced along the sagittal plane using the "Reslice" plug-in. This ensured that ectocranial to endocranial measurements would be taken in the same plane and not at an angle. Type II cranial landmarks were identified by increasing plane thickness in either the anterior, posterior or superior direction. For example, to find glabella and opisthocranion, the mean coronal plane was increased in thickness until a small amount of bone was visible at the intersection of the bone, the coronal plane, and the midpoint or sagittal plane (see Figure 3). Vertex was found by increasing the thickness of the mean Frankfurt horizontal plane until a point along the sagittal plane was visible on the superior aspect of the cranium. Vertex was not identified on crania that did not exhibit a cranial landmark for bregma and 'NA' was used. The vertex radius was identified using the "Path3D" and "Segment3D" plug-ins. First, a segment was created between both external auditory meatii (EAM). A point was placed on the center of the segment using the sagittal plane. A 3D path was drawn from bregma to lambda by clicking the cursor repeatedly. The path was aligned

with the sagittal plane using the “Align path to plane” function. Then, using the “Explode path to points” function, the previously created path was turned into points; one point for each click. A segment was created from the point between the EAM and each of the points in the path. The longest segment was designated the vertex radius. Bregma, vertex, and the vertex radius were not identified on reconstructed mesh of individuals with open fontanels, because predicting age using CVT requires a thickness measurement. CVT was marked ‘NA’ for all juvenile crania where the landmark could not be accurately placed.

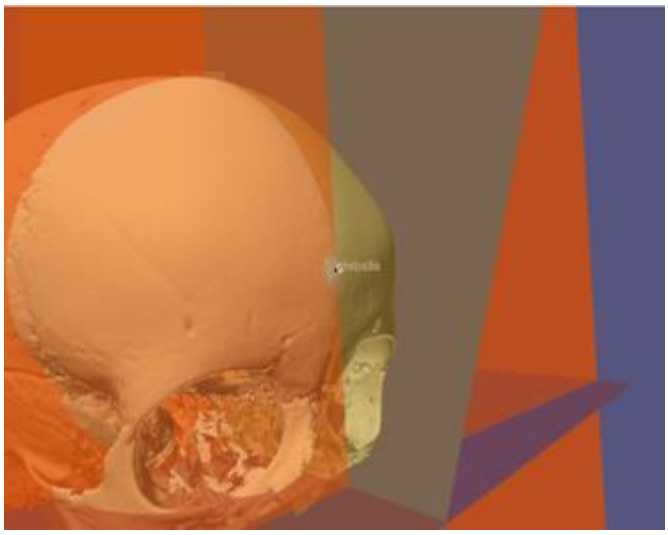

Figure 3 Point placement using planes in TIVMI.

This image shows how Type II landmarks were located. In this instance, glabella was found by increasing the thickness of coronal plane until a small segment of bone was visible at the planes intersection with the sagittal plane. The same procedure was used to find opisthocranion.

When collecting CVT measurements at cranial landmarks, the mesh image was hidden from the active screen, while the landmark points remained visible. The 3D image, which displays the original radiographic slices, was also visible in the sagittal plane. The same threshold value used in mesh calculation was used to illustrate the vault

in the radiographic image. The slices were moved so that the landmarks aligned with the image.

CVT measurements were collected using half maximum height (HMH) protocol. Measuring objects using the HMH protocol is highly accurate, because measurements are based on the best interface or meeting point between tissues (Spoor et al, 1993). To calculate thickness using HMH values, a segment was extended through the ectocranial and endocranial surface of the crania at the cranial landmark, bypassing the estimated landmark location. The "HMH on Segment3D" plug-in was used, which created a new point every time a difference in density was detected at a tissue intersection. Two points conforming to the cranial landmark at the ectocranial and endocranial surface were isolated and a segment drawn between them with the "Make 3D segment from two points" plug-in. The observed value was collected as the HMH measurement. The "Segment3D" plug-in automatically created and displayed this measurement in millimeters. Measurements at nasion and glabella passed through a sinus on some individuals, but not all individuals. All measurements, regardless of sinus presence, were used in model creation.

Images for individuals from the CT sample with the accession numbers 4, 10, 15, 16, 25, 64, 67, and 78 were excluded from the dataset used to develop the method, because they exhibited evidence of cranial surgery or other pathology that would affect growth and development, and CVT.

CVT Collection on Radiographic Images

Cranial landmarks were collected using ImageJ® on radiographic data. ImageJ® is an open source software program that has the capacity to measure different types of

images. Type I cranial landmarks were visually placed on the radiographs. Type II landmarks, like glabella and opisthocranion, were estimated by measuring the maximum cranial length with the "line tool" in ImageJ®. Vertex was identified by drawing a line from porion to infraorbitale and moving it superiorly until the superior most point on the cranium was identified. The vertex radius was identified by measuring the maximum radial distance between bregma and lambda from a point at the center of the EAM. CVT measurements were collected, and HMH values were manually calculated following the protocol in Spoor and colleagues (1993). The length of one pixel was defined for each radiograph through known measurements and scales using the "Set Scale" option in the Analyze tab in ImageJ®.

Points were marked on the cranium using the "point tool". The smallest distance from ectocranial to endocranial surface was measured using the "line tool". Following the HMH protocol (Spoor et al.,1993), two measurements were taken for each landmark. The average of these two landmarks was the CVT measurement used in statistical calculations.

CVT Collection on Dry Bone

The Lyon's Bluff collection contains many juvenile crania in various states of preservation. Crania that were intact or cranial fragments that exhibited cranial landmarks used in this study were selected for CVT measurement. CVT measurements on dry bone were collected using a Miyutoyo dental caliper. Type I cranial landmarks, including lambda and bregma were visually placed and marked with a pencil, while type II landmarks, including glabella, vertex and opisthocranion were estimated and their

centroid marked with a pencil. CVT was taken at marked cranial landmarks to the nearest hundredth, perpendicular to the bone and recorded in an Excel spreadsheet.

Dental Age (Transition Analysis)

Dental age estimations were performed on all samples following Moorrees, Fanning and Hunt's (1963) procedure for scoring dental maturation on individual teeth. Individual tooth scores for each individual were compiled and processed following Shackelford and colleagues (2012) method of age estimation of dental remains using transition analysis. Data was collected by visual examination of radiographic images, radiographic CT slices and available teeth not in occlusion. Black and white color levels were adjusted on each radiographic image using Photoshop (CS4) to delineate dental characteristics such as crown and root boundaries. Each observable tooth was scored and the numeric value was entered into a Microsoft ® Excel® (version 14.5.5) data sheet. Dentition that appeared radiopaque or radiolucent in the image were not scored and labeled 'NA'. Dental development age estimation was performed on the CT sample by scoring individual teeth on the radiographic CT slices. The author moved through multiple slices in TIVMI in order to view the entire suite of dentition and scored each tooth following the same methodology used for radiographs. Dental development age estimation was performed on CT scans by scoring individual teeth on the radiographic image slices. The author moved through multiple slices in order to view the entire suite of dentition and scored each tooth following the same methodology used on the radiographs. Dry bone dental estimates were scored using loose teeth associated with the remains, as *in situ* crown and root development was not observable.

Scores were determined using Moorrees and colleagues' (1963) coding system and recorded in a Microsoft ® Excel® spreadsheet. The following deciduous teeth: mandibular canines, first and second molars, and the following permanent teeth: the maxillary first and second incisor, and mandibular incisors, canines, premolars and molars were used to estimate age. Maxillary dentition was substituted into the scoring sheet when mandibular teeth were unobservable following established procedures in Shackelford and colleagues (2012). Tooth scores for each individual were analyzed using transition analysis, which is based on a combination of MLEs for individual teeth (Shackelford et al, 2012). A final MLE, with high-end and low-end estimates, was given for each individual.

Model and PI creation and other statistical analyses

CVT measurements were compiled in Microsoft ® Excel® spreadsheets and tested for normality using the Shapiro-Wilks test. CVT measurements that did not show a normal distribution underwent numerical transformations; measurements for nasion, glabella and vertex radius were converted to log or cubed root of the measurement. In the case of cubed root, the CVT measures were multiplied by (1/3), while the log transformation followed the log(CVT) equation.

CVT values that were normally distributed were plotted against the cubed root of known age in R software and fit with a loess curve to illustrate growth trajectories for each cranial landmark. Data for these landmark points were further analyzed in R software using the Earth package (Milborrow, 2011) to create MARS models in order to understand the relationship between age and CVT. In the model formula, cubed root chronological age was the response variable (y) and the CVT measurement was the

predictor variable (x). The following equation (generalized) was used to create the univariate models:

model<-earth(cubed_root_age~CVT, data=dataset, keepxy=TRUE,
varmod.method='lm', trace=0, ncross=10, nfold=10) (Eq. 1)

Equation 1 is the formula used to create a univariate model in the Earth package within R software. The regression formula reads as follows: the response variable, cubed root of age, minus the predictor variable, CVT. The dataset was the CT samples used in model creation. The varmod.method function selected the variance model, which was used to estimate prediction intervals. The 'lm', meaning linear model, estimated the standard deviation as a function of the predicted response. Ncross was set to do 10 cross validations. The model built 10 nfold cross-validated models. Each cross validation had 10 folds.

This equation was modified slightly for the multivariate models (see Equation 2).

model<-earth(cubed_root_age~CVT1+CVT2+CVT3+CVT4, data=dataset,
keepxy=TRUE, varmod.method='lm', trace=0, ncross=10, nfold=10) (Eq. 2)

Equation 2 is the formula used when creating multivariate Earth models in R. The regression formula reads as follows: the response variable, cubed root of age, minus multiple predictor variables, CVT at multiple cranial landmarks. The multivariate equation also uses 'lm' varmod.method and the same number of cross validations and cross validation folds.

Initially, the Earth package creates models to overfit the data, then trims them down through a forward and backward pruning pass. The pruning passes find the subset of terms that give the lowest generalized cross validation in a particular model. During

model construction, the Earth package tests multiple models with a subset of the test data to gauge accuracy and find the best model. The Earth package created multiple models for each cranial landmark to find the smallest residual standard error, which was used to create the PIs. PIs are based on the out of fold data and a *k*-fold cross-validation test to gauge the accuracy of the PIs. In order to find the predicted ages of test radiographs, CVT was entered into an equation (see Equation 3), and the measurements were placed within the PIs generated by the model.

Predict(object, newdata=dataset, interval="pint", level=.95 (3)

This equation was used to generate prediction intervals for the test data and unknown age data. The object is the Earth model. The newdata is the data set being tested against the model. The interval= "pint" is set to use a prediction interval, and the level means that it is testing the data at the 95% PI.

This equation was used on CVT measurements from the test data. The output of the equation gave lower, upper and fit age estimates for each of the radiographs at each cranial landmark. These estimates were compared to the chronological age associated with each radiographic image. Following Konigsberg and colleagues (2008), 50% coverage bands of CVT were compared to 50% coverage bands of dental development and their relationship discussed. These coverage bands were graphed using stock charts in Microsoft Excel® and compared to plotted points of chronological age. Graphs for CVT estimations at the 95% coverages were compared to plotted points of chronological age. These tests quantified how well the CVT method performs as compared to aging by dental development and chronological age on both the radiographic and CT samples. Results are discussed in Chapter VI.

CHAPTER IV

RESULTS

Summary Statistics

The CT dataset was plotted to illustrate the frequency of individuals at given ages that make up the sample (see Figure 4).

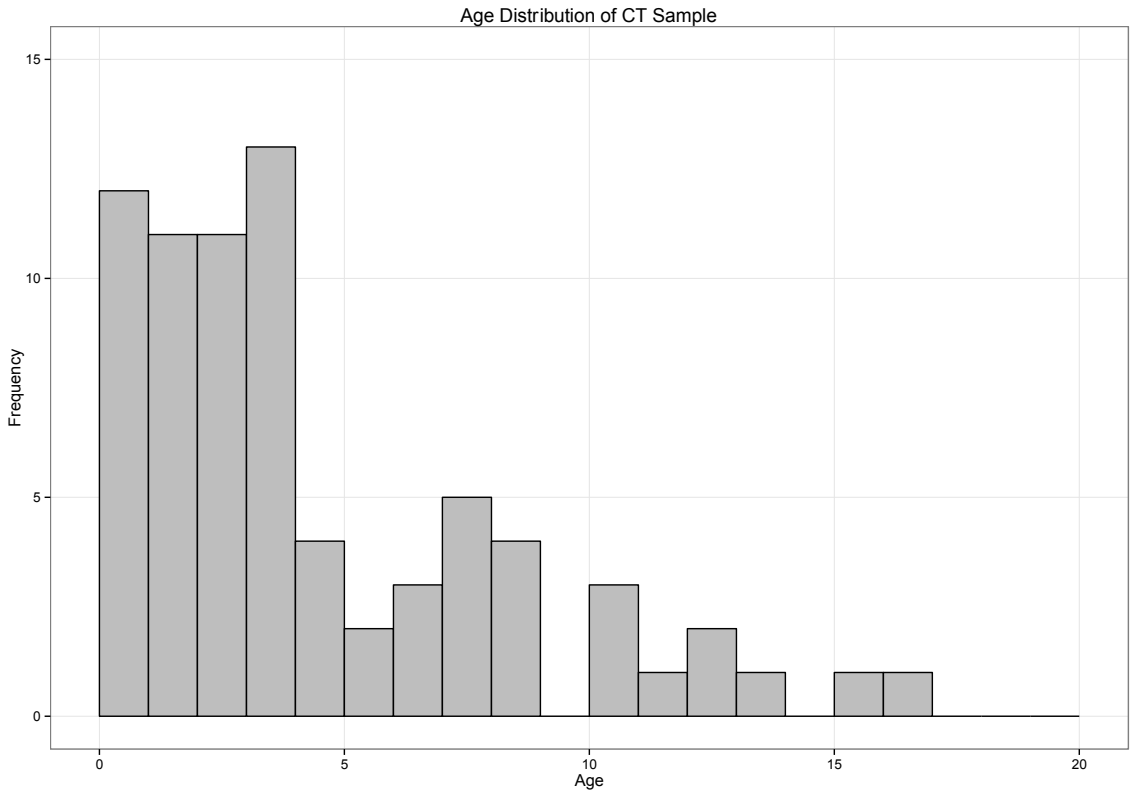

Figure 4 Distribution of ages in the CT sample.

The figure shows the distribution of ages in the CT sample.

The graph shows that the majority of the sample is composed of younger individuals aged between birth and 5 years old. More than half of the sample is under the age of 10 years old, and there are very few individuals over the age of 15 years old. The sample is composed of 37 females and 37 males.

CVT measurement values

The CVT HMH values from the CT data were tested for normality using the Shapiro-Wilkes test. Bregma, vertex, lambda, and opisthocranion produced *p-values* above 0.05, indicating that the data for those cranial landmarks was normally distributed. The results of the Shapiro-Wilkes test for nasion, glabella, and the vertex radius produced *p-values* below 0.05, indicating these datasets did not exhibit a normal distribution (see Table 1).

Table 1 Shapiro-Wilkes test on non-transformed CVT measurements.

Normality test on HMH CVT measurements[1]							
	nasion	glabella	bregma	vertex radius	vertex	lambda	opistho
W	0.92	0.92	0.98	0.93	0.97	0.97	0.99
p-value	2.00E-04	5.00E-04	0.76	0.01	0.41	0.17	0.67

[1]This table illustrates the results of the Shapiro-Wilkes test for each set of HMH CVT measurements from the CT data

For additional verification of normality, the CVT datasets for nasion, glabella and vertex radius were plotted in a QQ plot (see Figures 5, 6 and 7).

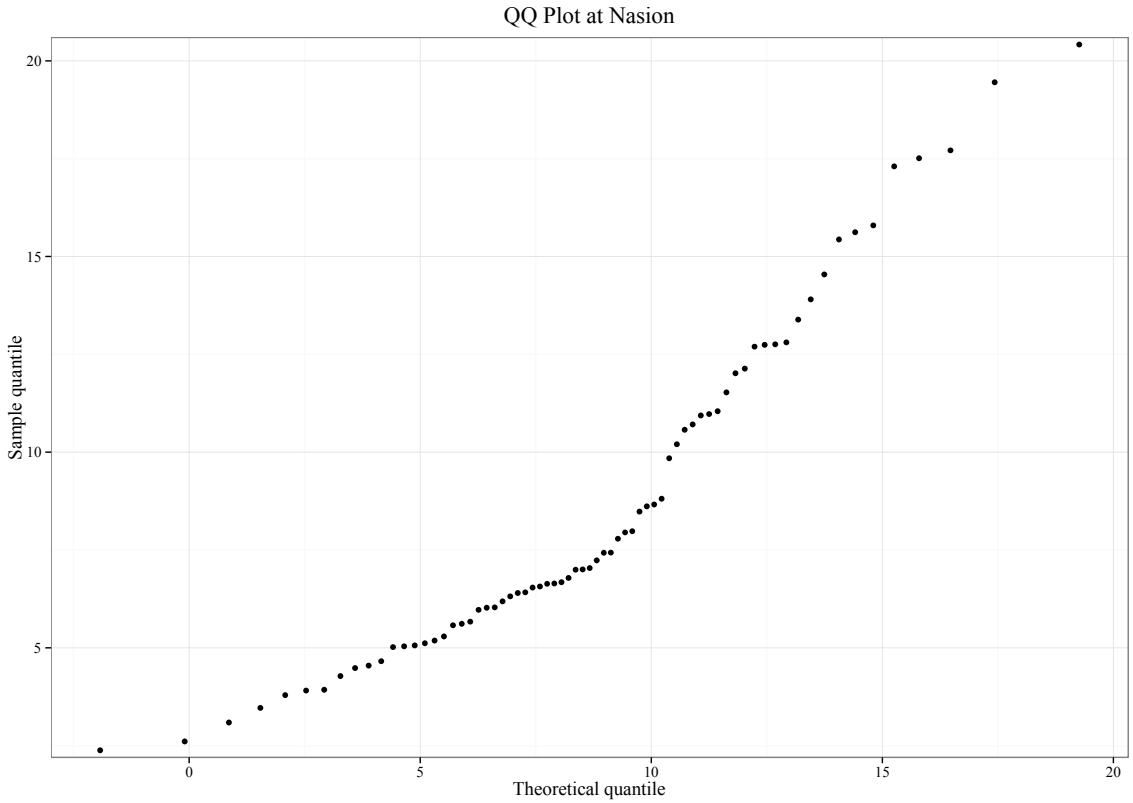

Figure 5 QQ plot of CVT at nasion

The above plot is the measured HMH CVT values for nasion. The data is skewed to the left, confirming that untransformed CVT measurements are not normally distributed.

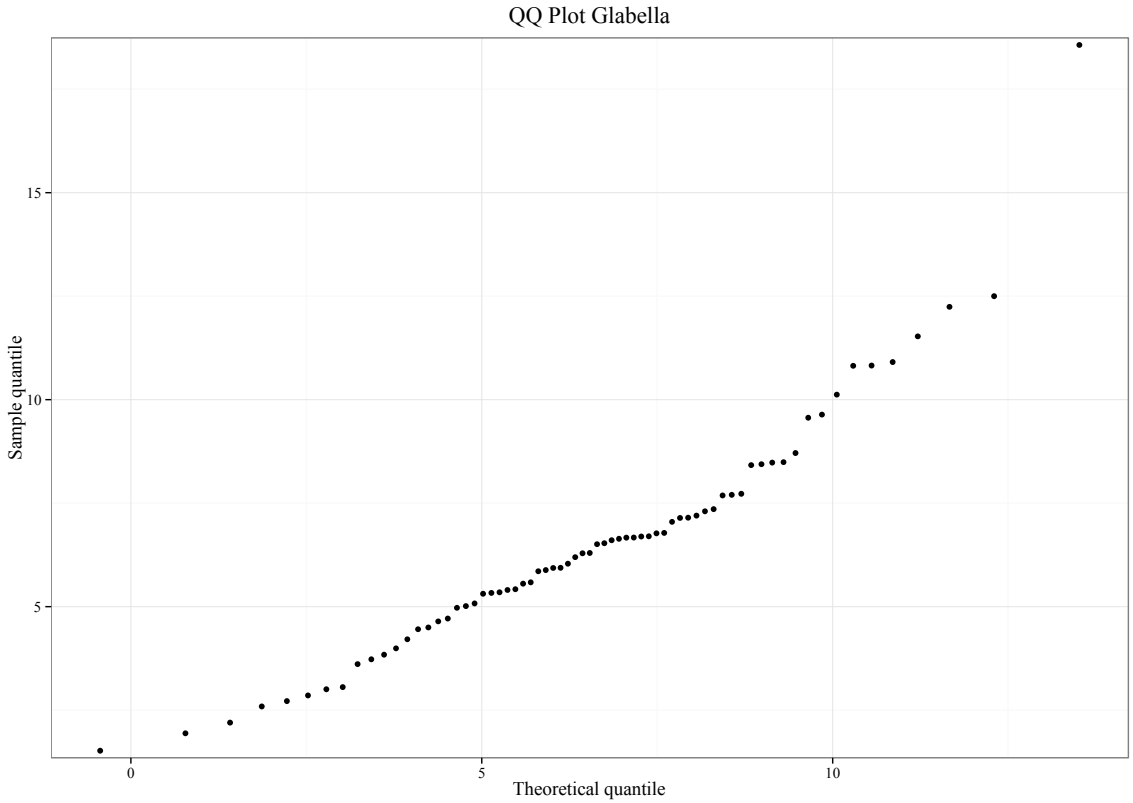

Figure 6 QQ plot of CVT at glabella

The above plot shows the measured HMH CVT values for glabella. The data is skewed to the left, confirming that untransformed CVT measurements are not normally distributed.

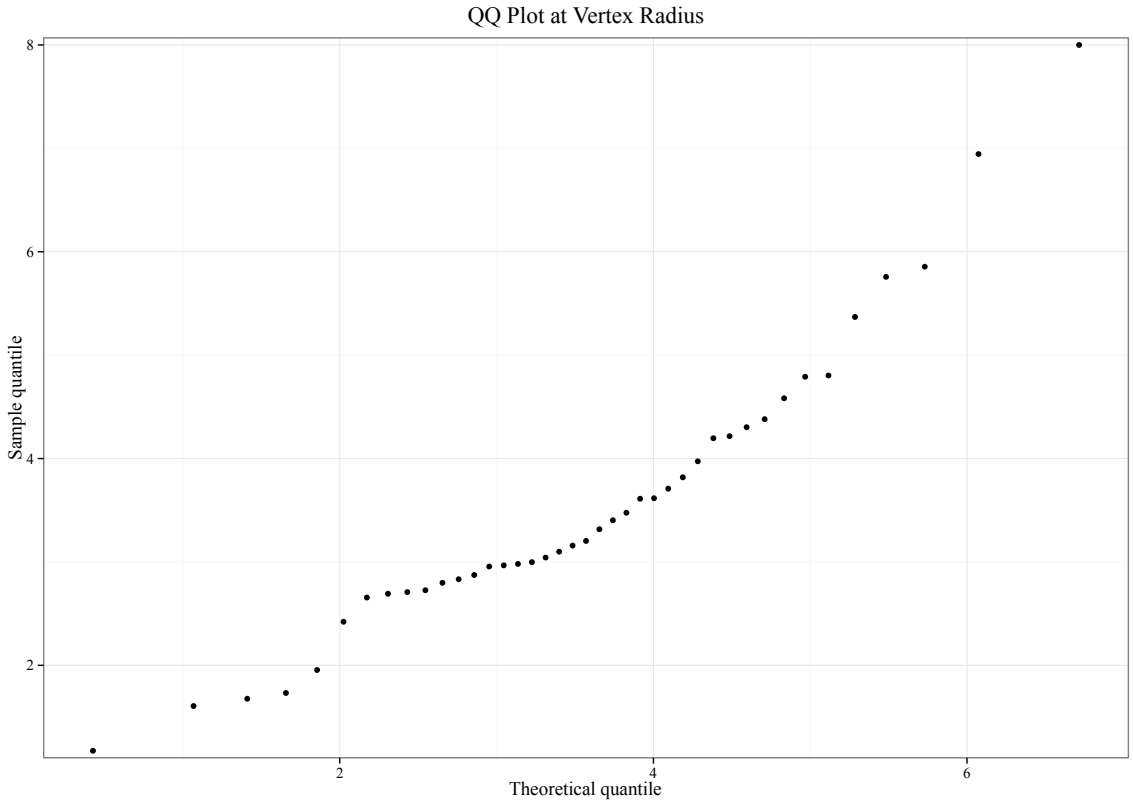

Figure 7 QQ plot for CVT at the vertex radius.

The above plot shows the measured HMH CVT values for the vertex radius. The data is irregular at the lower end of the plot, confirming that untransformed measurements are not normally distributed.

All three plots confirm that untransformed CVT measurements at nasion, glabella and vertex radius were not normally distributed. In an attempt to normalize the data, numerical transformations were performed on the measurement values. The CVT measurement data for nasion was transformed using the log of CVT. When tested again, the Shapiro-Wilkes test produced a *p-value* of 0.46, indicating a normal distribution. The CVT measurement data for glabella was transformed using the square root of CVT. When tested a second time, a *p-value* of 0.29 was produced, indicating that the distribution was normal. The CVT measurement for the vertex radius was transformed

using the log of CVT. When tested again, a *p-value* of 0.48 was produced, indicating the transformed data followed a normal distribution. In model construction at nasion and vertex radius, log of CVT was used; at glabella, the square root of CVT was used.

CVT measurements were taken 10 times on the same CT scan using TIVMI. The standard error was calculated for each CT scan using Microsoft Excel®. Then, the average standard error was calculated for all CVT measurements at that landmark. The standard error for each landmark is listed in Table 2.

Table 2 Standard error for CT measurements using TIVMI.

Standard error on multiple CVT measurements						
landmark	nasion	glabella	bregma	vertex	lambda	opistho
std error	0.04	0.03	0.03	0.03	0.02	0.02

Standard error calculations are low for all cranial landmarks, indicating measurements are slightly off from the mean, but not by a large degree.

Hypothesis One

The first hypothesis states that: CVT measurements at select cranial landmarks (nasion, glabella, bregma, vertex, vertex radius, lambda, and opisthocranion) will conform to expected growth curves using a locally smoothed (loess) fit.

To address this, scatterplots were created in R software where cubed root chronological age was plotted against CVT. Each scatterplot shows a smoothing line based on loess regression to better illustrate whether the data conformed to a growth curve or not (see Figure 8).

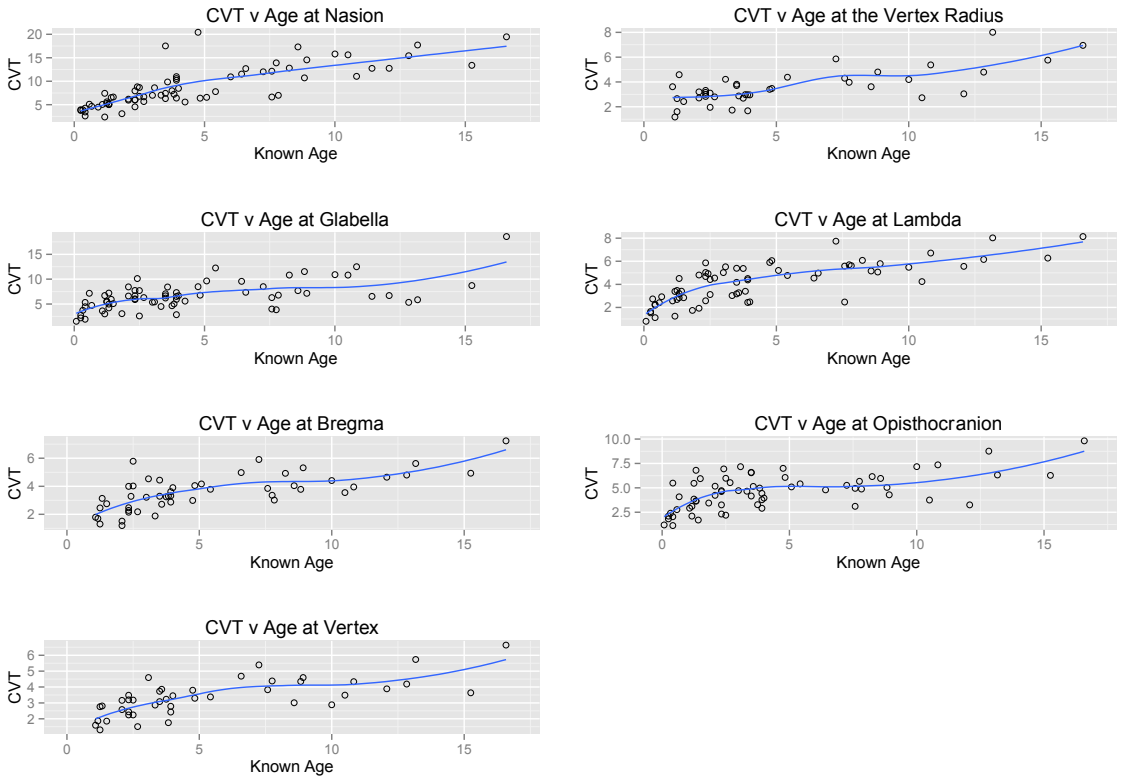

Figure 8 Plotted CVT values for each cranial landmark.

The above plot shows HMH CVT values plotted against known age for each cranial landmark. A smoothing loess line (in blue) indicates that there is an increased thickness with age at all landmarks. Some plots show a more linear increase in thickness, while others shows burst of rapid growth followed by steady growth.

The plots show that CVT increases with increasing age at every landmark. The loess lines indicate that CVT at certain cranial landmarks: bregma, vertex and opisthocranion, followed growth more closely than CVT at nasion, glabella, vertex radius and lambda. CVT at glabella and the vertex radius show an increase in thickness with age, but do not illustrate a typical growth curve. Nasion and lambda did not exhibit rapid increases in growth, but instead CVT increased steadily across the entire plot.

Hypothesis one was supported for bregma, vertex and opisthocranion. It was rejected for glabella, vertex radius, nasion and lambda.

Hypothesis Two

Hypothesis two states: CVT measured on radiographic images of juvenile crania will conform to age estimation models developed on CT scans.

In order to test this hypothesis, MARS models were created to understand the statistical relationship between chronological juvenile age and CVT at cranial landmarks, based on methods used by Stull and colleagues (2014). MARS used cubed root chronological age as the response variable (y) and CVT as the predictor variable (x); exceptions were at nasion and vertex radius, where log CVT was used, and glabella, where square root CVT was used. Univariate MARS models were created for CVT and age at each cranial landmark: nasion, glabella, bregma, vertex, vertex radius, lambda, and opisthocranion. Multiple models were created and the program selected the best model with the smallest residual error. PIs were created using the out of fold cross-validation that quantify—in years—the accuracy of the measurement in predicting chronological age.

MARS univariate models results

MARS models were built using available data for each cranial landmark on each CT scan. Not all CT scans allowed a measurement at every landmark used in this study; as some landmarks, like bregma had not formed at the time the scans were taken. The majority of the data used in model creation came from juveniles younger than 3 years old. Data for juveniles aged between 4 and 16 years old was severely lacking, with a single individual available for a year age interval at 11, 13, 14, and 16. The oldest individual used in model creation was 16.58. Predicted ages on juvenile crania older than 4 years old were less accurate than those made on younger aged juveniles. Predicted ages with a

fit age older than 16.58 were not shown, because they are outside of the sample range. These limitations will be discussed in more detail in Chapter V.

The univariate model analysis initially included four model interpretation plots: a model selection plot, a residual vs. fitted plot, a cumulative distribution plot, and a QQ plot of the residuals. The model selection plot illustrated the number of predictors used in the selected model. The residuals vs. fitted plot showed the residual spread, or difference between the values predicted by the model (predicted age) and the actual values (known age), for each predicted response. In an ideal residuals vs. fitted plot, points are evenly spread out across the plot, showing that the assumptions of linearity, randomness and homoscedasticity have been met (Field et al., 2012). The three largest residual values were labeled in this graph, a default of the Earth package. The line in center of the plot represents a normal distribution, which, ideally, should be straight. The QQ graph showed the normality distribution of the residuals (Milborrow, 2015). In the cumulative distribution plot, the line should start at zero and move rapidly to one. The point at which the vertical and graphed line connect, illustrate the percentage that the predicted value is within *x* units of the observed value. Smaller values suggest a better model for predicting age.

Summary statistics revealed the fit of the model to the data and the relationship between CVT and age. In the Earth package, the following values were used to assess the model: RSS (residual sum of squares), RSq (R-squared), CVRSq (Cross validated R-squared), GCV, and GRSq (generalized R squared). The RSS value measured the discrepancy between the data and the model. A lower RSS value indicated a better fit of the model to the data. The RSq measured the predictive ability of the model; the

quantification of an age estimate that can be explained by CVT. Values range from -1 to 1, and the closer the RSq value was to 1, the better the CVT model could explain age (Milborrow, 2015). The cross-validation statistics measure the accuracy of the model on different samples not used in model creation. This value is typically lower than the RSq value because of noise created by the residuals. The generalization statistics, GCV and GRSq, assessed how well the model generalizes to other data sets, allowing conclusions to be drawn beyond the sample (Field et al., 2012).

PIs were plotted for each of the landmarks using the plotmo() function. The PIs and their standard deviations were calculated during model creation by the Earth package. Test measurements were entered in the model, and the Earth package output produced numerical PIs including the fit age, upper and lower age ranges. These predicted age estimates were exported as a CSV file and compared with chronological age. Linear regression models were created to get the standard error (SE) for the univariate models.

Nasion

The models interpretation plots for the Earth model at nasion is shown in Figure 9.

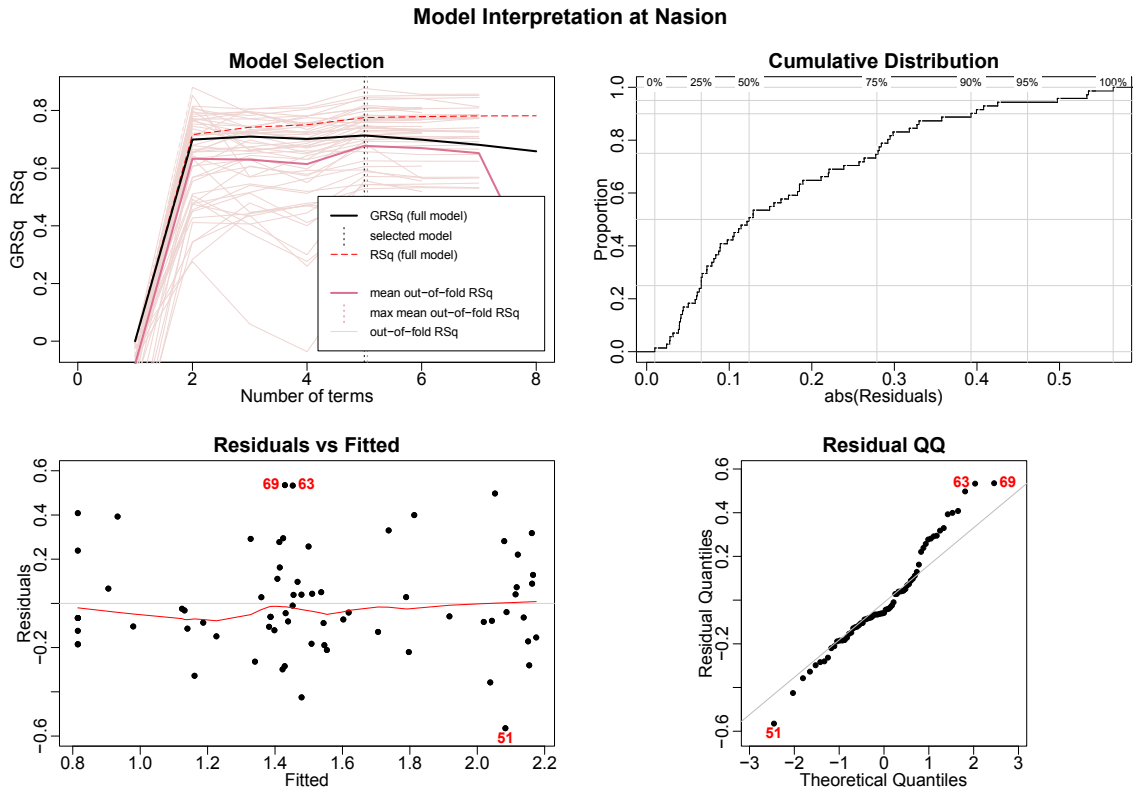

Figure 9 Model interpretations plots for CVT at nasion

The model selection plot explains that the best model at nasion used five terms. The residuals vs. fitted plot illustrates the residuals are clustered at the center and ends of the plot. The QQ plot shows that there is divergence from normality at both tails, but more at the right tail. Points 63, 69 and 51 are the largest residuals in the plot. These plots indicate that age predictions using the CVT model at nasion are not very accurate. Summary statistics for the model are listed below (see Figure 10 and Table 2).

```
Call: earth(formula=cbrt_known~CVT_log, data=nasion_hmhcvt, keepxy=TRUE,
      trace=0, ncross=10, nfold=5, varmod.method="lm")

                  coefficients
(Intercept)          0.8150273
h(CVT_log-0.631363)  4.4567425
h(CVT_log-0.75351)  -3.4421566
h(CVT_log-1.00874)   4.6258682
h(CVT_log-1.1074)   -6.3137911

Selected 5 of 8 terms, and 1 of 1 predictors
Termination condition: RSq changed by less than 0.001 at 8 terms
Importance: CVT_log
Number of terms at each degree of interaction: 1 4 (additive model)
GCV 0.06683216  RSS 3.618349  GRSq 0.7134777  RSq 0.7752262  CVRSq 0.640279

Note: the cross-validation sd's below are standard deviations across folds

Cross validation:   nterms 3.88 sd 1.12    nvars 1.00 sd 0.00

     CVRSq   sd     MaxErr   sd
      0.64 0.14       -0.8 0.59

varmod: method "lm"    min.sd 0.0264    iter.rsq 0.011

stddev of predictions:
            coefficients iter.stderr iter.stderr%
(Intercept)   0.19286907   0.0787431           41
cbrt_known    0.04644631   0.0518793          112

                              mean    smallest
95% prediction interval   1.033037   0.9044218
                         largest     ratio
95% prediction interval 1.151998   1.27374

                                       68%    80%
response values in prediction interval   73     87
                                       90%    95%
```

Figure 10 Summary statistics for the Earth model at nasion (output example).

This image illustrates the R output for the summary.statistics() function for the Earth model at nasion. The same results are shown in a table form in Table 3.

Table 3 Summary statistics for the Earth model at nasion.

Statistic	Acronym	Value
generalized cross validation	GCV	0.07
residual sum of squares	RSS	3.62
general r squared	GRSq	0.78
r squared	RSq	0.78
cross-validated r squared	CVRSq	0.64
standard deviation	sd	0.14
maximum error	MaxErr	-0.80
standard deviation	sd	0.59

This table shows the summary statistics from the Earth model for CVT at nasion.

The RSS value is 3.62, which indicates that the model does not fit the data very well. The RSq value is 0.78, which means that 78% of the model for age can be explained by CVT; there is a strong relationship between the two variables. The CVRSq value is 0.64, which is lower than the model's RSq, but still captures a significant percentage of the model. The GRSq value is 0.78, which indicates that the model is good at predicting age using CVT in a different data set. The 95% PIs for CVT are shown below (see Figure 11).

Figure 11 95% prediction intervals at nasion.

This plot illustrates the prediction intervals for the model at nasion in light pink; the CVT measurements at the cubed root of age; and the fit line.

Figure 10 shows the log of CVT regressed on cubed root of age. The shaded area represents the 95% prediction interval generated by the model. This graph shows that as age increases, there are two rapid increases in thickness at 9 months and just after a year until thickness plateaus. A variance model for nasion was plotted (see Figure 12). This model illustrates how well the confidence limits in dark grey compare to prediction intervals in pink.

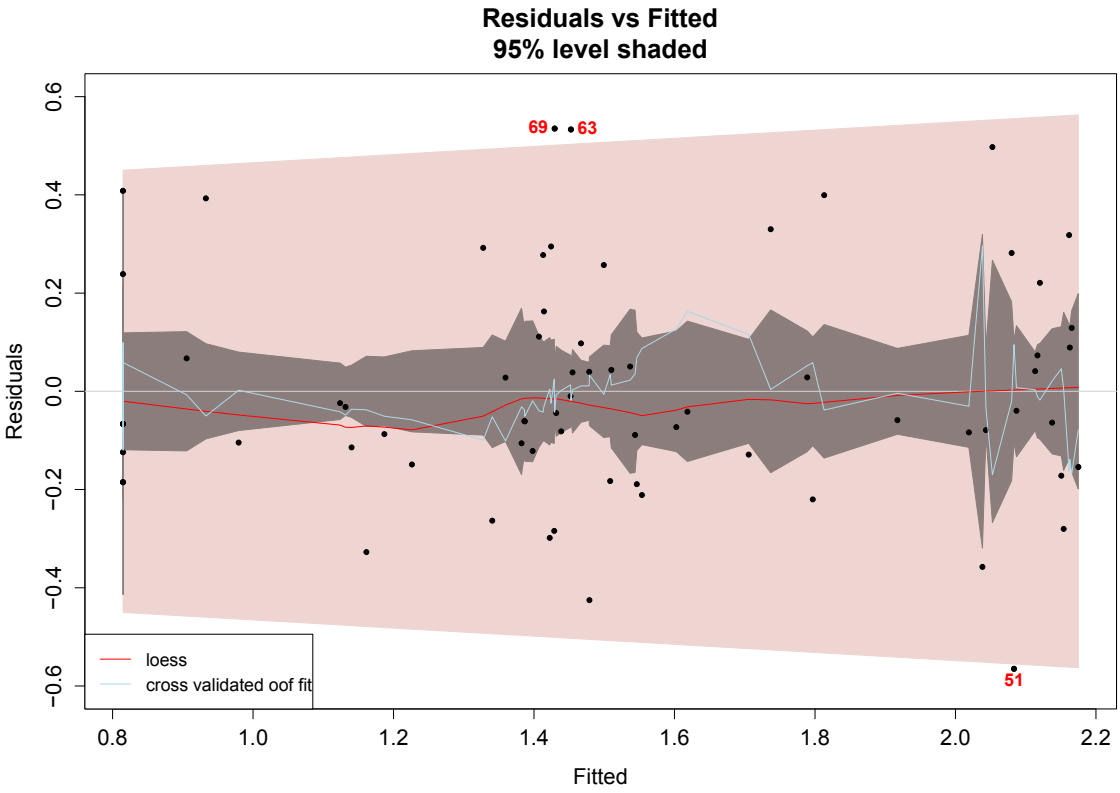

Figure 12 Prediction bands in a residuals plot for nasion.

The dark grey bands show the confidence limits; the wider pink bands show the prediction limits; the red line is a loess fit to the residuals; the blue line is the cross-validation mean fit.

The graph shows that CI band thickness is wide and varied throughout the plot, indicating model uncertainty. The loess line weakly corresponds with the grey line, while the cross-validation line does not correspond to the grey line. All of this data indicates that model created for nasion is not useful for predicting age from CVT.

Glabella

The Earth model at glabella was created using square root values of CVT. Model interpretation plots are shown below (see Figure 13).

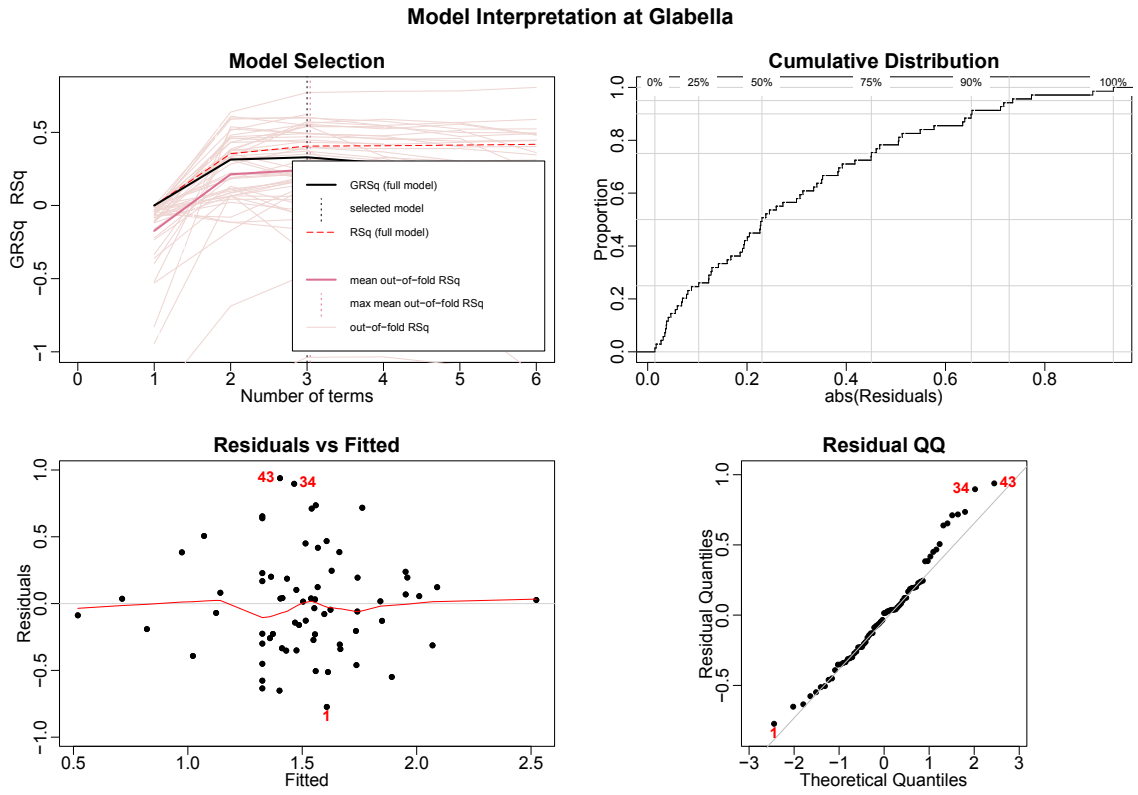

Figure 13 Model interpretation plots for CVT at glabella.

The model selection plot shows that the best model uses three terms. The residuals vs. fitted plot shows that the residuals cluster to the center, which means the model is less accurate as the predicted value increases. The QQ plot shows that the residuals diverge from normality at the right tail. Points 34, 43 and 1 are the largest residuals. This data indicates that the model is not accurate in predicting age using CVT at glabella. Summary statistics for the model at glabella are shown below (see Table 4).

Table 4 Summary statistics for the Earth model at glabella

Statistic	Acronym	Value
generalized cross validation	GCV	0.17
residual sum of squares	RSS	10.02
general r squared	GRSq	0.33
r squared	RSq	0.41
cross-validated r squared	CVRSq	0.05
standard deviation	sd	0.63
maximum error	MaxErr	1.20
generalized cross validation	sd	0.69

This table shows the summary statistics from the Earth model at glabella.

The RSS value is 10.02, which indicates that the model does not fit the data. The RSq value is 0.41 and tells us that 41% of age can be explained by CVT. The CVRSq is 0.05, which is much lower than the model's RSq value. This indicates that a smaller percentage of age is explained by the CVT. The GRSq value is 0.33, which explains that the model is not good at predicting age values in a different data set. Overall, this data indicates the model is not useful for predicting age using CVT. The 95% PIs are plotted below (see Figure 14).

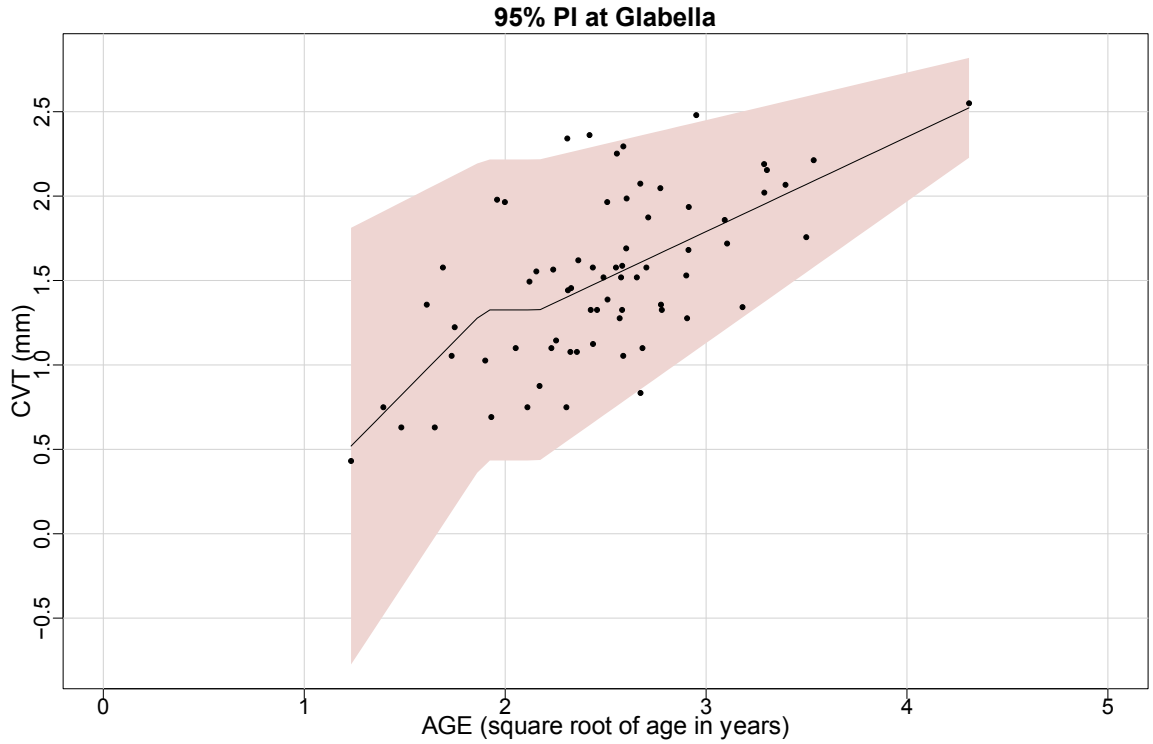

Figure 14 95% prediction intervals at glabella.

This plot illustrates the prediction intervals in light pink; the thickness measurements at each age in the CT sample; and the fit line.

This plot shows that as age increases, the PIs narrow. The plot illustrates rapid growth of CVT at glabella just before 4 years of age, with a small leveling off period, then a steady increase in thickness until after 16 years old. The plot truncates at ~17 years old indicating that predictions above that age are less reliable. A variance model for glabella was plotted (see Figure 15).

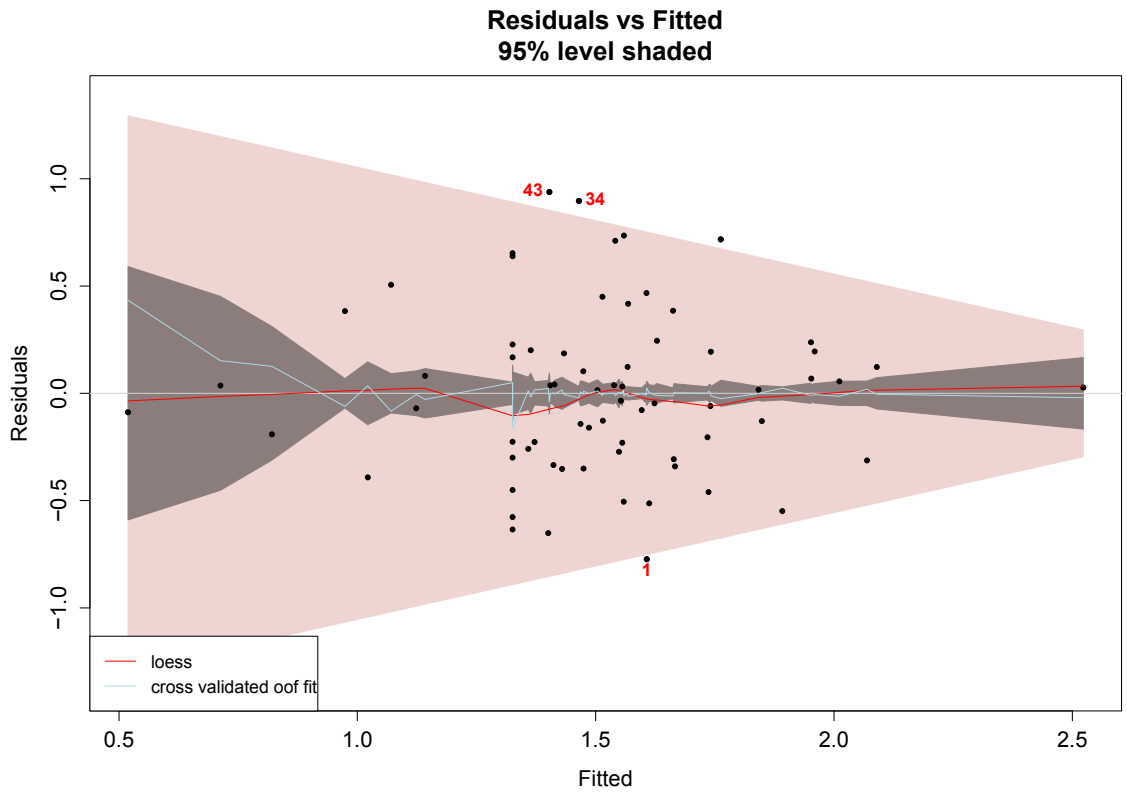

Figure 15 Prediction bands in a residuals plot for glabella.

The dark grey bands show the confidence limits; the wider pink bands show the prediction limits; the red line is a loess fit to the residuals; the blue line is the cross-validation mean fit.

The plot shows that the prediction limits are wider at the low and high ends, indicating that the model is more uncertain at those values. The confidence limits narrow across the plot, indicating greater certainty as the values shift to the right. The loess and cross-validation mean fit lines are close to the grey centerline of the model in the mid range values. The plot indicates that the model is useful for predicting age at middle and upper values, but uncertain at the lower values.

Bregma

The Earth model at bregma was created using CVT measurements. The model interpretation plots are shown below (see Figure 16).

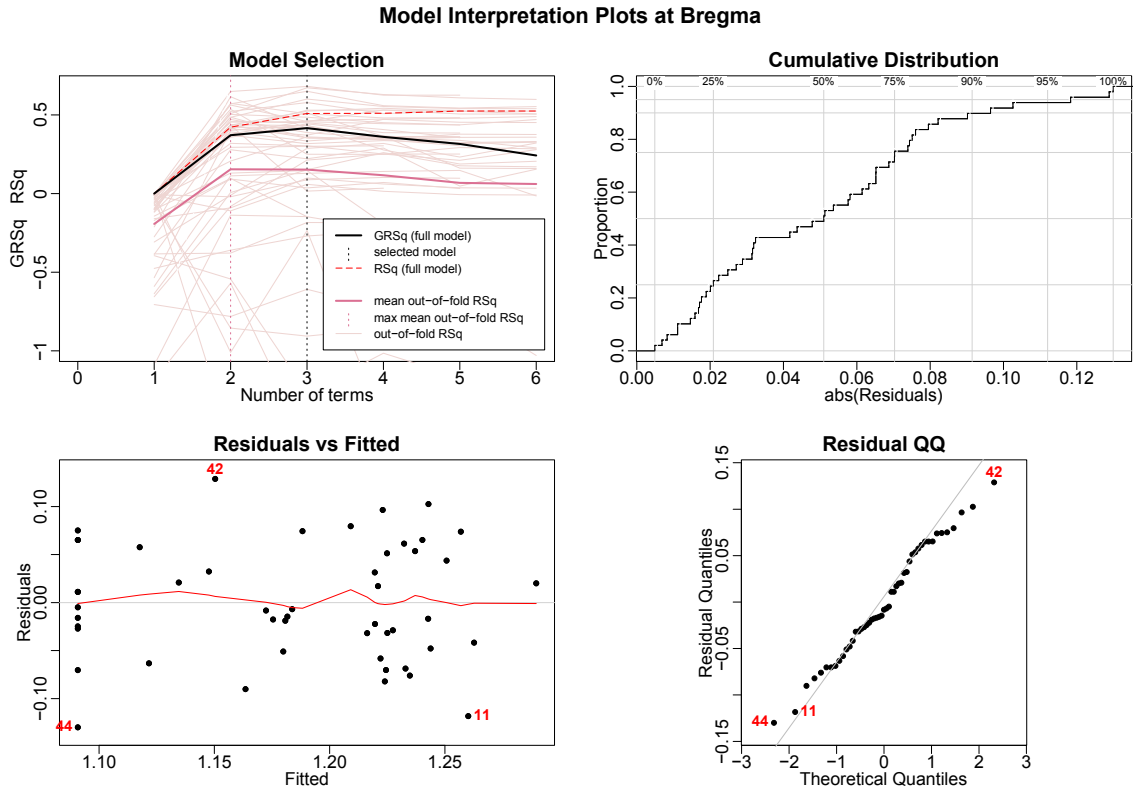

Figure 16 Model interpretation plots for CVT at bregma.

The model selection plot shows that the selected model uses three terms. The residuals vs. fitted plot shows the loess line is constant along the center of the plot. The residuals are evenly distributed throughout the plot, indicating that the model is a good fit for the data. The QQ plot shows the residuals diverge from normal at the right tail, and points 42, 44 and 11 are the largest residuals. Overall, the model assessment plots

indicate that the model at bregma is useful for predicting age. Summary statistics for the model are shown in Table 5.

Table 5 Summary statistics for the Earth model at bregma

Statistic	Acronym	Value
generalized cross validation	GCV	4.00E-3
residual sum of squares	RSS	0.18
general r squared	GRSq	0.42
r squared	RSq	0.51
cross-validated r squared	CVRSq	0.12
standard deviation	sd	0.54
maximum error	MaxErr	-0.19
generalized cross validation	sd	0.13

This table shows the summary statistics from the Earth model at bregma.

The RSS value is 0.18, indicating that the model is a good fit for the data. The RSq value is 0.51, which means 51% of the age prediction can be attributed to CVT. The CVRSq is 0.12, which is lower than the model's RSq value; indicating the cross-validation results capture lesser percentage of the model. The GRSq value is 0.42, which indicates that the model is useful for predicting values in a different data set. The 95% PIs for the model are shown below (see Figure 17).

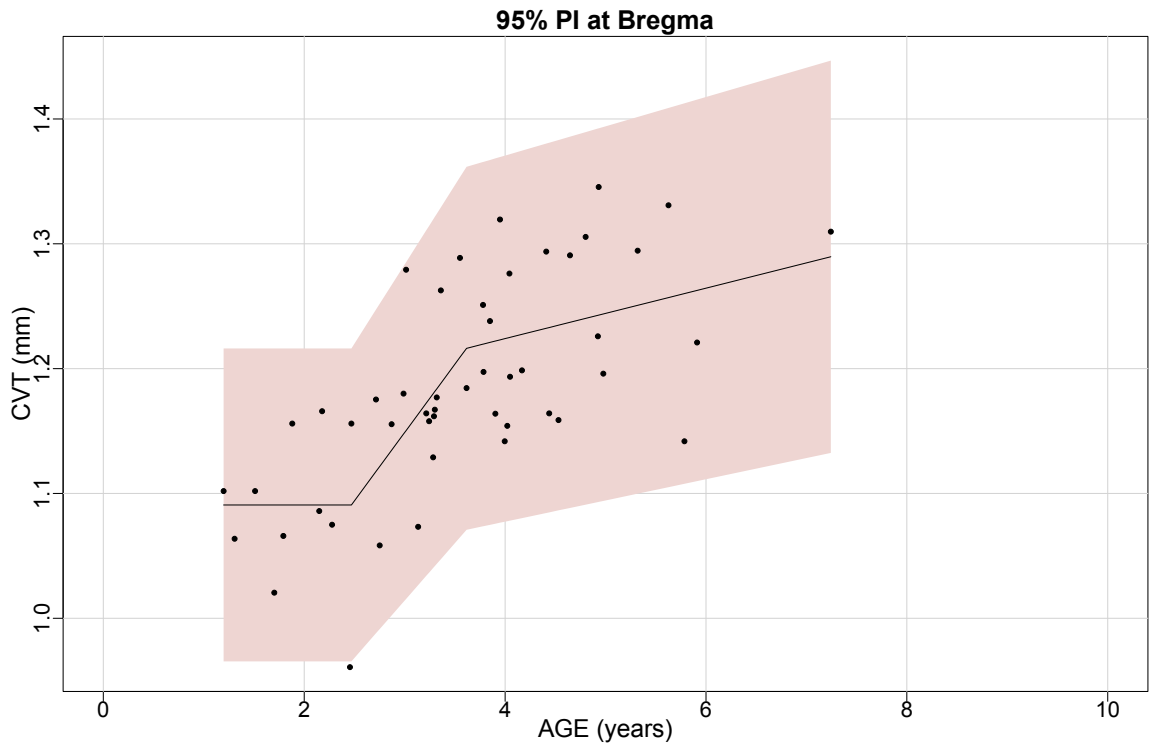

Figure 17 95% prediction intervals at bregma

This plot illustrates the prediction intervals (light pink); the thickness measurements at each age in the CT sample; and the fit line (black).

To plot shows that there is a rapid increase in CVT at bregma beginning after 2 years of age and slowing just before 4 years of age. This spurt is consistent with the first juvenile growth spurt, beginning shortly after birth and slowing around 3 years of age (Lewis, 2007:60). The PIs are narrow, and the plot shows that the CVT values vary by 0.4 mm over 7 years of age. This is a very small range of measurement and using this model to estimate age by CVT would be impractical and unreliable. The model truncates just over 7 years of age indicating older age predictions are less reliable. A variance model for bregma was plotted with residual values (see Figure 18).

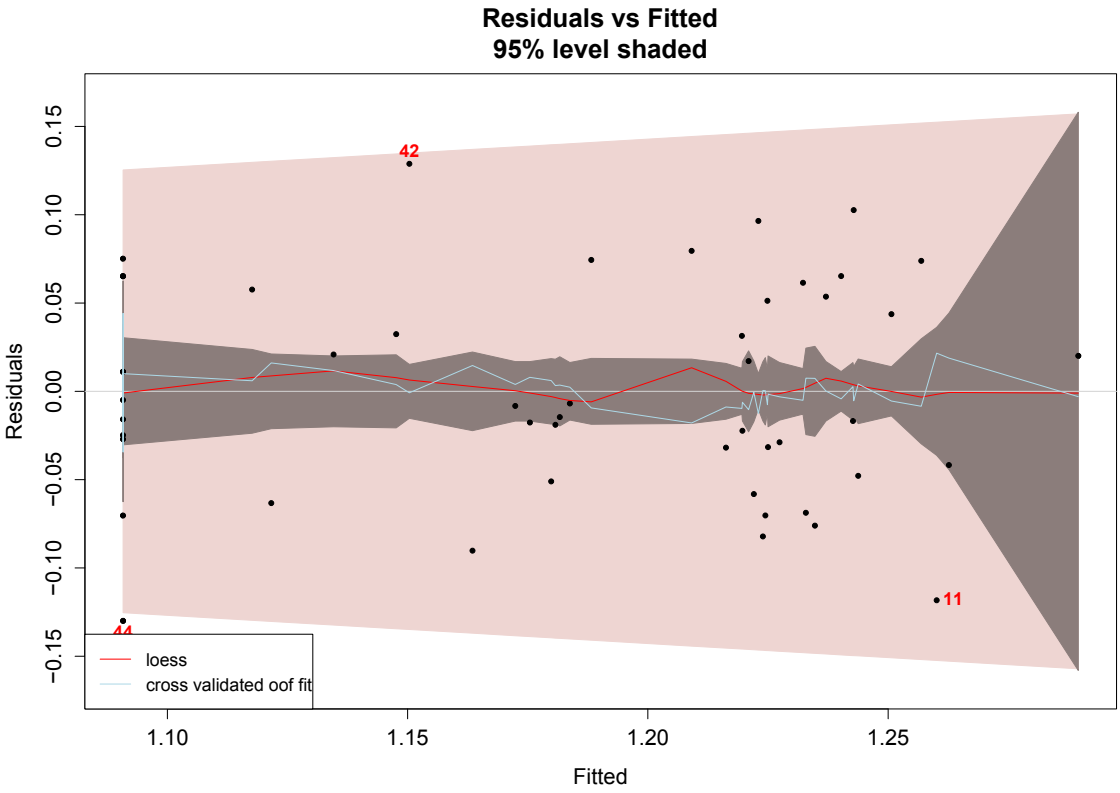

Figure 18 Prediction bands in a residuals plot for bregma.

The dark grey bands show the confidence limits; the wider pink bands show the prediction limits; the red line is a loess fit to the residuals; the blue line is the cross-validation mean fit.

The plot shows wide confidence limits that increase with higher values. The prediction limits. The residuals plotted in the variance model show that the confidence limits widen at the extreme high values, revealing that the model is more unpredictable on the upper limits. The PIs are wide to start, and are very wide at the upper limit.

Vertex

The Earth model at vertex was created using CVT measurement. The model interpretation plots for the model are show in Figure 19.

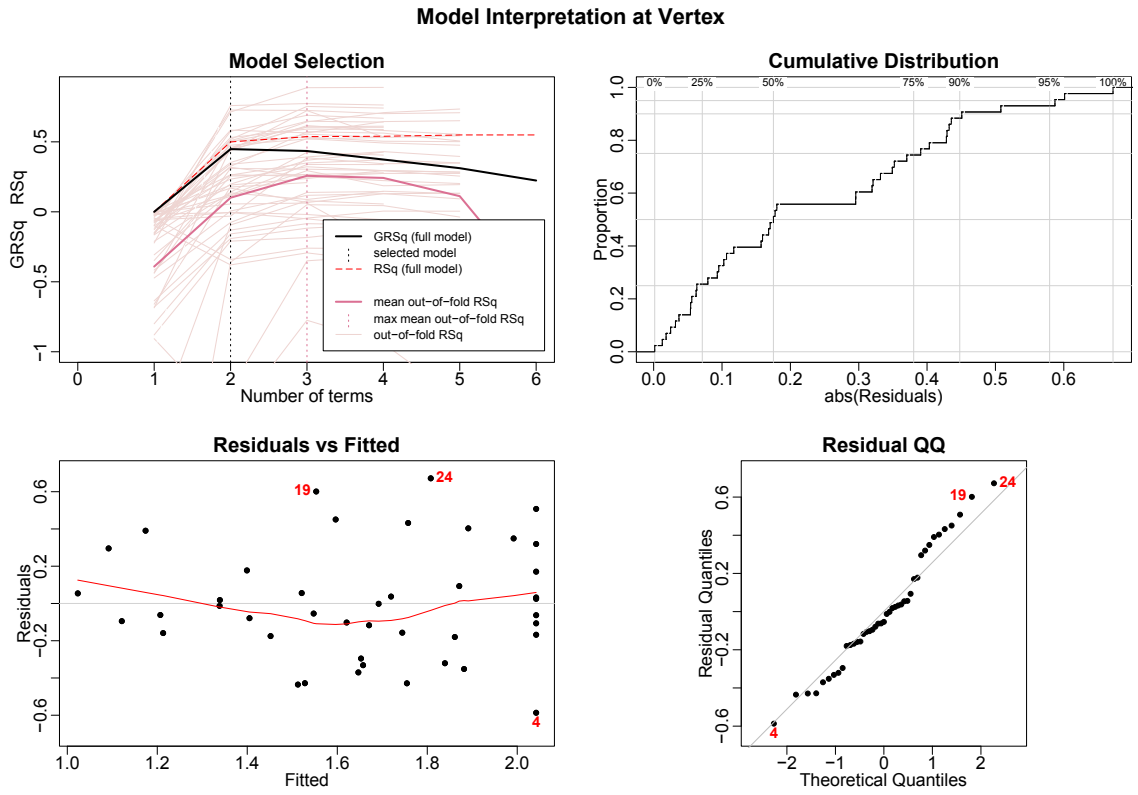

Figure 19 Model interpretation plots for vertex.

The model selection plot explains that the best model used two terms. The term selection line is also the point where the RSq and GRSq lines are the closest in contact; the ideal situation for an Earth model. The residuals vs. fitted plot shows the points are evenly distributed throughout the plot, with some clustering at the far end. The loess line is straight and indicates the model is a good fit for the data. The QQ plot shows that there is slight divergence from normality at the right tail. Points 19, 34, and 4 are the largest residuals. The model interpretation plots indicate that the vertex model is useful for predicting age. Summary statistics for the model are shown below (see Table 6).

Table 6 Summary statistics for the Earth model at vertex

Statistic	Acronym	Value
generalized cross validation	GCV	0.10
residual sum of squares	RSS	3.83
general r squared	GRSq	0.45
r squared	RSq	0.50
cross-validated r squared	CVRSq	0.16
standard deviation	sd	0.58
maximum error	MaxErr	0.84
standard deviation	sd	0.55

This table shows the summary statistics from the Earth model for CVT at vertex.

The RSS value is 3.83, which is high, and indicates that the model is not a good fit for the data. The RSq value is 0.50 and tells us that 50% of age predictions can be explained by CVT using the model. The CVRSq is 0.16, which explains that, using the cross validation data, a smaller percentage, 16%, of age is explained by CVT. The GCV is low, explaining The GRSq value is 0.45, indicating that the model is average at predicting values in a different data set. The 95% PIs for the model are shown below (see Figure 20).

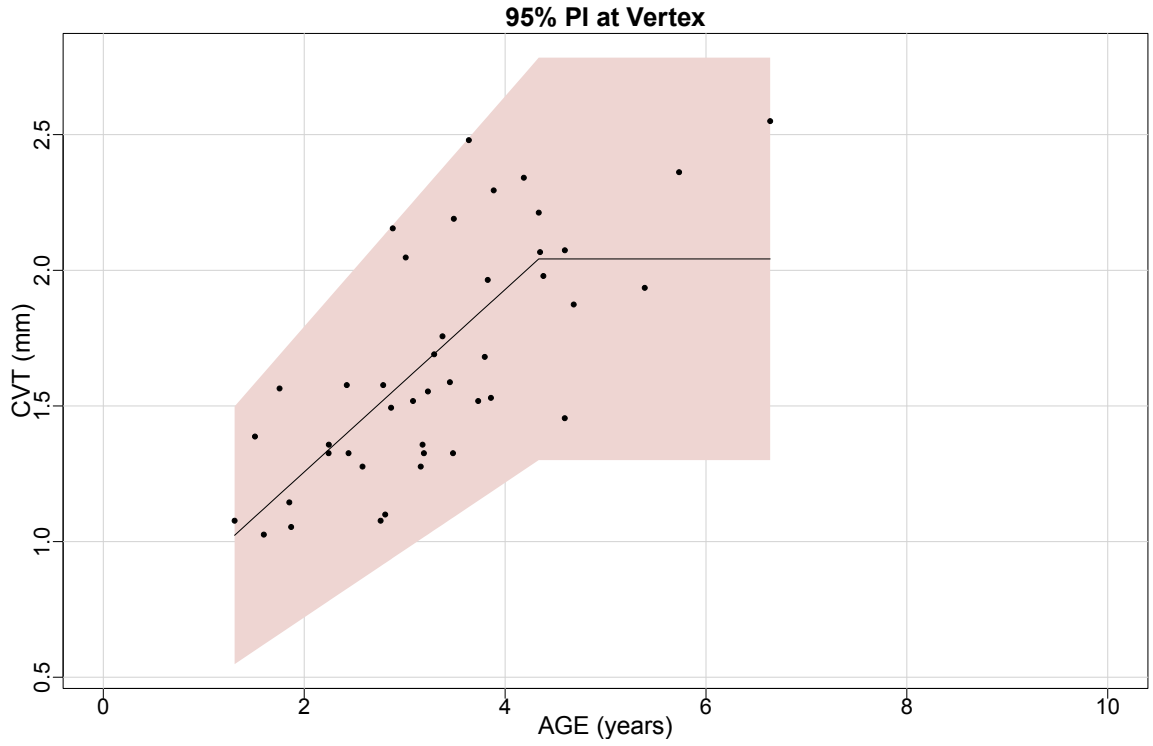

Figure 20 95% prediction intervals at vertex.

This plot illustrates the prediction intervals in light pink; the thickness measurements at each age in the CT sample; and the fit line.

The model created prediction intervals for juveniles aged 1.5 to 7 years of age; outside of that age range, the predicted ages are uncertain. The plot illustrates that CVT at vertex increases from 1.5 until 4 years old, then thickness plateaus. The range of thickness for the vertex landmark is 2 mm. A variance model for vertex was plotted with residual values (see Figure 21).

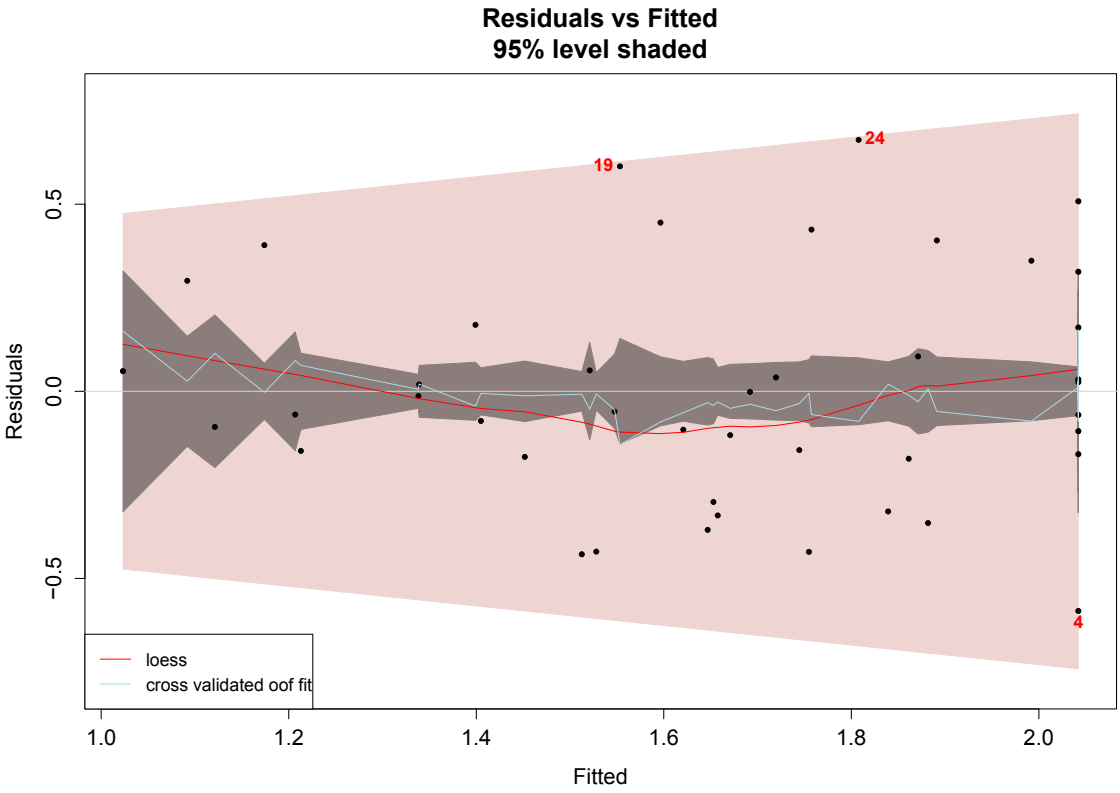

Figure 21 Prediction bands in a residuals plot for vertex.

The dark grey bands show the confidence limits; the wider pink bands show the prediction limits; the red line is a loess fit to the residuals; the blue line is the cross-validation mean fit.

The plot shows that prediction limits are widest at the lower values and indicates model uncertainty at those values, but overall the prediction limits are narrow. The loess line and cross-validation lines correspond fairly well with the grey line, indicating that the model fits the data.

The Vertex Radius

The Earth model at the vertex radius was created using the log of CVT. The model interpretation plots are shown below (see Figure 22).

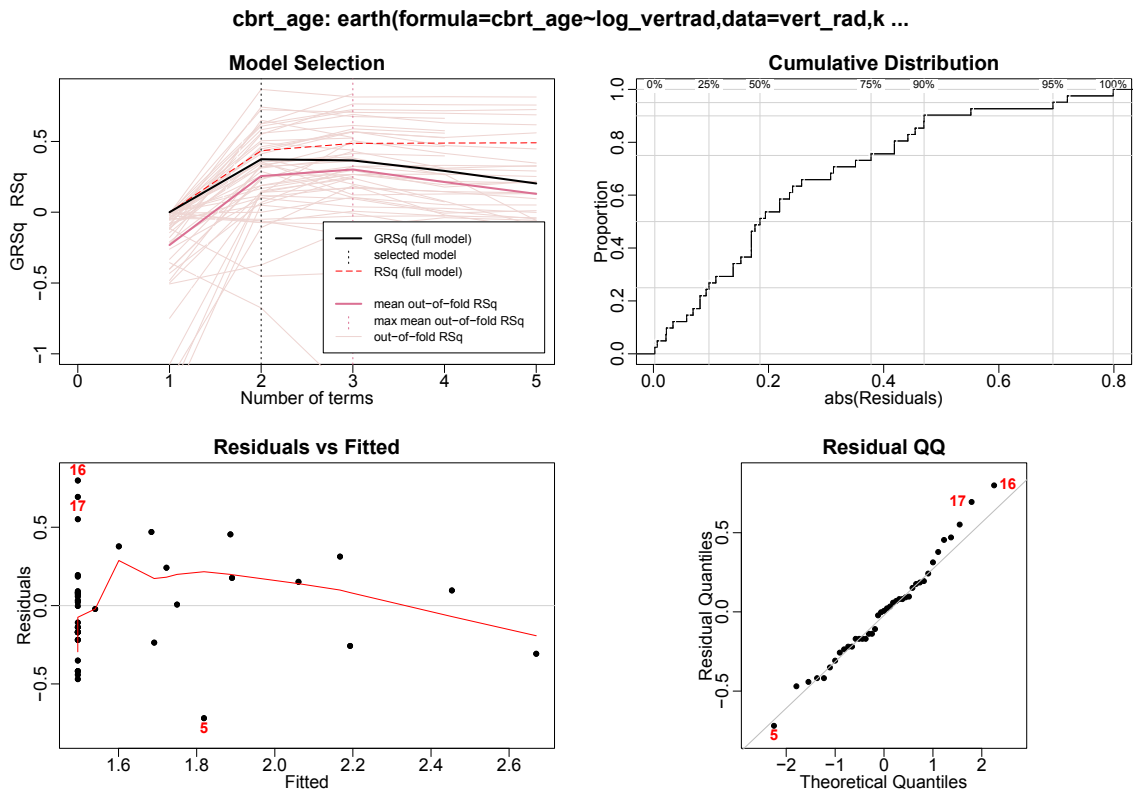

Figure 22 Model interpretation plots for the vertex radius.

The model selection graph explains that the best model used two terms. The residuals vs. fitted graph shows that the points are clustered at the lower end, indicating heteroscedasticity of the residuals. The QQ plot shows that there is slight divergence from normality at the right tail. Points 17, 14, and 5 are the largest residuals. Overall, the model assessment plots do not indicate that vertex is good at predicting ages using CVT. Summary statistics for the model at vertex radius are displayed below (see Table 7).

Table 7 Summary statistics for the Earth model at vertex radius

Statistic	Acronym	Value
generalized cross validation	GCV	0.12
residual sum of squares	RSS	4.20
general r squared	GRSq	0.37
r squared	RSq	0.43
cross-validated r squared	CVRSq	0.24
standard deviation	sd	0.35
maximum error	MaxErr	-1.00
generalized cross validation	sd	0.67

This table shows the summary statistics from the Earth model for CVT at vertex radius.

The RSS value is 4.20, which indicates that the model is not a good fit for the data. The RSq value is 0.43 and tells us that 43% of age can be explained by CVT in the model at vertex radius. The CVRSq is 0.24, indicating a smaller percentage of the cross-validated test data can explain age. The GRSq value is 0.37. This indicates that the model is not very good at predicting values in a different data set. Summary statistics suggest that this model is not useful for predicting age using CVT. The 95% PIs for the model at the vertex radius are shown below (see Figure 23).

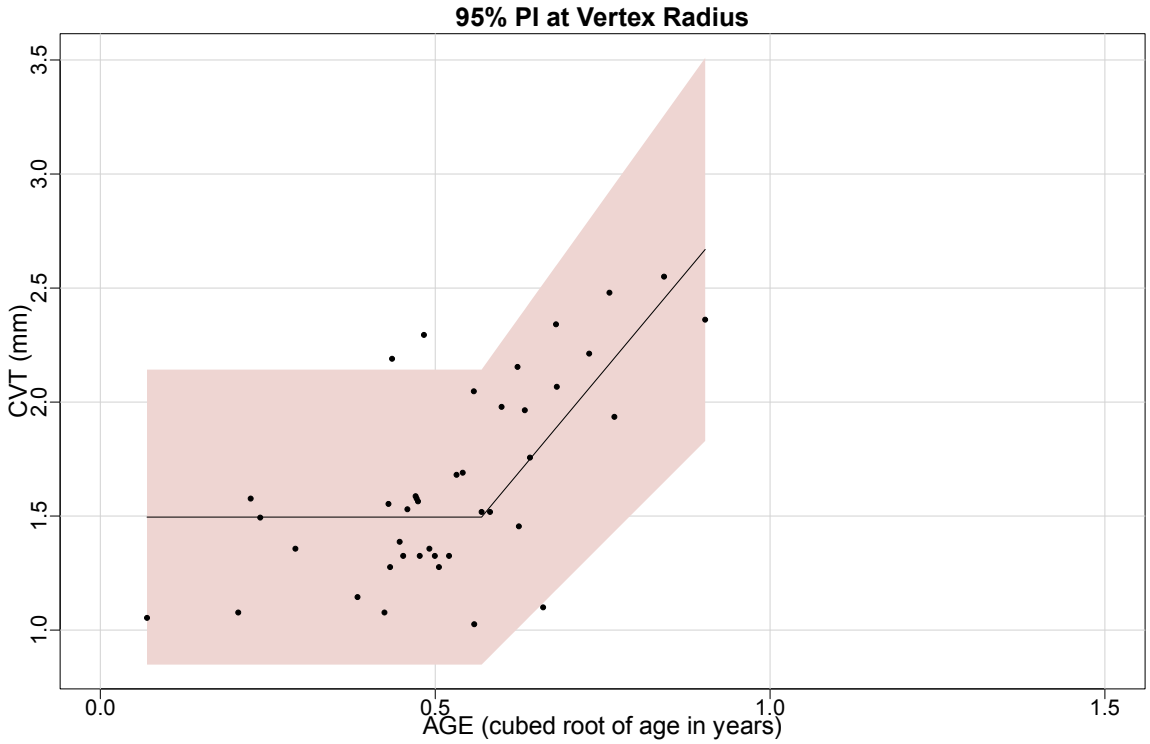

Figure 23 95% prediction intervals at the Vertex Radius

This plot illustrates the prediction intervals in light pink; the thickness measurements at each age in the CT sample; and the fit line

The plot shows that there is a rapid increase in thickness at 0.22 years of age. The model shows that thickness varies by 2.5 mm over less than a year. According to the plot, the model reliably predicts age from 0 to 3.4 years old. A variance model for the vertex radius was plotted with residual values (see Figure 24).

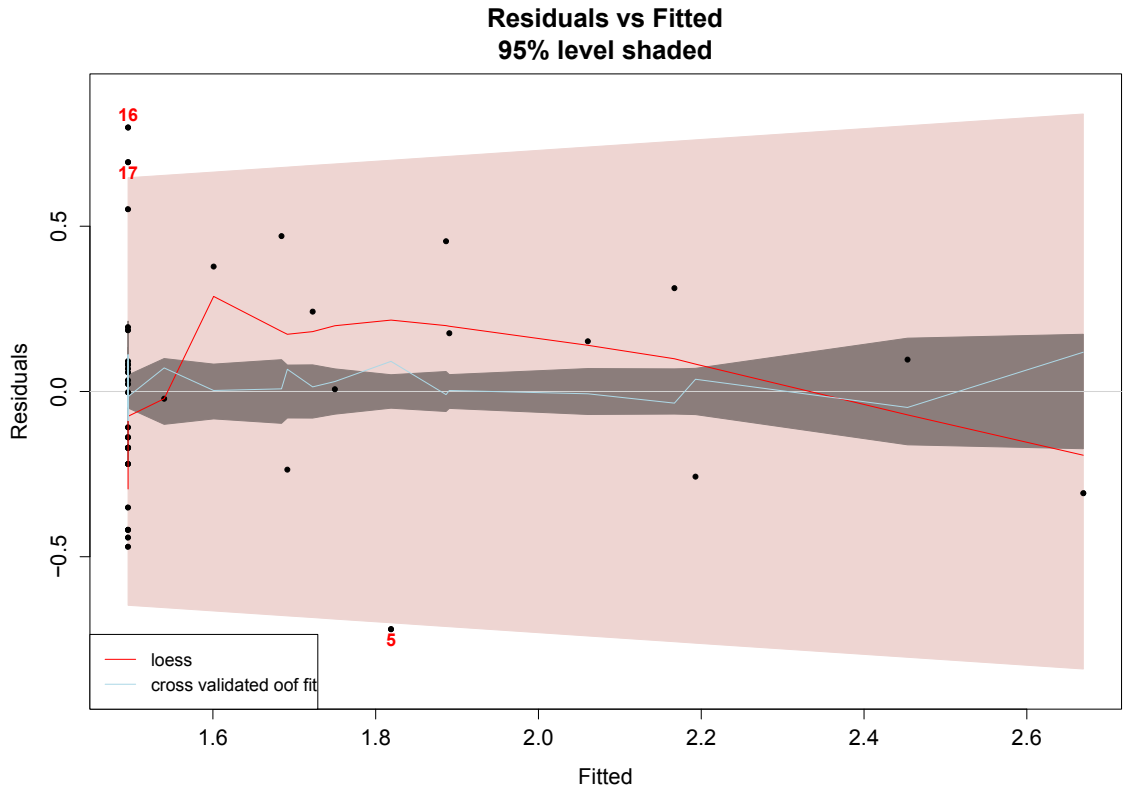

Figure 24 Prediction bands in a residuals plot for the vertex radius.

The dark grey bands show the confidence limits; the wider pink bands show the prediction limits; the red line is a loess fit to the residuals; the blue line is the cross-validation mean fit.

The graph shows that the prediction limit band thickness is narrow across the entire range. The cross validation line corresponds with the grey line better than the loess line. This plot indicates that the model has narrow prediction limits in age estimates and appears to be useful for predicting age.

Lambda

The Earth model for lambda was created assessing CVT measurements. The model interpretation plots are shown in Figure 25.

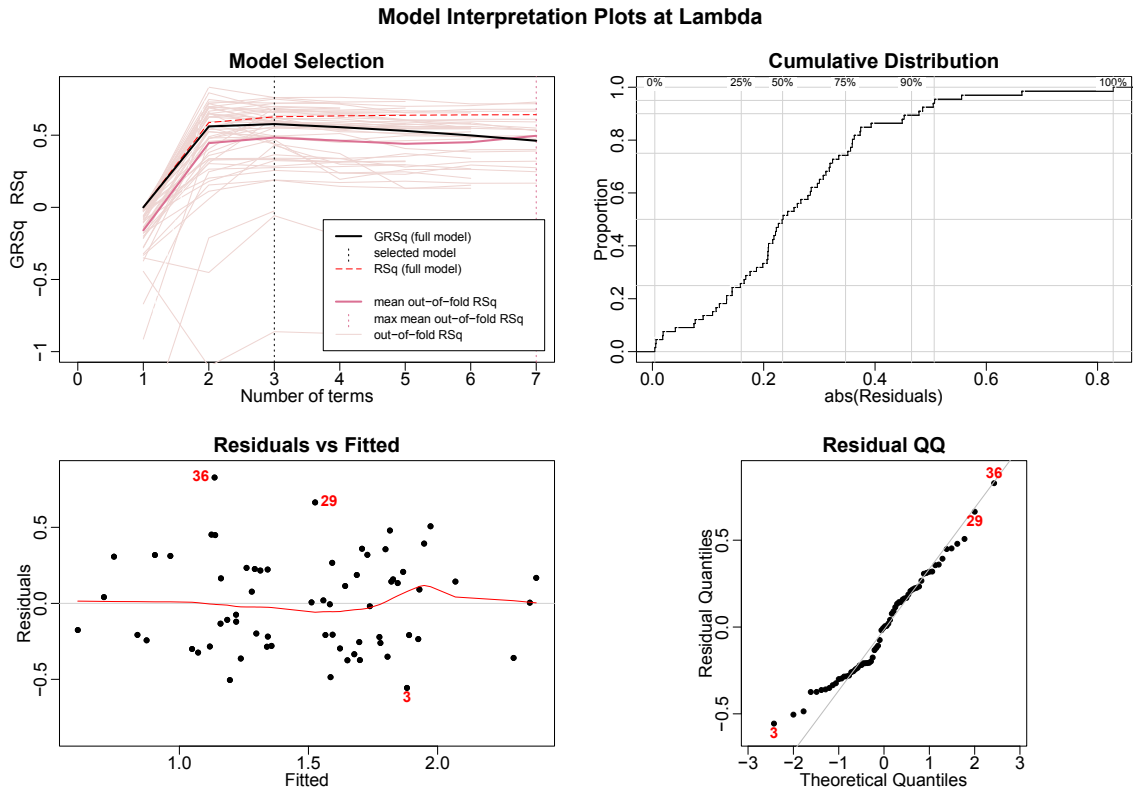

Figure 25 Model interpretation plots for lambda.

The model selection graph shows that the best model used three terms. The residuals vs. fitted plot shows a smooth loess line, indicating the mean residual is constant. The data is evenly distributed throughout the plot indicating the assumptions of homoscedacity and random error have been met. The QQ plot is straight, but indicates that the residuals diverge from normal distribution at the left tail. Points 3, 29, and 36 are the largest residuals. Model interpretation plots indicate that the model is useful for predicting age. The summary statistics for the model at lambda are shown in Table 8.

Table 8 Summary statistics for the Earth model at lambda

Statistic	Acronym	Value
generalized cross validation	GCV	0.11
residual sum of squares	RSS	6.08
general r squared	GRSq	0.58
r squared	RSq	0.63
cross-validated r squared	CVRSq	0.46
standard deviation	sd	0.30
maximum error	MaxErr	0.92
generalized cross validation	sd	0.64

This table shows the summary statistics from the Earth model for CVT at lambda.

The RSS value is 6.08, which indicates that the model is not a tight fit to the data. The RSq value is 0.63, meaning that 63% of the age can be explained by CVT in the model at lambda. The CVRSq is 0.34, which means a lower percentage of cross-validation CVT scores can explain age. The GRSq value is 0.58, indicating that the model is average at predicting values in a different data set. Overall, summary statistics indicate that the model is useful for predicting age using CVT. The 95% PI are plotted below (see Figure 26).

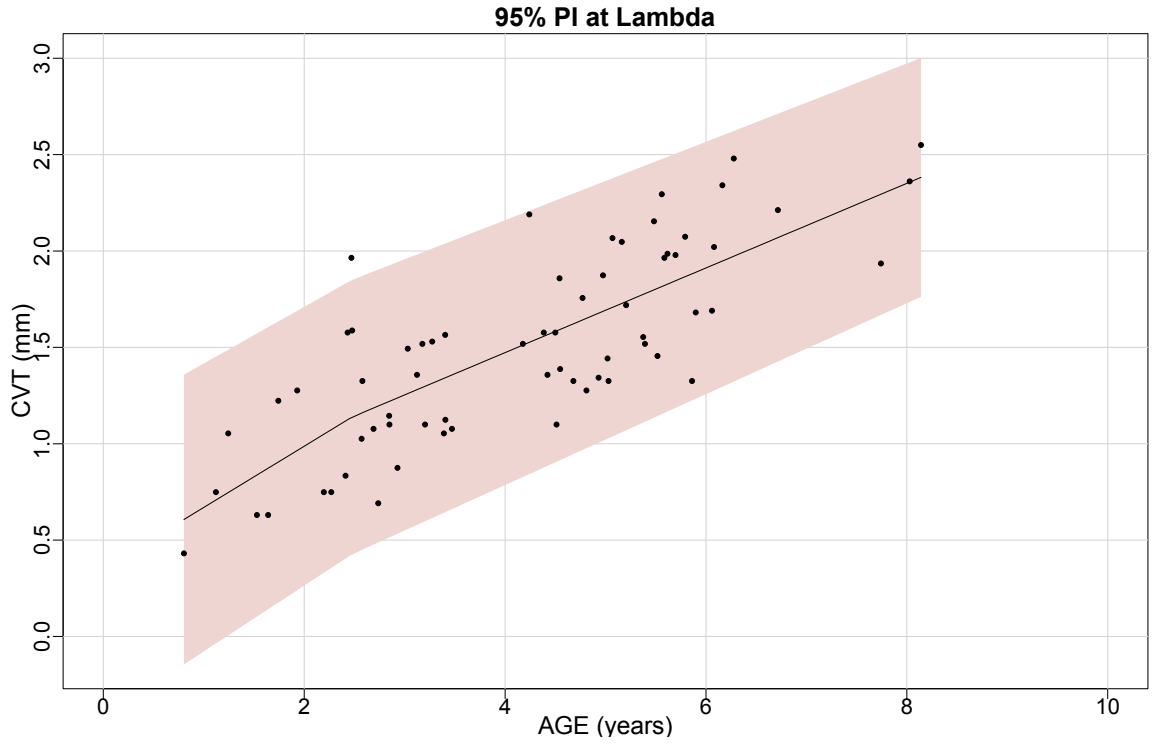

Figure 26 Prediction intervals at lambda

This plot illustrates the prediction intervals in light pink; the thickness measurements at each age in the CT sample; and the fit line.

The PIs for lambda range from 1 to 8 years of age. Outside of this age range, the predicted age is less certain. The plot indicates that CVT increases steadily from 1 to 8 years of age at lambda. There is a greater increase in thickness from 1 to 3 years of age, and then thickness continues to increase steadily until 8 years of age. The model truncates at 8 years of age, indicating that age predictions over this age are less reliable. A variance model for lambda was plotted (see Figure 27).

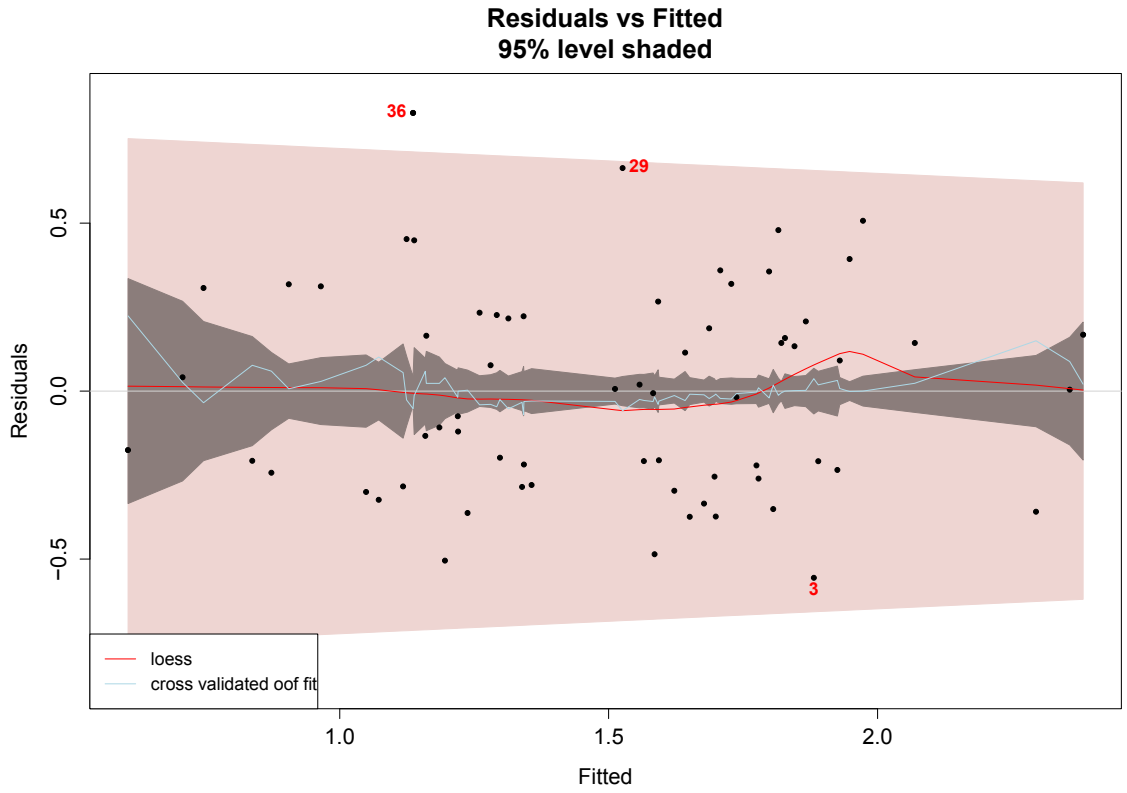

Figure 27 Prediction bands in a residuals plot for lambda.

The dark grey bands show the confidence limits; the wider pink bands show the prediction limits; the red line is a loess fit to the residuals; the blue line is the cross-validation mean fit.

The graph shows that the prediction limit band thickness is fairly thin across the plot, but widens at the ends. This shows that model created appears to be useful for predicting age from CVT at middle values. The loess and cross validation lines somewhat correspond with the grey line. The variance model confirms what is shown with the prediction intervals; the model is best suited for predicting the middle age ranges in the sample, 1 to 8 years old.

Opisthocranion

The Earth model for opisthocranion was created assessing CVT measurements. The model interpretation plots are shown in Figure 28.

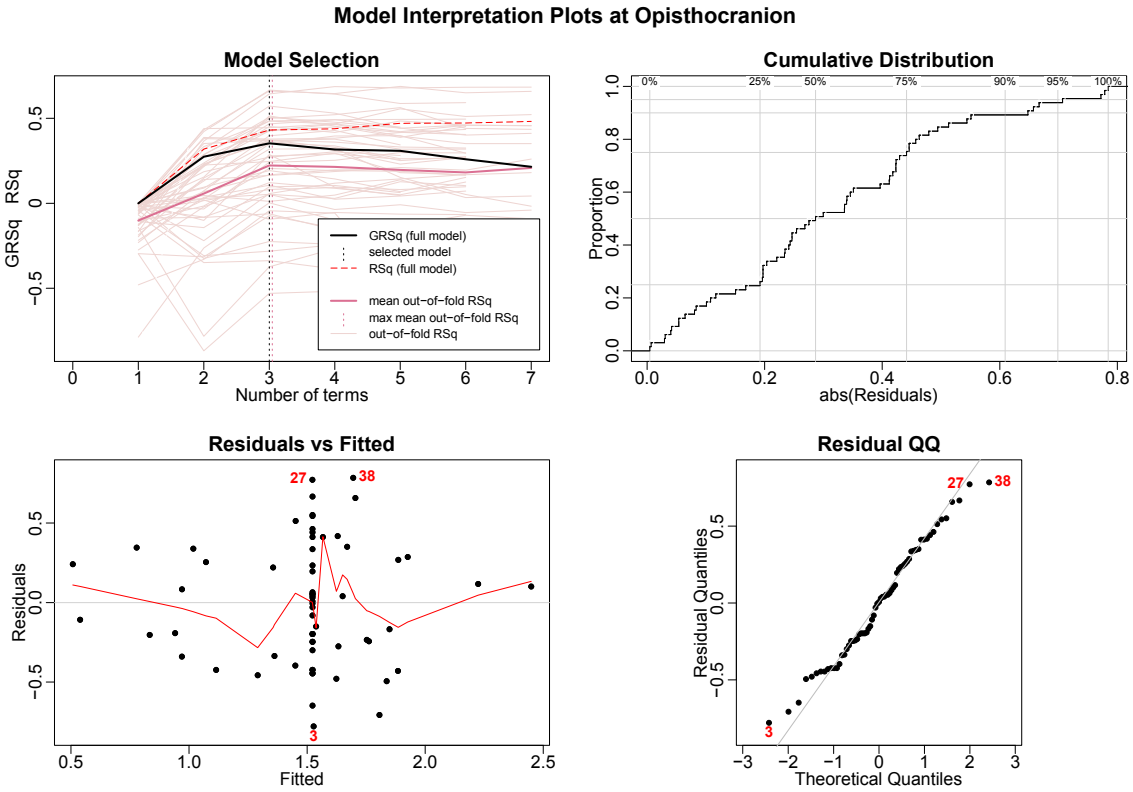

Figure 28 Model interpretation plots for opisthocranion

The model selection plot shows that the best model uses three terms. The residuals vs. fitted plot show that the loess line is not constant at the midrange values of the model. The residuals are clustered near the center of the model indicating heteroscedasticity. The QQ plot indicates the residuals are distributed normally; however there is a slight divergence of normality at the left tail. Cases 3, 27 and 38 are the largest

residuals. Model interpretation plots suggest that the model at opisthocranion is not useful for predicting age. Summary statistics are shown in Table 9.

Table 9 Summary statistics for the Earth model at opisthocranion

Statistic	Acronym	Value
generalized cross validation	GCV	0.17
residual sum of squares	RSS	9.19
general r squared	GRSq	0.35
r squared	RSq	0.43
cross-validated r squared	CVRSq	0.19
standard deviation	sd	0.29
maximum error	MaxErr	1.10
generalized cross validation	sd	0.77

This table shows the summary statistics from the Earth model for CVT at opisthocranion.

The RSS value is 9.19. This high value indicates that the model is not a good fit for the data. The RSq value is 0.43, and shows us that 43% of the age can be explained by CVT using the model. The cross-validation percentage of age explanation using CVT is only 19%, as the CVRSq is 0.19. The GRSq value is 0.35, which indicates that the model is average at predicting values in a different data set. Overall, the summary statistics suggest that the model at opisthocranion is not useful for predicting age. The 95% PI are plotted below (see Figure 29).

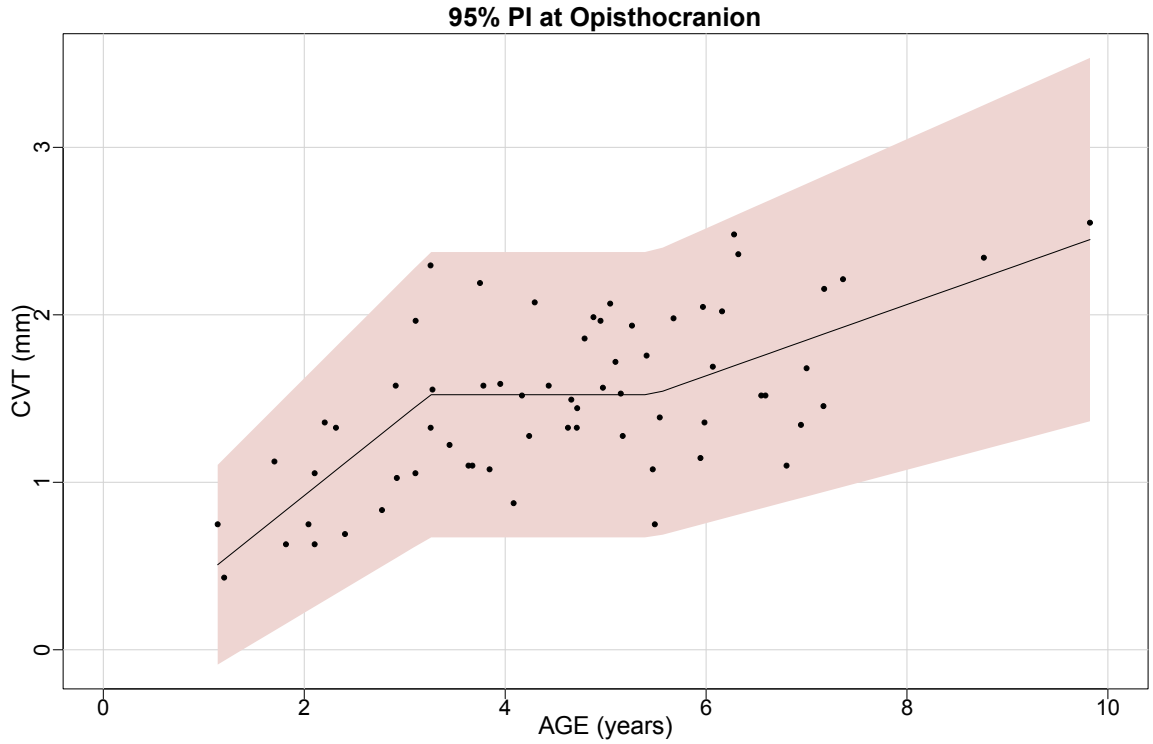

Figure 29 95% prediction intervals at opisthocranion

This plot illustrates the prediction intervals in light pink; the thickness measurements at each age in the CT sample; and the fit line.

The PIs range from 1 to 10 years old at opisthocranion. The PIs indicate that CVT at opisthocranion increases rapidly from 1 to 3 years of age, then CVT plateaus until just before age 6. Thickness increases again until age 10, but at a slower rate. A variance model for opisthocranion was plotted below (see Figure 30).

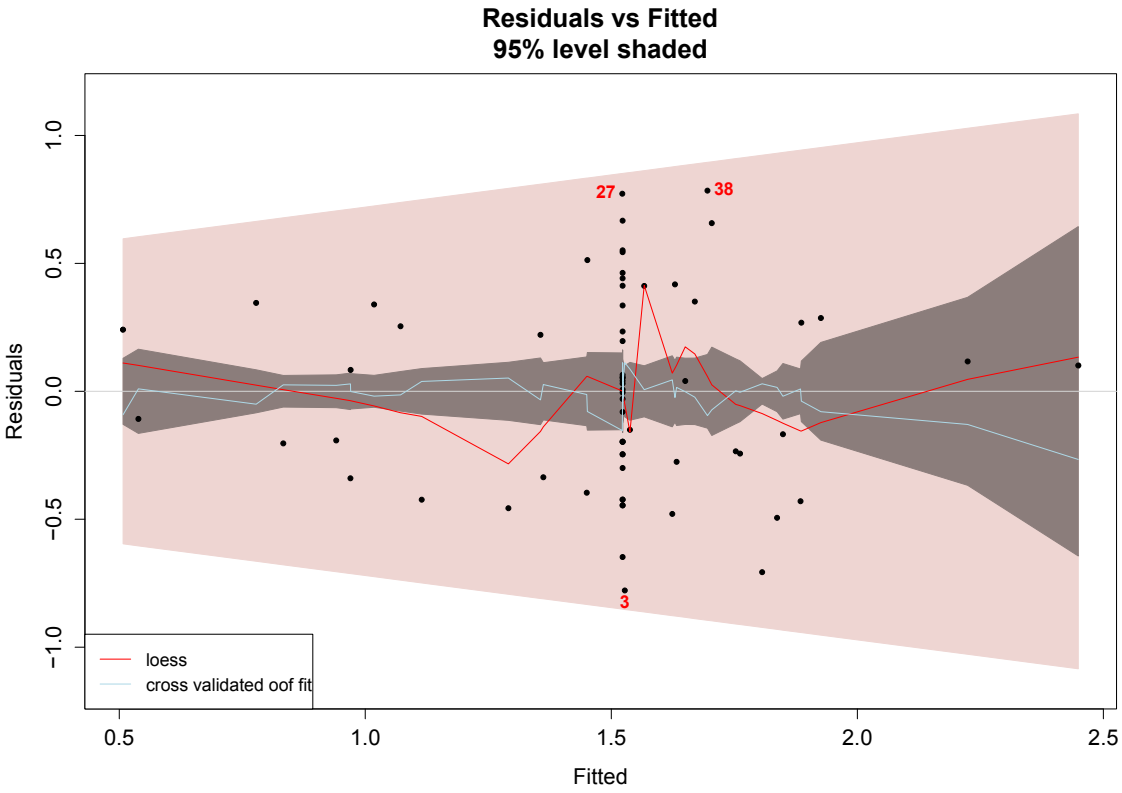

Figure 30 Prediction bands in a residuals plot for opisthocranion.

The dark grey bands show the confidence limits; the wider pink bands show the prediction limits; the red line is a loess fit to the residuals; the blue line is the cross-validation mean fit.

The variance model at opisthocranion shows that confidence limits and prediction limits increase at higher values, suggesting that the model is not a good predictor of age as CVT increases. The loess line indicates the model is unreliable in its predictive ability at midrange values.

Standard Error and Prediction Intervals

The standard error and prediction intervals for the univariate models are listed in Table 10. Standard error was calculated using linear models. Dummy variables were

created to illustrate the PIs response to age. Prediction interval size was calculated from the plots illustrated in Figures 31-37.

Table 10 Standard Error and Prediction Intervals for the univariate models

Landmark	SE	Size of 95% PI
nasion	0.07	1.5 to 17 years
glabella	0.14	80 to ~1500 years
lambda	0.19	4 to 25 years
opisthocranion	0.23	2.5 to 35 years
bregma	0.32	1 to 1.6 years
vertex radius	0.34	9 to 42 years
vertex	0.41	3 to 18 years

The table shows the standard error and size of the 95% prediction interval for each model. The standard error was calculated from a linear regression model using the Earth package because this statistic was not provided in the loess Earth models.

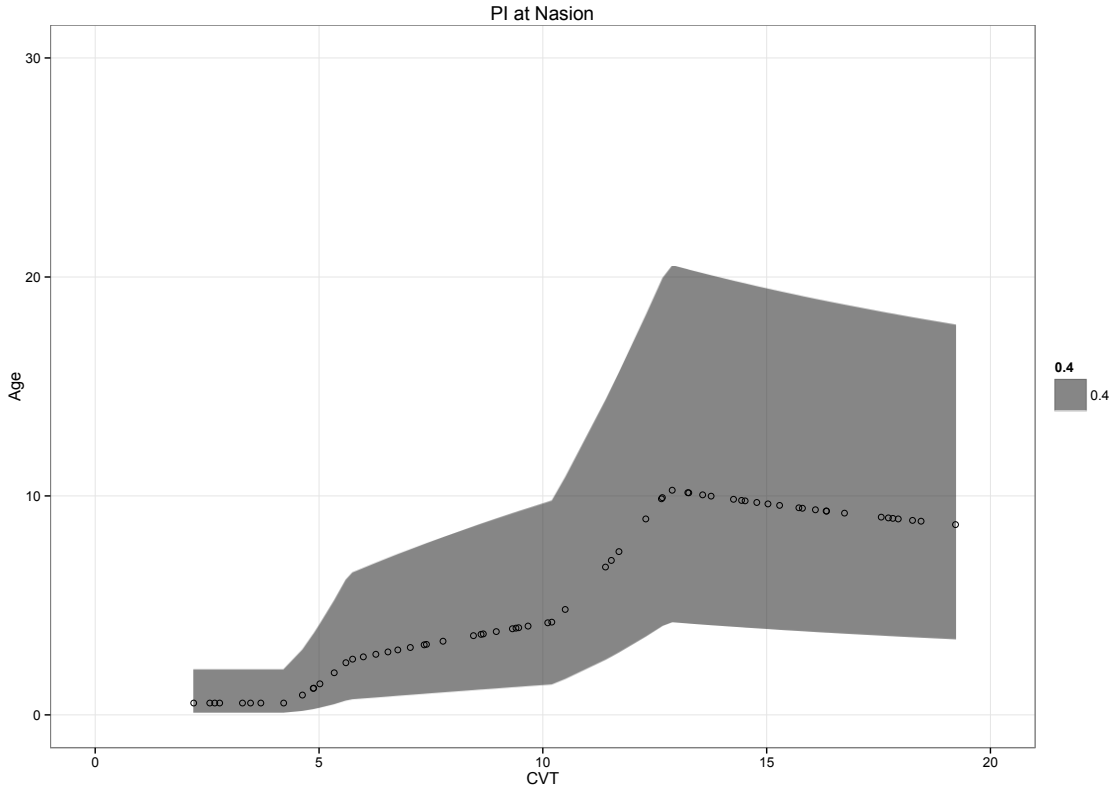

Figure 31 95% prediction intervals when age is regressed on CVT for Nasion. CVT thickness is expressed in millimeters and age in years.

The plot at nasion shows a narrow prediction interval at the low CVT measurements. The PI increases with increasing thickness, with widest increase occurring just after 10 mm.

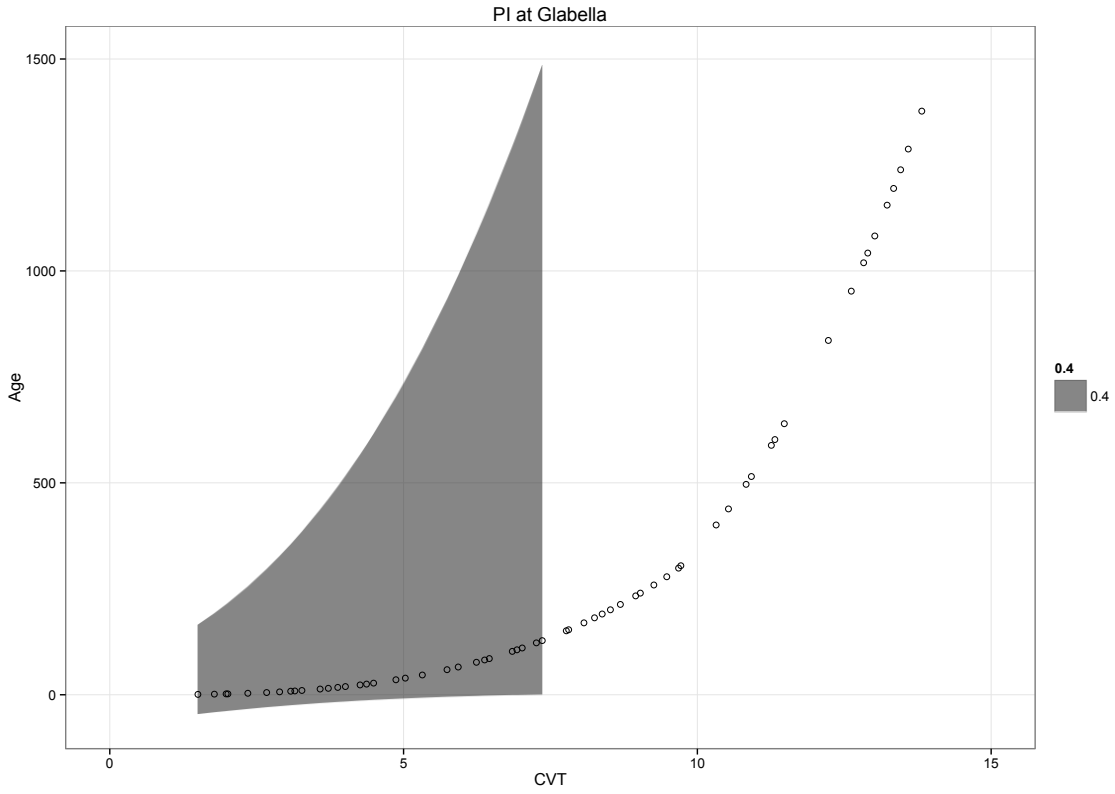

Figure 32 95% prediction intervals when age is regressed on CVT for Glabella. CVT thickness is expressed in millimeters and age in years. Black circles represent dummy measurements.

The PI plot for glabella truncates at 7 mm in thickness. Age estimates in the PIs increase exponentially, up to about 1500 years old, which are unrealistic.

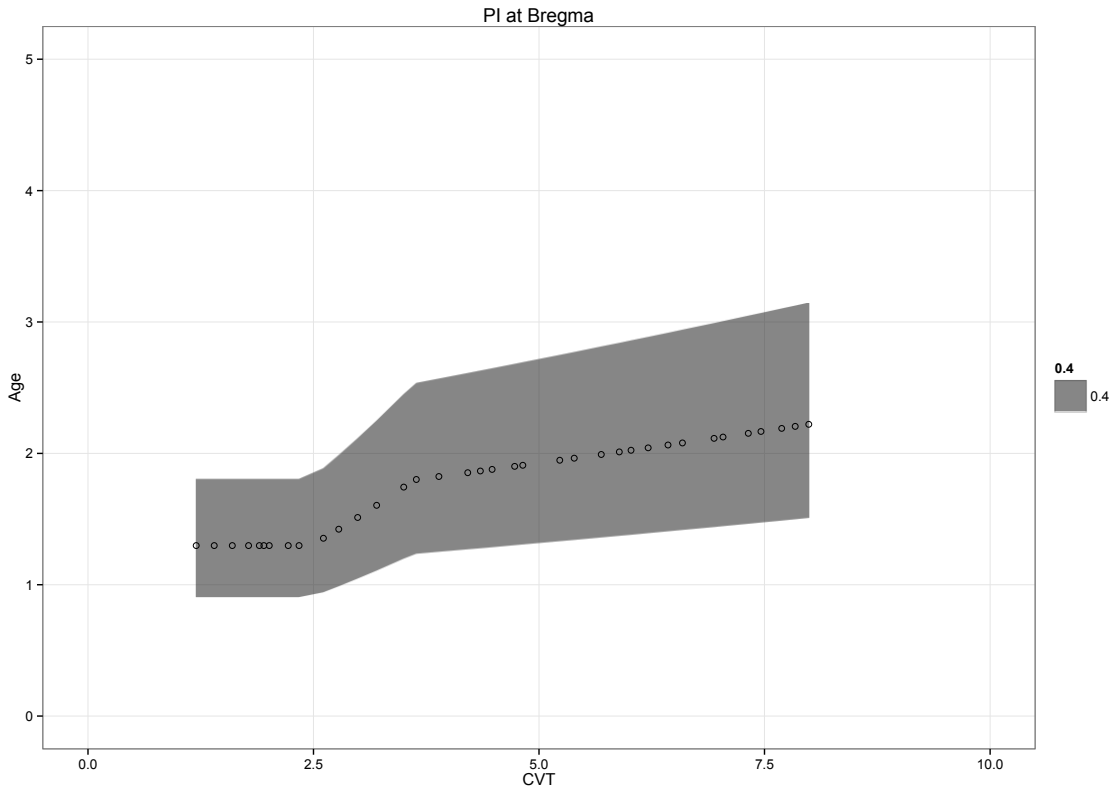

Figure 33 95% prediction intervals when age is regressed on CVT for Bregma. CVT thickness is expressed in millimeters and age in years. Black circles represent dummy measurements.

The plot for bregma shows that the PIs increase slightly when CVT increases. The PIs are narrow, starting at a width of 1 year and increasing to slightly over 2 years. Even though CVT varies in thickness, the predicted ages only fall within a 3-year window.

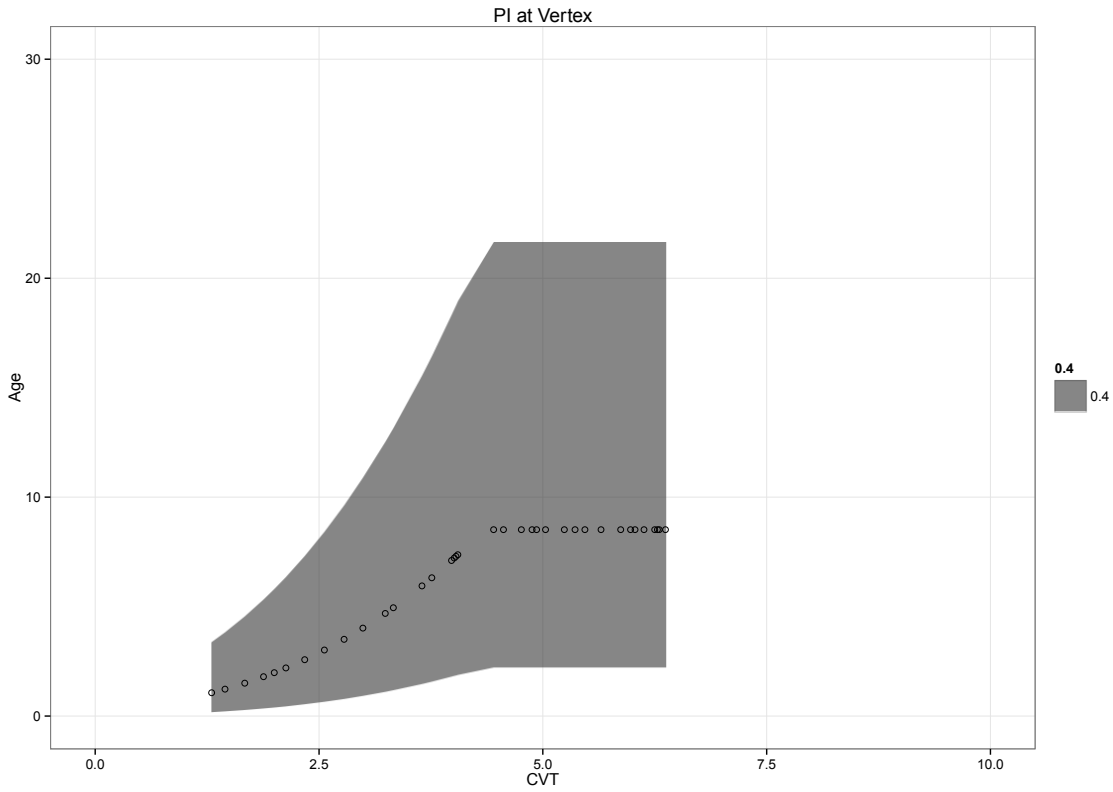

Figure 34 95% prediction intervals when age is regressed on CVT for Vertex.

CVT thickness is expressed in millimeters and age in years. Black circles represent dummy measurements.

The plot shows that PIs are narrow at smaller CVT measurements ranging to about 3 years. As CVT increases, so do the PIs.

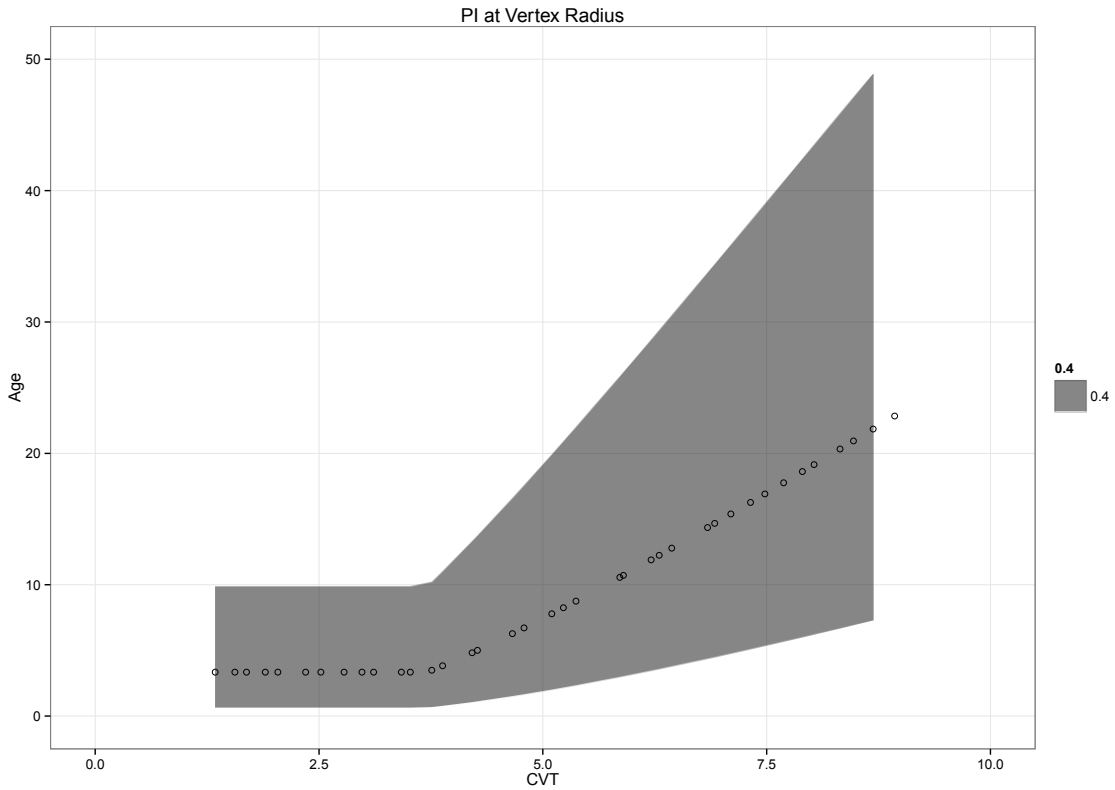

Figure 35 95% prediction intervals when age is regressed on CVT for the Vertex Radius.

CVT thickness is expressed in millimeters and age in years. Black circles represent dummy measurements.

This plot shows that the PIs are more narrow and smaller CVT measures and increase as thickness increases. The smallest predicted range is about 10 years, which is still very wide.

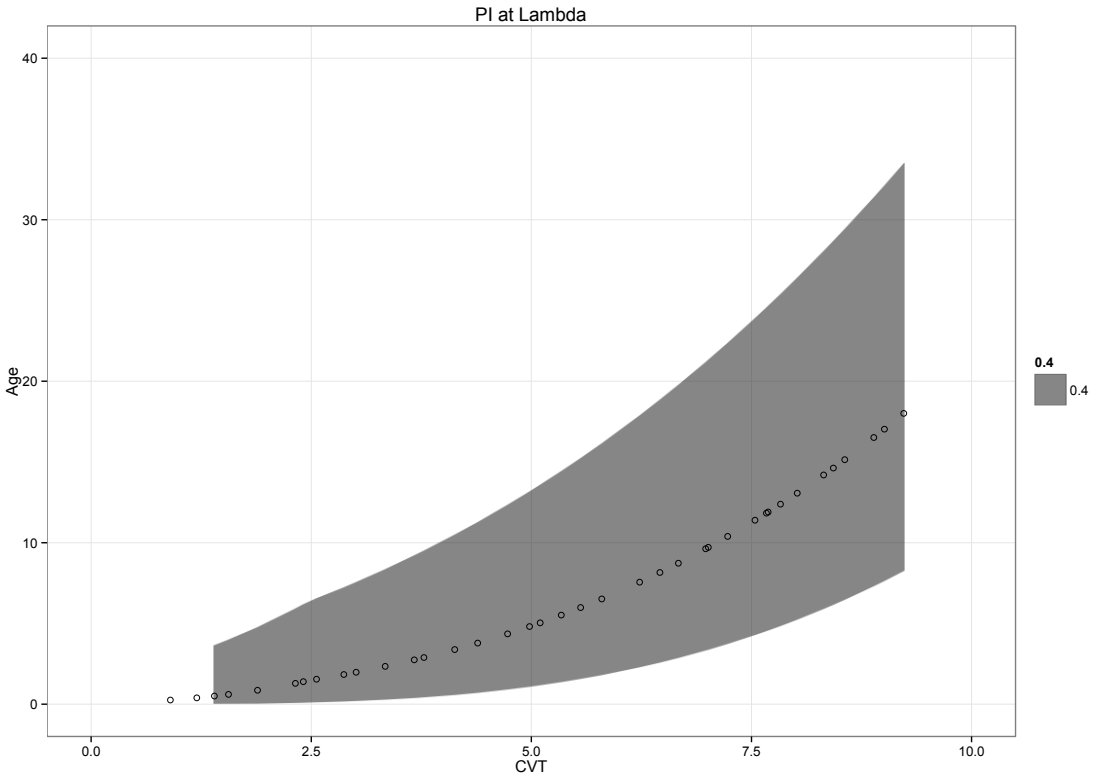

Figure 36 95% prediction intervals when age is regressed on CVT for Lambda.

CVT thickness is expressed in millimeters and age in years. Black circles represent dummy measurements.

This plot shows narrow PI intervals at smaller CVT measurements that increase with increasing thickness. The smallest predicted range is less than 5 years old, while the widest PI is about 25 years old.

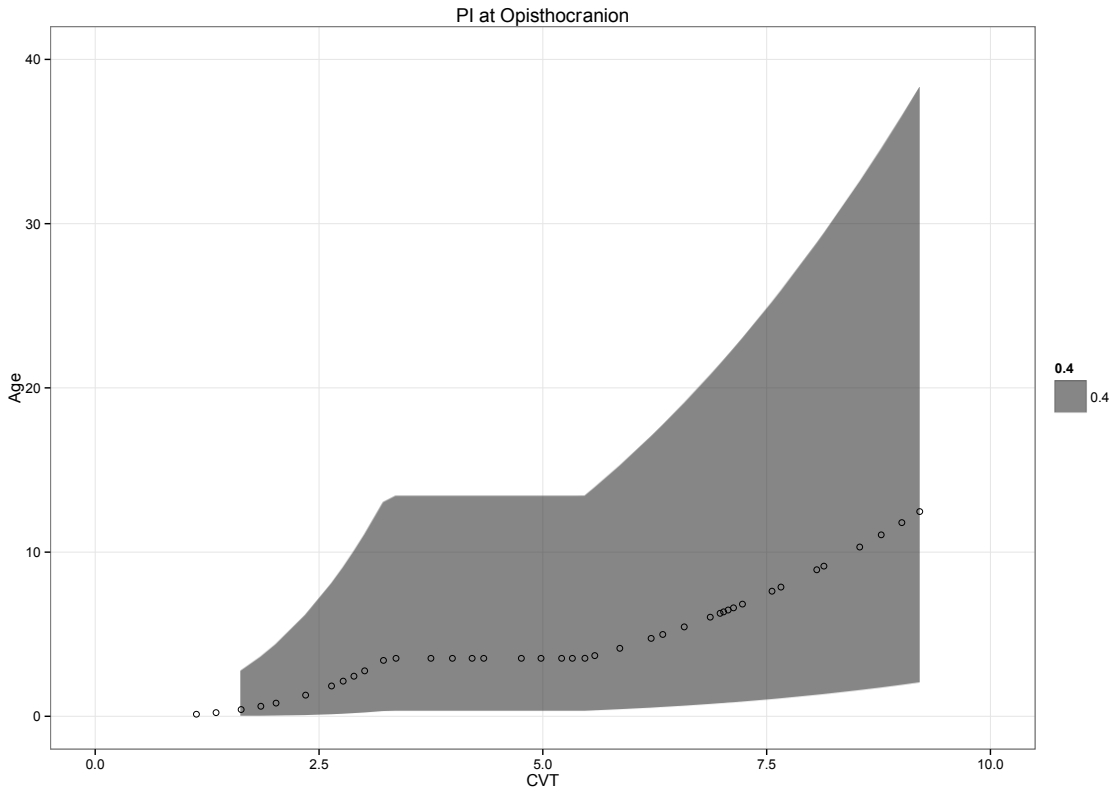

Figure 37 95% prediction intervals when age is regressed on CVT for Opisthocranion. CVT thickness is expressed in millimeters and age in years. Black circles represent dummy measurements.

The PIs at lower ages are narrower, starting at a width of 2.5 years. They increase in size after measurements of 6 mm. Larger CVT measurements have larger PI ranges; at their greatest range they are almost 35 years. This is consistent with results from the model assessment plots indicating greater uncertainty with increasing age.

All models show that as CVT increased, the PIs adjusted for age, usually becoming larger. For all models, except bregma, the high end of the PIs extended past 18 years of age into adulthood. The best model was for lambda, which had PIs that started at 4 years and ranged to 25 years at its greatest dimension. The worst model was for glabella. The low end of the PI started at almost 100 years old and the upper end

extended over 1000 years of difference. The PI plot illustrates that glabella is inaccurate and unrealistic at predicting age using CVT. Even though bregma has a small PI range, the model above shows us that measurements vary by less than 1 mm.

MARS multivariate model results

All seven cranial landmarks

Individual CT scans that had measurements available for all seven points were used to create a multivariate model. The model interpretation plots are shown in Figure 38.

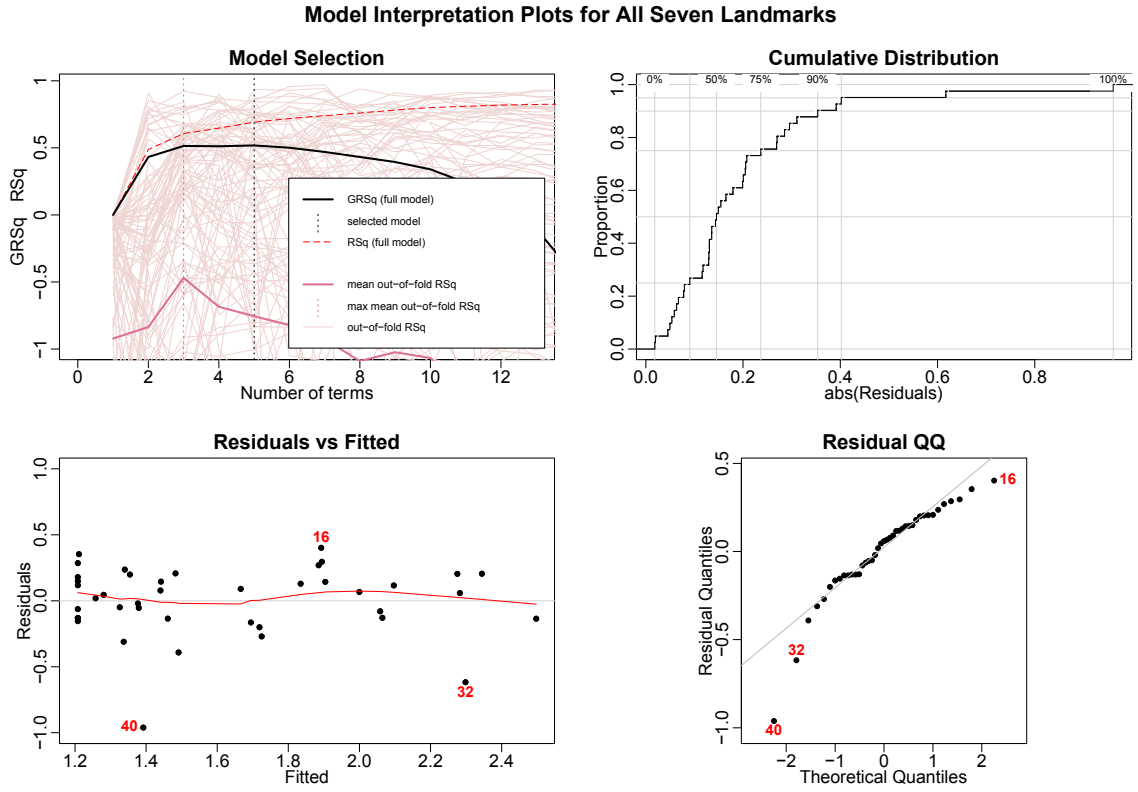

Figure 38 Model interpretation plots for entire suite of seven cranial landmarks

The model selection plot explains that five terms were used to create the best model. The residuals vs. fitted plot shows that the data is evenly spread over the plot, but slightly clustered at the lower values. The loess line follows the centerline. The QQ plot shows the largest residuals were 16, 32, and 40. Overall, the model appears to be useful for predicting age. Summary statistics for the seven point multivariate model are shown in Table 11.

Table 11 Summary statistics for the Earth model at all seven landmarks

Statistic	Acronym	Value
generalized cross validation	GCV	0.11
residual sum of squares	RSS	2.74
general r squared	GRSq	0.52
r squared	RSq	0.69
cross-validated r squared	CVRSq	-0.86
standard deviation	sd	4.30
maximum error	MaxErr	-1.50
generalized cross validation	sd	0.76

This table shows the summary statistics from the multivariate Earth model for CVT at the seven cranial landmarks.

The RSS value is 2.74. This value indicates that the model is not a good fit for the data. The RSq value is 0.69, which means that 69% of age can be explained using the CVT model for all landmarks. The CVRSq is -0.86, which indicates that the model is worse than using a mean. The GRSq value is 0.52, which is midway between 0 and 1. This indicates that the model is not useful for predicting values in a different data set.

Variable importance of cranial landmarks

Variable importance was estimated among the seven points in the model using the evimp() function in the Earth package (see Table 12).

Table 12 Multivariate model using suite of seven cranial landmarks

Variable importance of cranial landmarks in the multivariate model			
	# of subsets	GVC	RSS
log nasion	4	100.0	100.0
log vertex radius	3	40.7	54.3
vertex	1	11.2	25.4
opistho-unused	0	0	0
lambda-unused	0	0	0
bregma-unused	0	0	0
sqrt glabella-unused	0	0	0

The evimp() function produces information on the number of subsets (abbreviated # of subsets) of terms generated by the pruning pass until the best subset is selected; the RSS and GVC are scaled by a decrease, which are listed in the RSS and GVC columns.

The seven point model used three cranial landmarks: nasion, vertex, and the vertex radius. Of those points, nasion was the most important, used in 4 subsets and produced the highest net decrease in the RSS and GCV values. Opisthocranion, lambda, bregma and glabella were not used to create the model.

A second multivariate model was created using the highest ranked landmarks from the previous model; nasion, vertex radius, and vertex. The highest ranked multivariate model interpretation plots are shown in Figure 39.

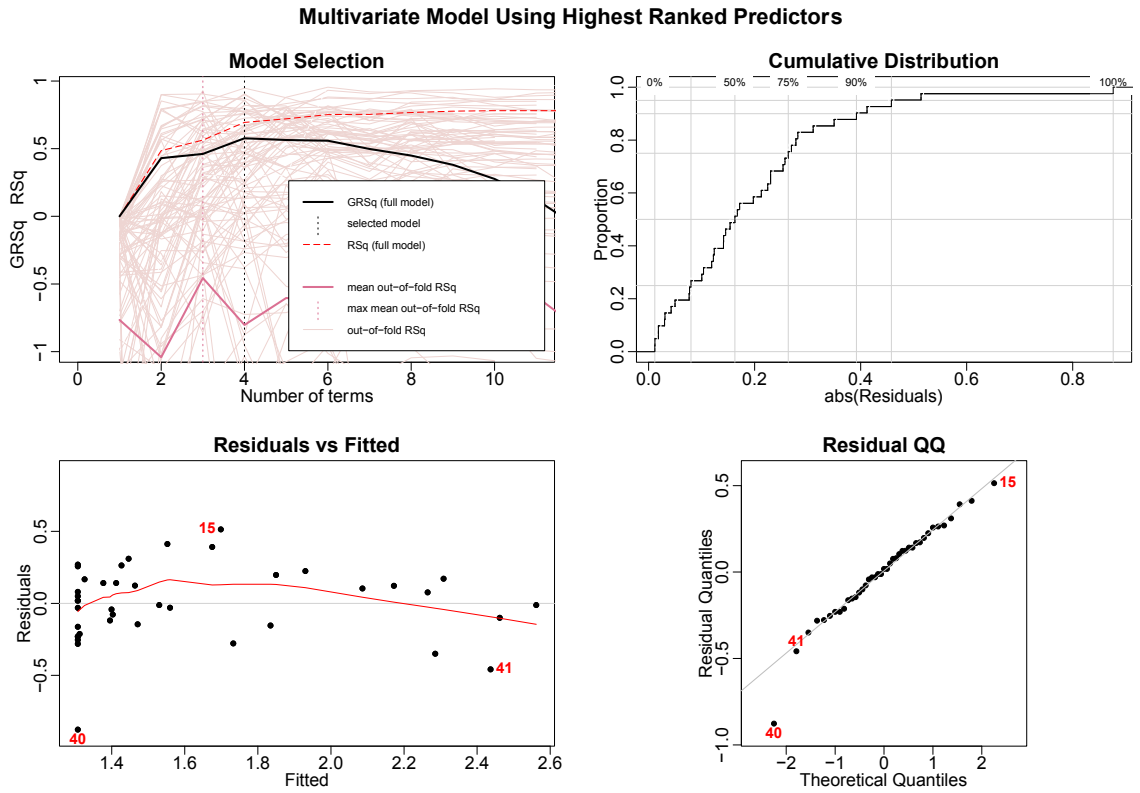

Figure 39 Model interpretations plots for best variables set (nasion, vertex, and vertex radius)

The model selection plot shows that four terms were used in selecting the best model. The residuals vs. fitted plot shows that points cluster toward the lower values, and the loess line is relatively straight. The QQ plot indicates a good fit with one large residual; number 40. Summary statistics are shown in Table 13.

Table 13 Summary statistics for the multivariate model of nasion, vertex and the vertex radius.

Statistic	Acronym	Value
generalized cross validation	GCV	0.09
residual sum of squares	RSS	2.71
general r squared	GRSq	0.58
r squared	RSq	0.69
cross-validated r squared	CVRSq	-0.73
standard deviation	sd	3.30
maximum error	MaxErr	-1.50
generalized cross validation	sd	0.68

This table shows the summary statistics from the multivariate Earth model for CVT at the three highest ranked cranial landmarks.

The RSS value is 2.71, and indicates that the model is not a good fit for the data. The RSq value is 0.69, which means 69% of age can be explained by CVT for this model. The CVRSq is -0.73, indicating the model is worse than explaining age using CVT than simply using the mean. The GRSq value is 0.58, which indicates that the model is moderate at predicting values in a different data set. Summary statistics suggest that the model is useful for predicting age. A variance model with prediction bands is shown in Figure 40.

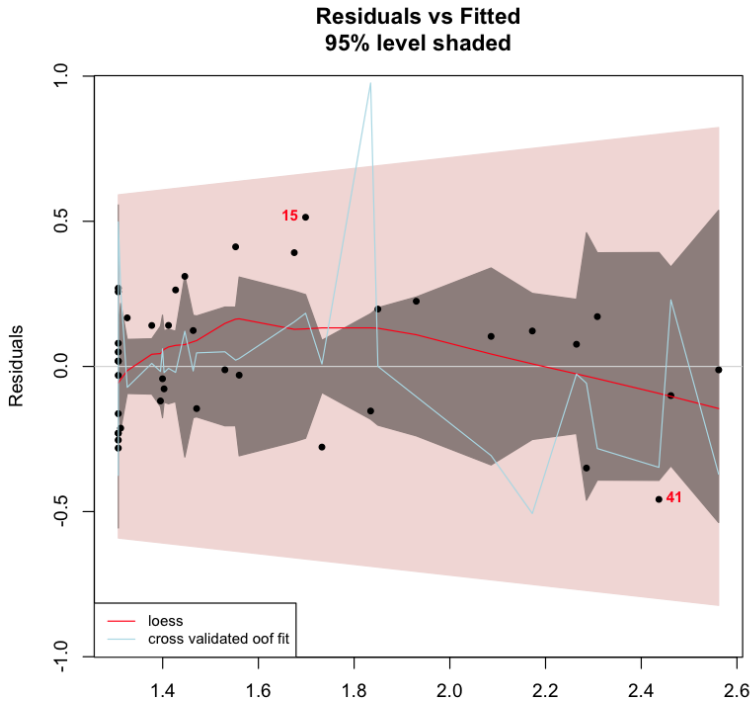

Figure 40 Prediction bands in a residuals plot.

The dark grey bands show the confidence limits; the wider pink bands show the prediction limits; the red line is a loess fit to the residuals; the blue line is the cross-validation mean fit.

The CIs are wide for the entire model. The loess line indicates a fit to the data, but the cross-validated mean fit line is very irregular. This plot indicates that the values predicted by the model are more uncertain. This model does not appear to accurately predict age using CVT.

The vault set of cranial landmarks

A third multivariate model was created for a vault set of landmarks; glabella, bregma, lambda and vertex. The plots for the Earth model are shown below (see Figure 41).

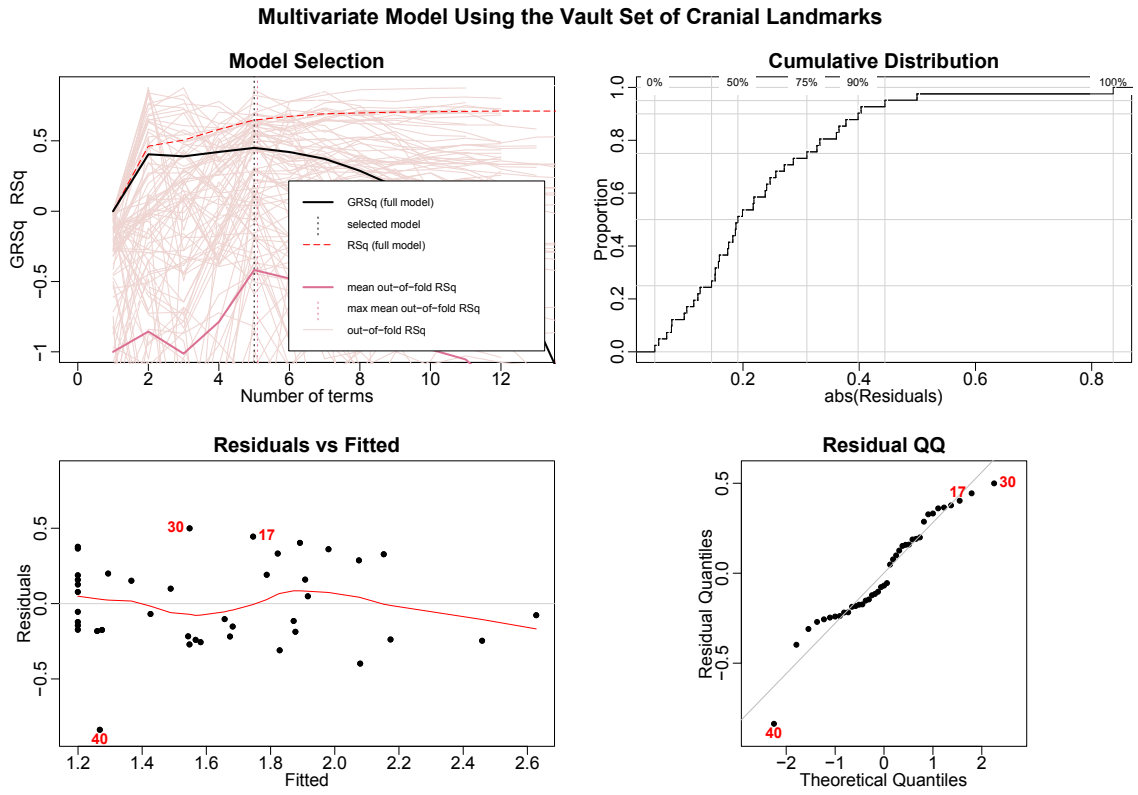

Figure 41 Model interpretation plots for the vault set (glabella, bregma, vertex and lambda)

The model selection plot shows that five terms were used in selecting the best model. The residuals vs. fitted plot shows that points cluster toward the lower and middle values, and the loess line is fairly straight. The QQ plot indicates a slight deviation from normal at the upper and lower tails. Points 17, 30, and 40 are the largest residuals. The model interpretation plots suggest that the vault set is not useful for predicting age. Summary statistics for the model are shown in Table 14.

Table 14 Summary statistics for the vault set model.

Statistic	Acronym	Value
generalized cross validation	GCV	0.13
residual sum of squares	RSS	3.12
general r squared	GRSq	0.45
r squared	RSq	0.65
cross-validated r squared	CVRSq	-1.00
standard deviation	sd	4.10
maximum error	MaxErr	-1.50
generalized cross validation	sd	0.73

This table shows the summary statistics from the multivariate Earth model for CVT at the three best cranial landmarks.

The RSS value is 3.12, which indicates that the model is not a good fit for the data. The RSq value is 0.65, meaning that 65% of age can be explained by CVT using the model. The CVRSq is -1.00 and much lower than the model's RSq value. This indicates that the model is worse at predicting age than just using the mean alone. The GRSq value is 0.45, and indicates that the model is average at predicting values in a different data set. Summary statistics suggest that the model is not useful for predicting age. The residual model with prediction bands is plotted in Figure 42.

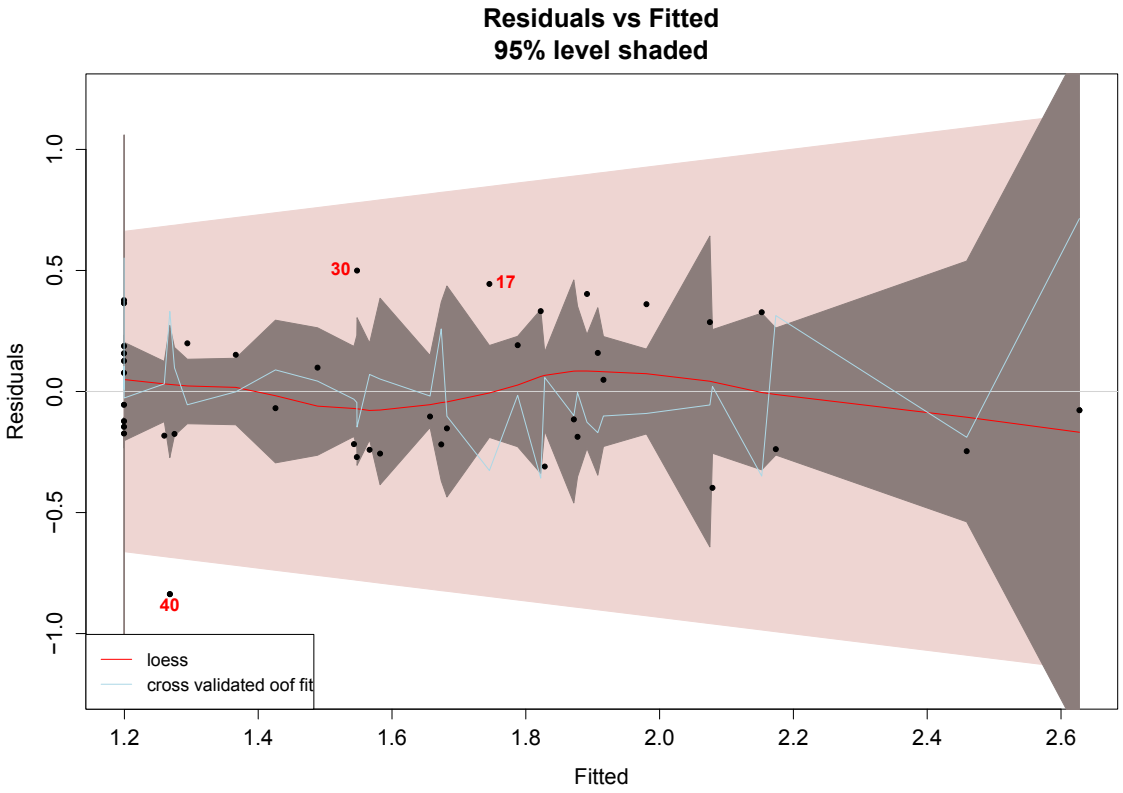

Figure 42 Prediction bands in a residuals plot.

The dark grey bands show the confidence limits; the wider pink bands show the prediction limits; the red line is a loess fit to the residuals; the blue line is the cross-validation mean fit.

The plot shows that the confidence limits increase as age increases. The prediction limits are irregular and large at high values, indicating the model is more uncertain in predicting older ages. The loess line follows the center, however the cross validation line is very irregular. Overall, the model does not appear to be very useful in predicting age from CVT.

Radiograph Test Results

The CVT models were used to estimate age in radiographic test data. Since measurements are required for this method of age estimation, the author evaluated only

images with a scale (n=2). In both test images, vertex and vertex radius were unavailable. A measurement for bregma was unavailable on image 114-00030-01-007-011 because the cranial sutures were not yet closed. Table 15 shows the lower, upper and fit ages at the 95% and 85% CI for each univariate model. Table 16 shows the fit predicted ages and the known chronological ages for two test cases.

Table 15 Prediction intervals at the 95% and 85% PI.

ID	Landmarks	PI Level	lower	fit	upper
118-00080-01-012-012	nasion	95%	0.94	3.27	7.88
		85%	1.38	3.27	6.39
114-00030-01-007-011	nasion	95%	0.05	0.54	2.03
		85%	0.11	0.54	1.50
118-00080-01-012-012	glabella	95%	0.23	3.30	12.15
		85%	0.71	3.30	9.04
114-00030-01-007-011	glabella	95%	0.01	1.46	9.55
		85%	0.07	1.46	6.43
118-00080-01-012-012	bregma	95%	0.90	1.30	1.80
		85%	0.99	1.30	1.65
118-00080-01-012-012	lambda	95%	0.80	4.13	11.89
		85%	1.36	4.13	9.29
114-00030-01-007-011	lambda	95%	0.00	0.41	3.26
		85%	0.01	0.41	2.13
118-00080-01-012-012	opisthocranion	95%	0.30	3.53	13.39
		85%	0.72	3.53	9.92
114-00030-01-007-011	opisthocranion	95%	0.00	0.57	3.43
		85%	0.04	0.57	2.34

Numerical values represent age in years.

Table 16 Predicted CVT age (fit values) and know ages on radiographs at cranial landmarks.

ID	nasion	glabella	bregma	lambda	opistho	known
118-00080-01-012-012	3.27	3.30	1.30	3.53	0.88	1.37
114-00030-01-007-011	0.54	1.46	NA	0.41	0.57	0.18

Numerical values represent age in years. When no measurement was available, NA was used.

The sample size was too small to use correlation tests; therefore, graphical representations of the prediction intervals for each landmark are shown in Figures 43 and 44.

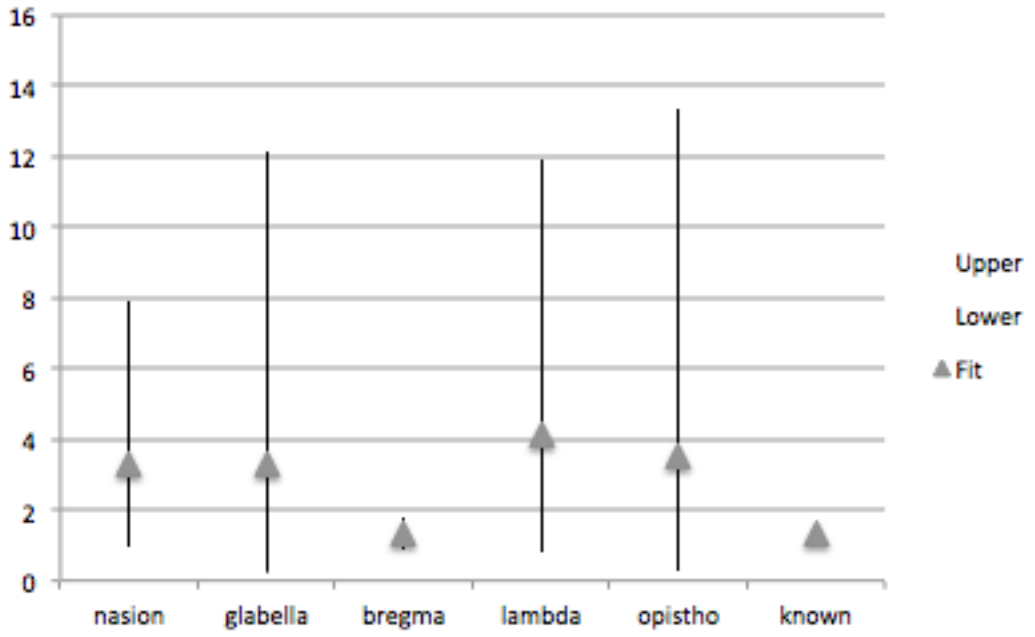

Figure 43 95% Prediction intervals for 118-00080-01-012-012.

The y-axis represents age in years and the x-axis represents cranial landmarks used and known age.

The fit ages produced using CVT for the test case 118-00080-01-012-012 range between 1.30 to 4.13 years. The CVT models for nasion, glabella, lambda and

opisthocranion produced wide PI ranges. For example, the fit age for nasion is 3.27 years old, but the PIs extend the range to 0.94 to 7.88 years. Therefore at nasion, the most accurate age estimation is from 0.94 to 7.88 years.

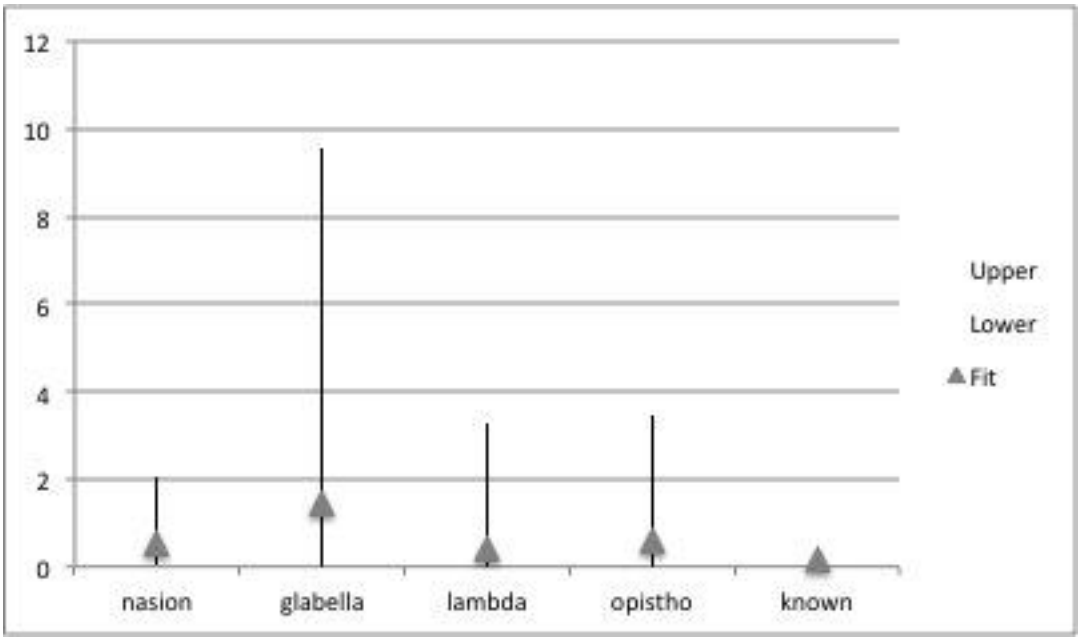

Figure 44 95% Prediction intervals for 114-00030-01-007-011.

The y-axis represents age in years and the x-axis represents cranial landmarks used and the known age.

The fit ages for the CVT model on the test case 114-00030-01-007-011 range from 0.41 to 1.46 years, and are close to the known chronological age of 0.18 years, except at glabella. The PIs for all models were narrow, ranging from 0.00 to 3.26 years, except at glabella where they ranged from 0.01 to 9.55 years.

This data supports hypothesis two. The known age for each individual fell within PIs generated by the models. The models over predicted age. Results indicate that age in older individuals is more over predicted than age in younger individuals.

Hypothesis three

Hypothesis three states: CVT will compare to chronological age and age-at-death estimates using transition analysis (Shackelford et al., 2012) on dental development scores of all available teeth (Moorrees et al., 1963); however, prediction intervals will not be as narrow as those produced by dental age-at-death estimates.

It was not possible to use correlation tests because the test sample size was too small. Instead, a chart showing the PIs with the fit age was compared to the MLE dental age (see Figures 45 and 46).

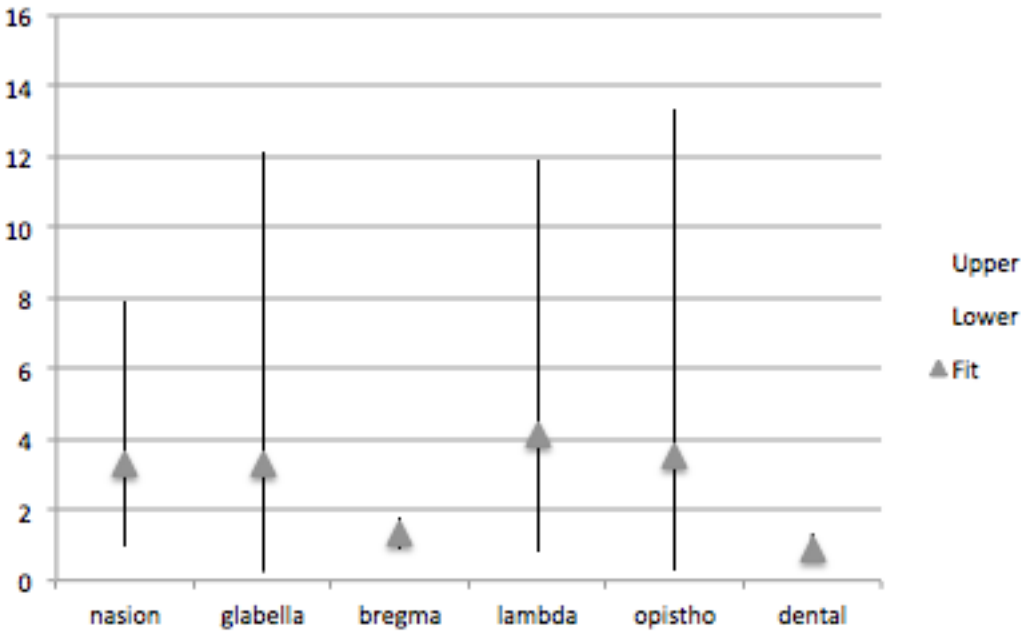

Figure 45 95% PIS for 118-00080-01-012-012 with dental age.

The y-axis represents age in years and the x-axis represents cranial landmarks used and the dental age.

The fit ages produced by all models, except bregma, are higher than the MLE dental age. The PIs are much wider than the dental age interval. The most narrow PI, nasion, ranges from 0.94 to 7.88.

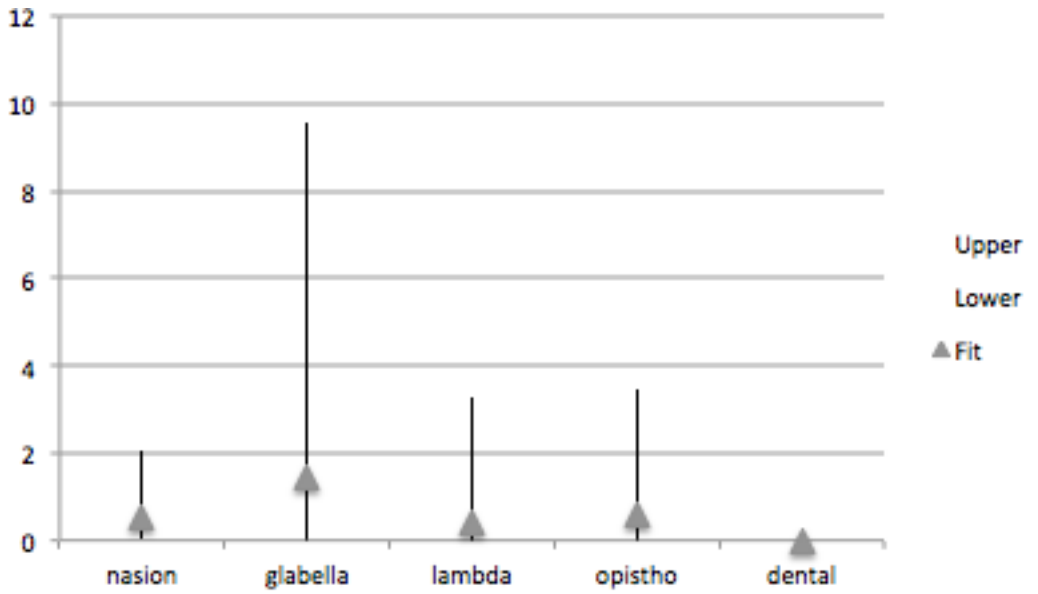

Figure 46 95% PIs for 114-00030-01-007-011 with dental age.

The y-axis represents age in years and the x-axis represents cranial landmarks used and the dental age.

Overall results showed that fit estimates overestimated age, except at bregma on the older test case (118-00080-01-012-012). The prediction intervals were very large for all points, with the exception of bregma. In the test of the second radiograph (114-00030-01-007-011), results shows that fit estimates were closer to the dental estimates; however, the prediction interval at glabella was still very large and extended past 9 years old. Results indicated that CVT age estimates correlated more closely with dental age-at-death estimates in the test case of the younger individual.

Hypothesis three is therefore supported; all PIs for the CVT models compared to dental age at death estimates, but were wider. As age increased in the test sample, the models over predicted age. CVT predicted ages were higher than dental age at death estimates. Models that did not support hypothesis three on the first test case were at glabella, lambda, and opisthocranion. The PIs were very large and did not correspond well with the predicted dental range. On the second test case, the model at glabella did not support hypothesis three, as the PI was very large and did not correspond with dental age. Alone, results from the model at glabella did not support hypothesis three on either of the test cases.

Case Studies

Age estimation using CVT was performed on unknown age cranial samples from the FAB Lab and the BARL. These crania (n=24) came from three sources: (1) individuals recovered from forensic contexts; (2) archaeological remains recovered from the Lyon's Bluff site in Oktibbeha County, Mississippi; (3) an archaeological cranium from the Mitrou site in Central Greece, which dates to the protogrometric period (1070-900 BC) (Tartaron, 2008; Rutter, 1993; Morris, 1989; Pedley, 2007). CVT was measured on a radiograph and CT scan for the forensic case, on dry bone from the Lyon's Bluff collection, and on a CT scan from the Mitrou site. These results are discussed separately as case studies because sample size and unknown demographics prevent them from contributing to method development or testing.

Case Study #1: An Unknown Forensic Case

An unknown juvenile cranium, designated MSU2014-02, was aged using CVT on radiographic images and a CT scan. Aging by transition analysis on dental development produced an age range of 3.81 to 7.84 with a MLE age of 5.51 years old. CVT age estimates using the radiographic data are listed in Table 17. CVT age estimates using the CT scan are listed in Table 18 and shown in Figure 47.

Table 17 CVT PIs for case MSU 2014-02 using radiographic data

CVT PIs at the 95% and 85% PI for case MSU 2014-02 (radiographic image)				
	PI level	lower	fit	upper
nasion	95%	0.99	3.41	8.16
	85%	1.45	3.41	6.63
glabella	95%	0.31	3.28	12.13
	85%	0.71	3.28	9.03
bregma	95%	0.99	1.43	2.00
	85%	1.10	1.43	1.84
vertex	95%	2.20	8.51	16.14
	85%	3.36	8.51	17.31
vertex radius	95%	1.97	7.77	19.84
	85%	3.03	7.77	15.89
lambda	95%	2.17	7.37	17.54
	85%	3.16	7.37	14.26
opisthocranion	95%	0.71	5.99	20.59
	85%	1.47	5.99	15.54

Numerical values are age in years for the unknown individual. Transition analysis of dental development produced an age range of 3.81 to 7.84 with a mean age of 5.51 years old.

Table 18 CVT PIs for case MSU 2014-02 using CT data

CVT PIs at the 95% and 85% PI for case MSU 2014-02 (CT image)				
	PI level	lower	fit	upper
nasion	95%	1.21	3.93	9.15
	85%	1.73	3.93	7.48
glabella	95%	1.83	6.37	15.29
	85%	2.70	6.37	12.41
bregma	95%	1.22	1.78	2.50
	85%	1.35	1.78	2.30
vertex	95%	1.52	6.22	16.14
	85%	2.37	6.22	12.88
vertex radius	95%	0.61	3.35	9.84
	85%	1.06	3.35	7.66
lambda	95%	2.36	7.76	18.19
	85%	3.40	7.76	14.85
opisthocranion	95%	0.32	3.67	13.81
	85%	0.76	3.67	10.24

Numerical values are age in years.

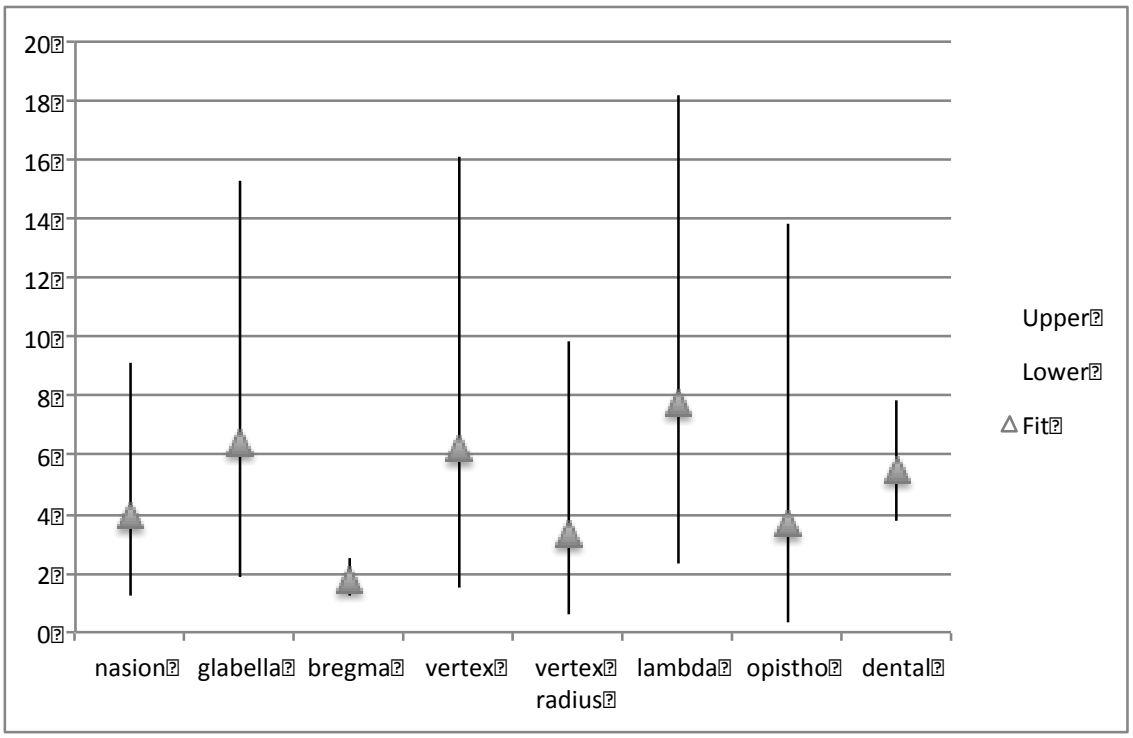

Figure 47 Chart showing univariate model PIs for MSU2014-02.

The y-axis represents age in years and the x-axis represents cranial landmarks used and the dental age.

Measurements on the CT scan and radiograph were slightly different. Because slight differences in CVT measurements can affect predicted ages, measurements using TIVMI, where HMH values are automatically calculated, were used over manually calculated HMH measurements in radiographs.

Results show that each model differed in its ability to predict age. Glabella, vertex and lambda produced a mean fit closest to the MLE dental age, but their PIs were very large. The widest PI, at lambda, includes all ages between 2.36 to 18.19 years old in the estimate. The mean values for nasion, bregma, vertex radius and opisthocranion underestimated age by approximately 2 to 4 years. The model for bregma showed the

narrowest PIs, but under predicted age by about 4 years. Results for the multivariate models are shown at the 95% and 85% PI levels in Table 19.

Table 19 Multivariate models using the CT data

Multivariate PIs at the 95% and 85% PI for case MSU 2014-02 (CT image)				
	PI level	lower	fit	upper
7 cranial landmarks	95%	0.93	5.00	14.58
	85%	1.61	5.00	11.37
highest ranked	95%	0.72	3.58	10.10
	85%	1.21	3.58	7.93
vault-set	95%	1.90	11.57	35.41
	85%	3.45	11.57	27.34

Numerical values are age in years. Transition analysis of dental development produced an age range of 3.811 to 7.839 with a mean age of 5.509 years old.

Results show that the PIs were wide in the multivariate models. The 7 cranial landmarks model was the best predictor of age. The fit age was close to the estimated dental age. The fit age for the highest ranked model under predicted age. The vault-set over predicted the fit age by 6 years and showed the largest PIs with the upper end extending to 35 years old. Results are shown in Figure 48. The 7 cranial landmarks model was the best predictor of age for the multivariate models, but it showed a large PI range. Glabella and vertex were the best predictors of age using univariate models. All three models produced an accurate fit age, but PIs were wide. The PI range for all three models was about 15 years, which is not useful for estimating a narrow age range.

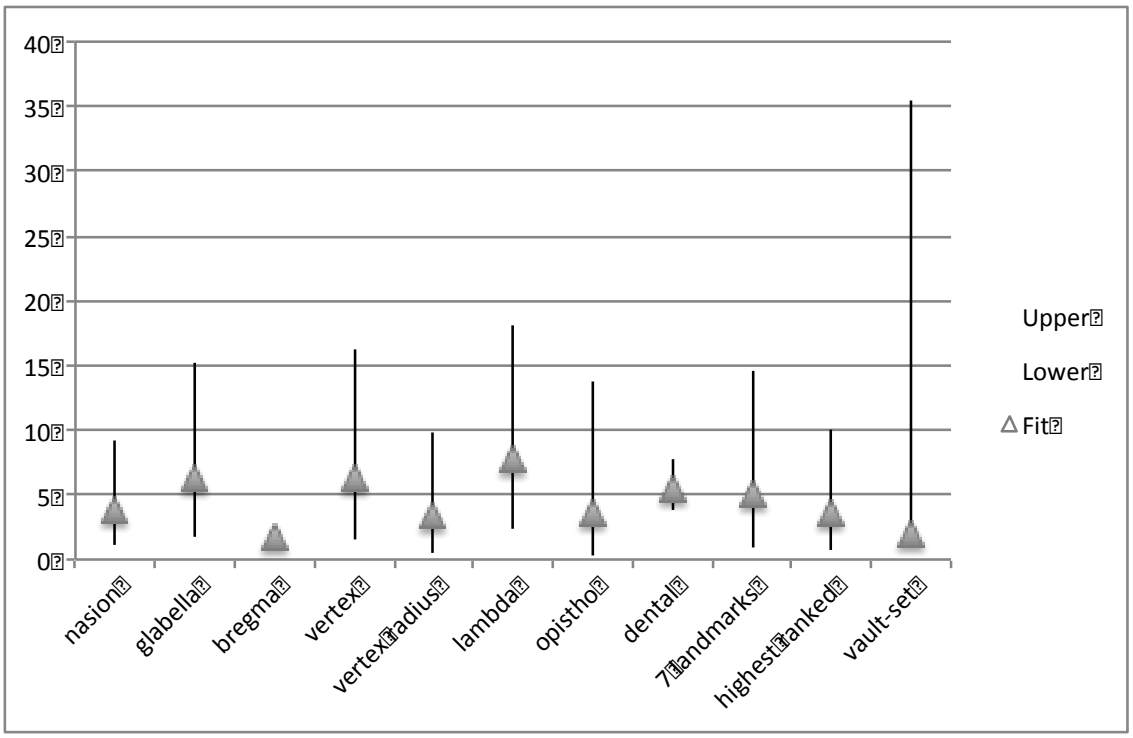

Figure 48 All models and PIs for MSU2014-02.

The y-axis represents age in years and the x-axis represents cranial landmarks used and the dental age.

Case Study #2: Lyon's Bluff Archaeological Crania

Dry bone and fragmentary CVT measurements were collected on the Lyon's Bluff collection. These crania (n=22) were aged by the author using transition analysis on dental development (Moorrees et al., 1963; Shackelford et al., 2012) on teeth not in occlusion and by measuring CVT on dry bone. Scatterplots of dental age estimates and CVT are shown in Figures 49-54. Each plot includes a fit line to illustrate the relationship of the two variables.

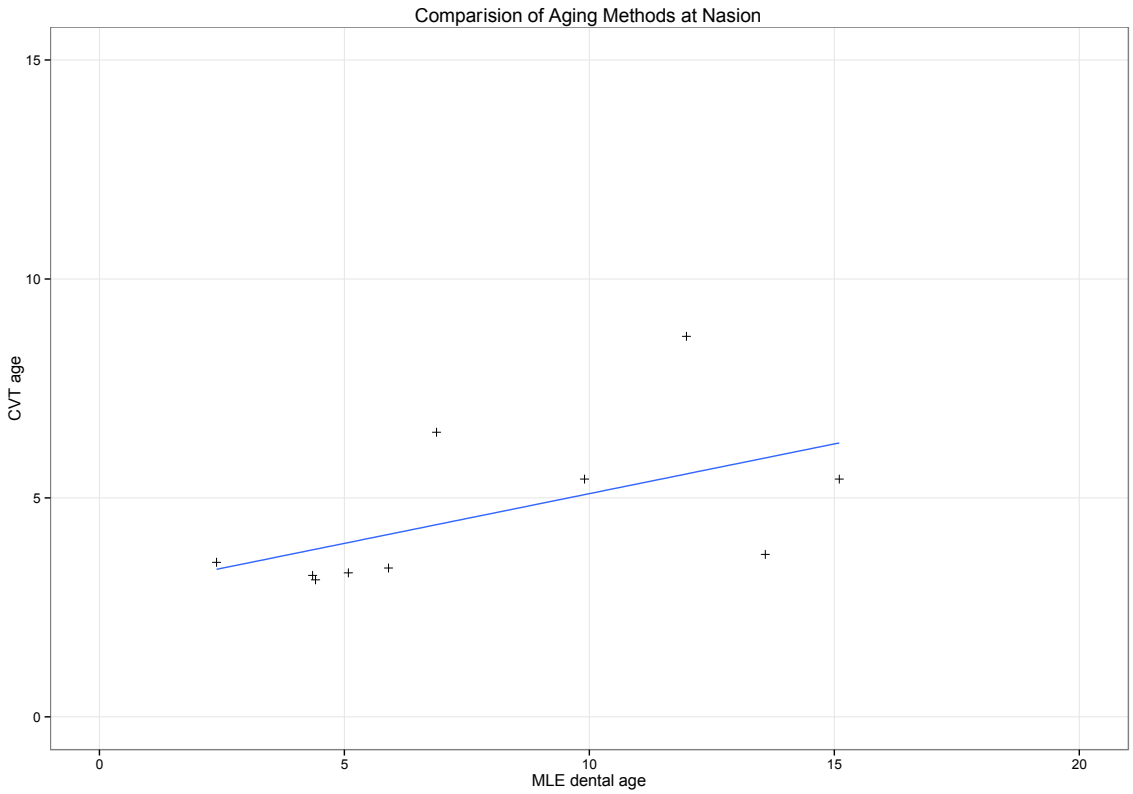

Figure 49 Dental age plotted against CVT age at nasion in the Lyon's Bluff sample.

There is a positive relationship between the two aging methods, however the points are not close to the fit line. This indicates that the age estimates from the two methods weakly compare to each other.

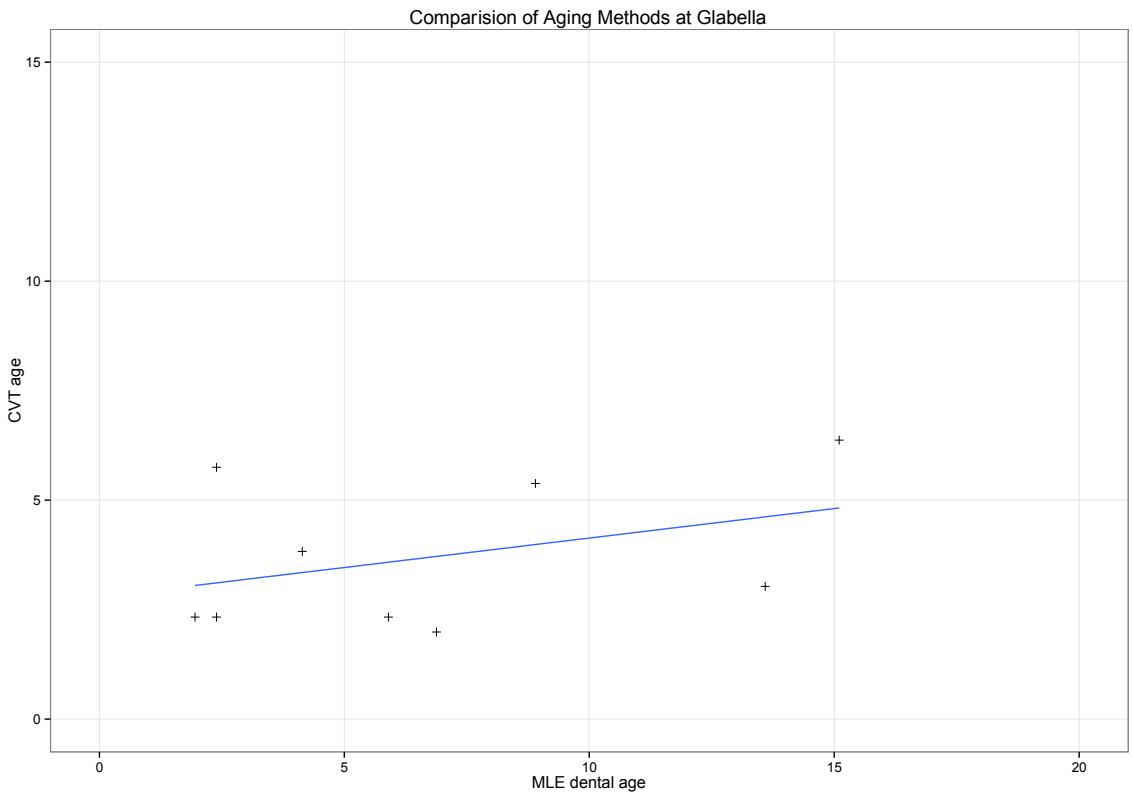

Figure 50 Dental age plotted against CVT age at glabella in the Lyon's Bluff sample.

There is a slight positive relationship between the two methods. The fit line shows a slight increase in as predicted ages increase. Points do not conform to the line and indicate these two methods do not compare well.

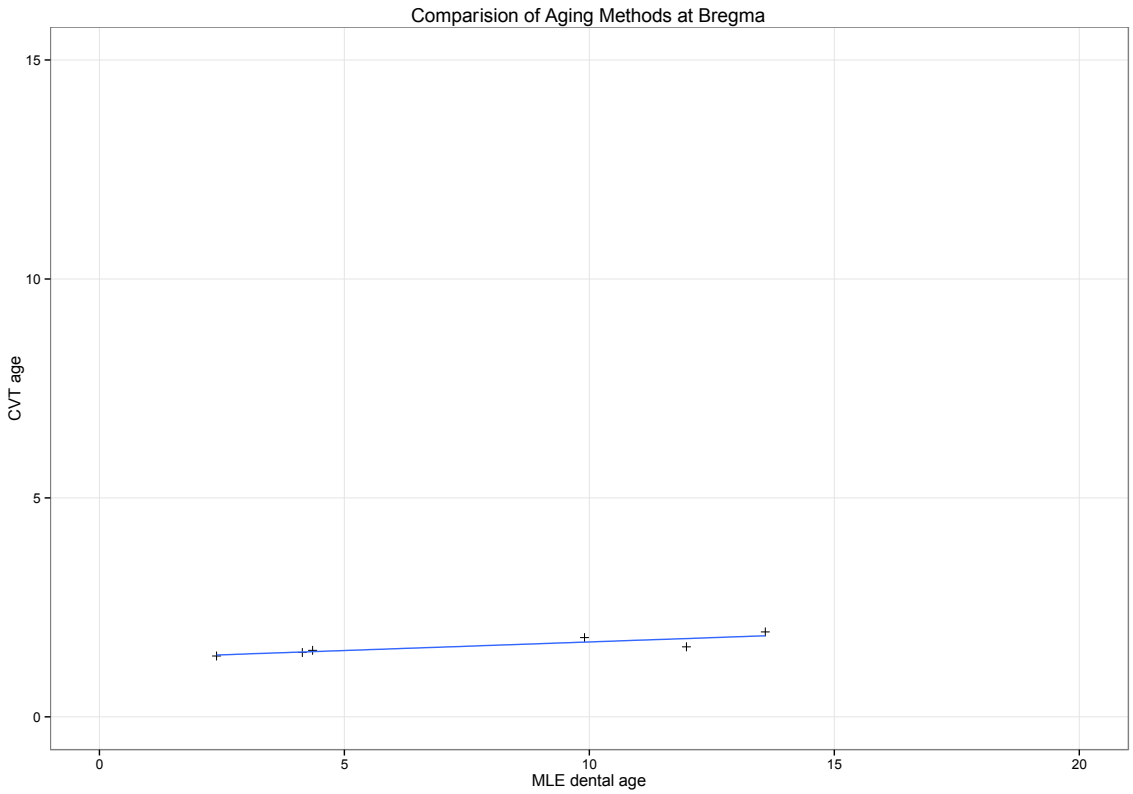

Figure 51 Dental age plotted against CVT age at bregma in the Lyon's Bluff sample.

There is a very weak correlation between the two methods at bregma. The fit line does not increase for CVT as the dental age estimate increase.

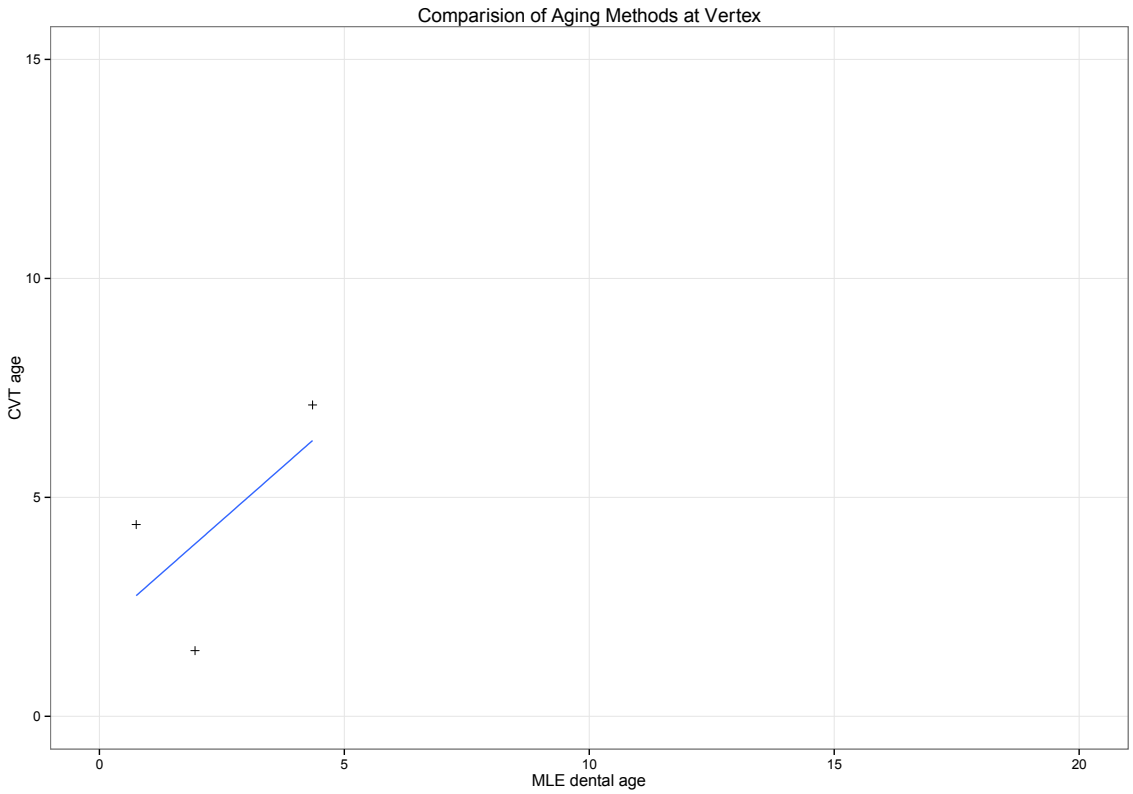

Figure 52 Dental age plotted against CVT age at vertex in the Lyon's Bluff sample.

The scatterplot shows a positive relationship between the two methods; however the sample size is small, consisting of three points.

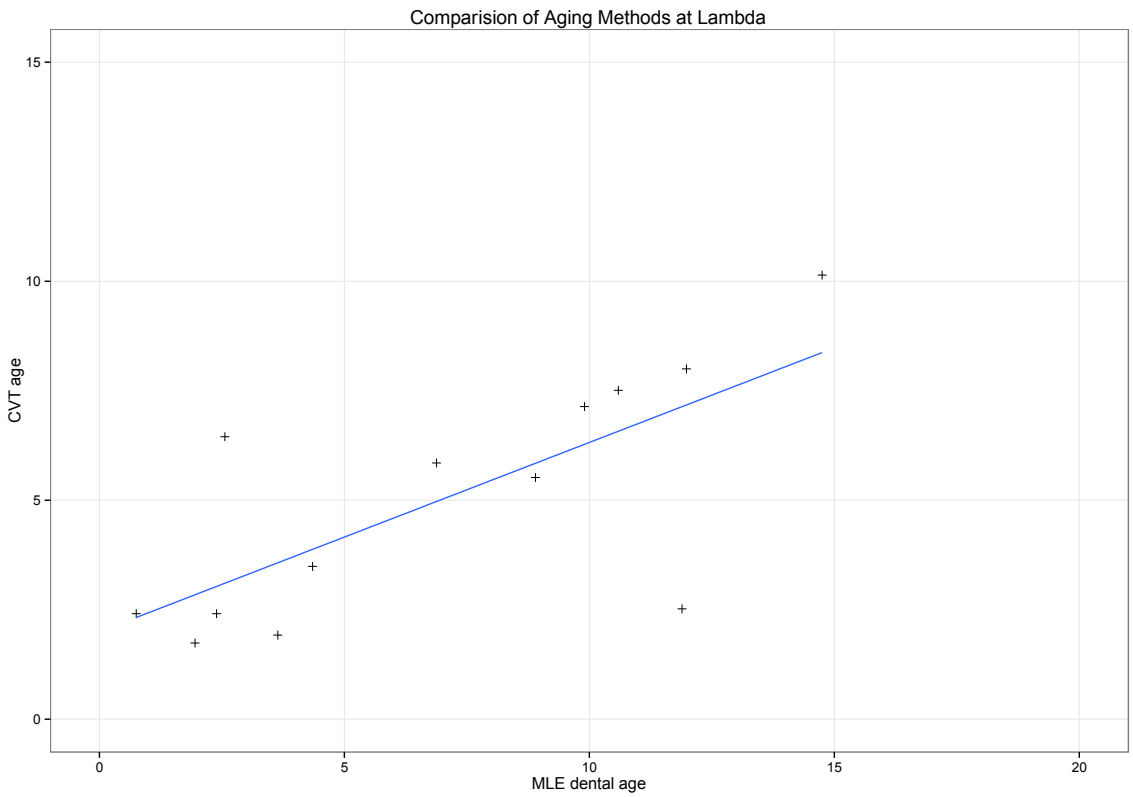

Figure 53 Dental age plotted against CVT age at lambda in the Lyon's Bluff sample.

The scatterplot shows a positive relationship between both methods at lambda. The predicted ages increase at a slower rate in the CVT sample.

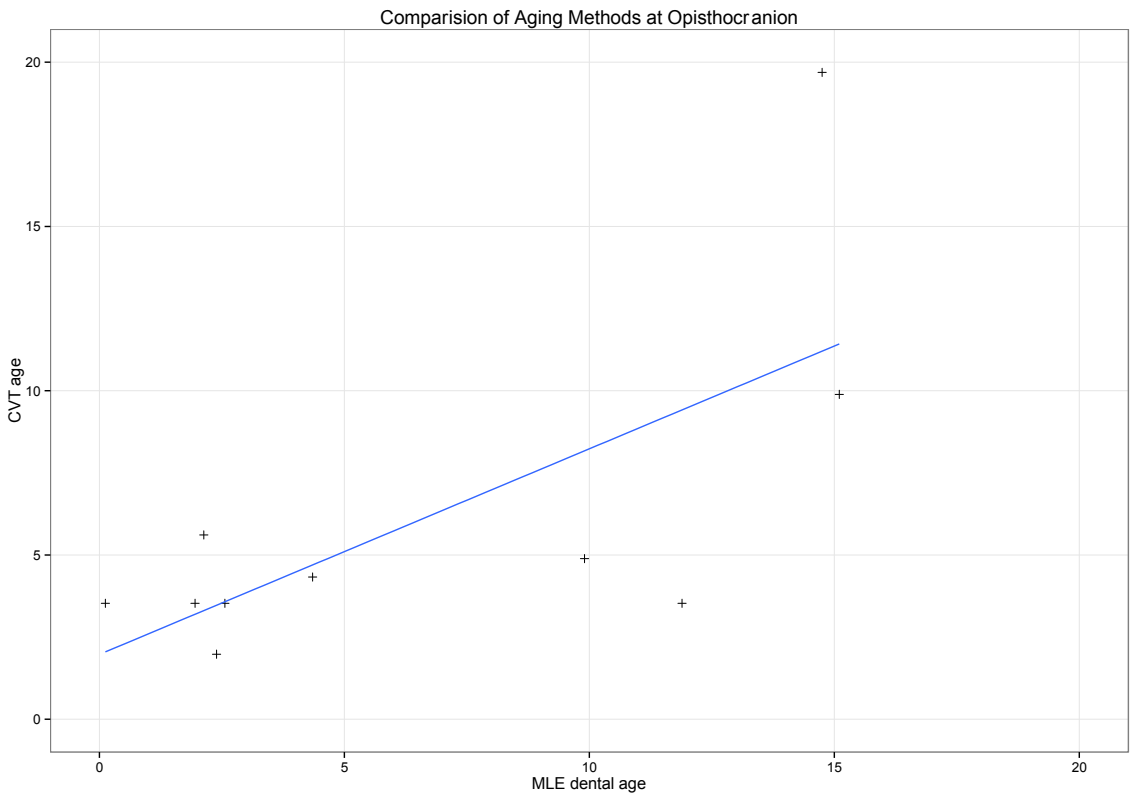

Figure 54 Dental age plotted against CVT age at opisthocranion in the Lyon's Bluff sample.

The scatterplot shows a positive relationship between both aging methods at opisthocranion. There are outliers as the age increases in both samples.

Predicted age ranges using CVT were compared to the predicted age ranges based on dental development and results are listed in Table 20. Bolded values indicate predicted ages that are outside of the sample range used in model creation. They were included to show the models ability to predict, but should not be used until the model can be supplemented with more known age samples that cover their range. Correlation tests between CVT and dental age on the entire sample indicated different levels of correlation at different cranial landmarks (see Table 21).

Table 20 Predicted CVT fit compared to predicted dental fit in Lyon's Bluff

CVT fit compared to dental fit							
ID	nasion	glabella	bregma	vertex	lambda	opistho	dental
67_2	-	-	-	-	-	5.61	2.13
67_3	-	-	-	4.38	2.41	3.53	0.75
67_5	-	-	-	-	2.52	3.53	11.89
67_11	-	-	-	-	**10.14**	**19.68**	14.75
67_14	**3.23**	-	1.52	7.11	3.49	4.33	4.35
67_15	**6.50**	1.99	-	-	5.85	-	6.88
67_18B	**3.13**	3.83	1.47	-	-	-	4.41
67_20	**3.29**	-	-	-	-	-	5.01
67_21	**5.43**	5.75	1.81	-	7.14	4.89	9.90
67_23	-	2.33	-	1.50	1.74	3.53	1.95
68_6	-	-	-	-	6.45	3.53	2.56
68_17	-	-	-	-	7.51	-	10.59
68_19	-	-	-	-	1.92	-	3.64
68_21	**3.53**	2.33	1.39	-	2.41	1.98	2.39
68_29	**8.69**	-	1.60	-	8.00	-	11.98
68_31	**5.43**	6.37	-	-	-	9.89	15.10
68_34	**3.40**	2.33	-	-	-	-	5.90
68_35	-	5.38	-	-	5.52	7.11	8.90
01_01	**3.71**	3.03	1.94	-	-	-	13.59

Numerical values are age in years. Bold ages are those predicted outside of the model's range. These values are less reliable.

Table 21 Correlation between CVT and dental age in Lyon's Bluff

	nasion	glabella	bregma	vertex	lambda	opistho
t	-1.78	0.45	0.24	-2.40	2.53	1.36
df	7	6	3	1	11	9
p-value	0.12	0.67	0.82	0.25	0.03	0.21
cor	-0.56	0.18	0.14	-0.92	0.61	0.41

Results for the correlation test using Pearson's r.

The correlation values range from -1 to 1. A positive or negative integer indicates the directionality of the relationship, and the closer the value of the integer to 1 indicates its strength; 1 is the strongest score. Results show that predicted age using CVT at certain cranial landmarks varied in correlation strength with age estimates using transition analysis on dental development. Correlation values between the two methods were weak for models at bregma and glabella, moderate for models at opisthocranion and nasion, and strong for model at lambda. The scatterplot for vertex suggests a correlation between CVT and age, however correlation test data produces a strong negative correlation. There were only three samples for vertex. Results of the comparison between the two methods suggest that the model at lambda was accurate and comparable to dental age for predicting age in the Lyon's Bluff sample. Results suggested that the models for predicting age at nasion and opisthocranion were less accurate than using dental age, and the models for predicting age at bregma and glabella were not accurate when compared to dental age estimates.

Case Study #3: Mitrou Archaeological Cranium

CVT was used to estimate age in a juvenile cranium from the Mitrou archaeological site. The cranium was not complete. Measurements were available for nasion and glabella and an estimated measurement was available for bregma. Measurements were unobservable at vertex, vertex radius, lambda, and opisthocranion because the cranial bone was absent at those landmark locations. Age estimates using the univariate models are listed in Table 21. A multivariate model was created for the three points available on the cranium. Data for the multivariate model is also in Table 22. Dental age was estimated to be between 3.83 and 6.50 with a fit of 5.01 years old. Figure

55 compares the fit ages and prediction intervals for the various landmarks used in estimation.

Table 22 Results for the Mitrou Cranium

Predicted ages at the 95% PI for the Mitrou Cranium			
Cranial Landmark	*lower*	*fit*	*upper*
nasion	0.04	0.54	2.03
glabella	0.71	4.33	13.31
bregma (est)	0.98	1.42	1.97
multivariate	0.48	2.40	6.80

Numerical values are age in years.

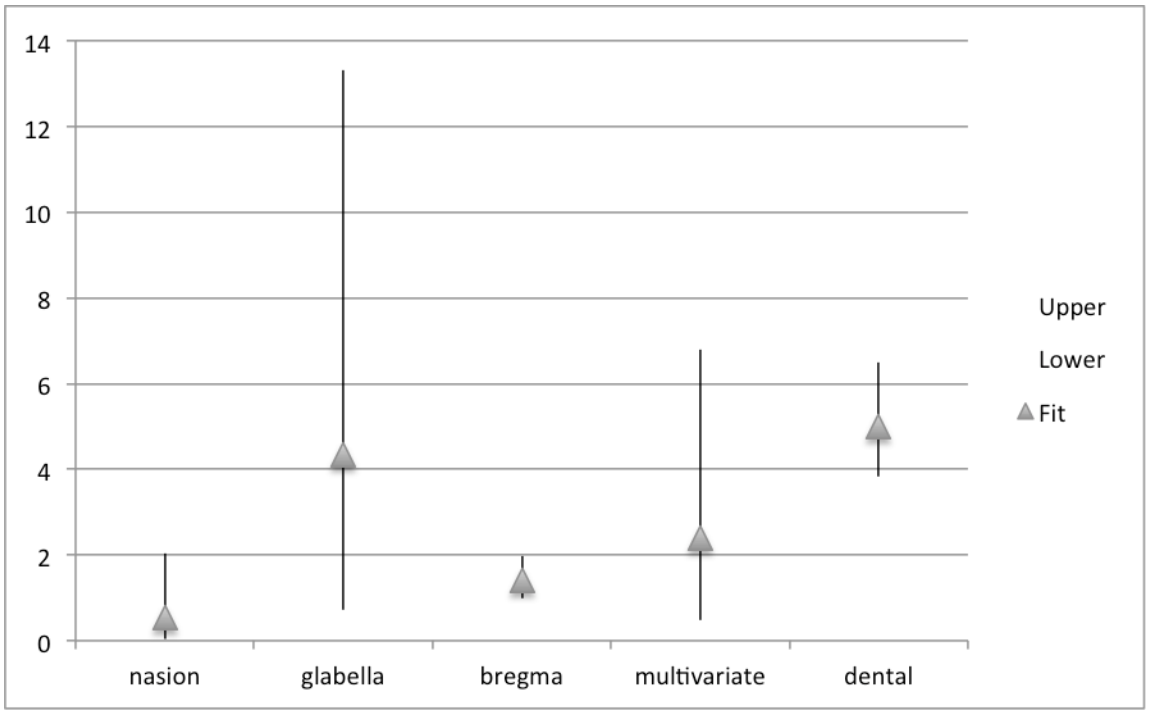

Figure 55 Models and PIs for Mitrou cranium

The y-axis represents age in years and the x-axis represents cranial landmarks used and the dental age.

The model for glabella predicted the closest fit age to the dental age, however the upper and lower PIs were very wide. Their width includes approximately 13 years. The

models at nasion and bregma under predicted age in the Mitrou cranium. The multivariate model (nasion, glabella, and bregma) prediction includes the dental range, however the predicted fit age was lower than the dental MLE by approximately 3 years. The models at nasion, bregma and the multivariate model were not accurate in predicting age in the Mitrou cranium. The model for glabella performed the best, predicting a fit age consistent with the dental fit age. Because the prediction interval ranges were large, the model at glabella would not be useful in creating a narrow age estimate.

CHAPTER V

DISCUSSION AND CONCLUSIONS

Predicting age using CVT

Results indicated that CVT at certain cranial landmarks is useful for predicting age at death in juveniles. Models indicated that certain landmarks were more useful than others, in particular, vertex and lambda.

Univariate and Multivariate Models

CVT at all cranial landmarks increased with increasing age. MARS models parsed out the relationship and clarified the degree of accuracy with which CVT predicted age. In all models, the PIs widened as age increased. The upper PI range varied for all models, and, in many instances, extended to include ages over 18 years old. Each model is discussed in detail below.

Nasion

The univariate model at nasion produced high R squared values for the general model and cross-validated model. These high scores indicated that a large percentage of age could be explained by an increase in CVT. Plots illustrating the residual spread showed clustering, and the RSS (residual sum of squares) value was high; indicating the model was not a good fit for the data. The variance model further showed that the model had a moderate degree of uncertainty when predicting age using CVT. The plot of the age

regressed on CVT showed the PIs, which were narrow for measurements between 2.5 to 10 mm. After 10 mm, the PIs rapidly widened where at 12.5 mm, their width extended to 15 years. Alone, nasion was not useful for predicting age using CVT. Moderate correlation values indicated that more data would be useful to clarify predictive ability of CVT at nasion.

Glabella

R squared values for the univariate model at glabella were low, indicating that age could not be explained very well using CVT in the model. Model interpretation plots and the RSS (residual sum of squares) value indicated the model was not a good fit for the data. The variance model confirmed that the model had a high degree of uncertainty when predicting age using CVT. The PI plot of age regressed on CVT showed that the model had a large predictive age range for all CVT values. A trend indicated that as CVT increased, the PIs widened exponentially and extended into the 1000's of years old. The PIs and predicted fit age were so high that the model at glabella was unrealistic to use for estimating age in juveniles. The CVT model at glabella is not useful to use when predicting age in juveniles.

Bregma

Results showed that the R squared values for the univariate model at bregma were midrange, indicating that about 50% of age could be explained by CVT using the model. The model interpretation plots and the RSS value indicated a good fit of the model to the data. The variance model suggested greater uncertainty in predictions at high values. The plot showing age regressed on CVT indicated narrow predictive age ranges varying from

less than 1 year to about 1 year and 6 months. The statistics suggest that the model for bregma is useful for predicting age, but the model was based on a very small measurement difference (0.4 mm) for CVT values. This small variance could be problematic as small measurement differences could greatly affect age predictions. Adjusted PI values on dummy variables indicated a range of a little over 3 years in the model's predictive ability. Such a small age range is neither useful nor practical for age estimation. Bregma is not useful for predicting age by CVT because the estimation range is limited to very young juveniles (newborns to 3 years old).

Vertex

The univariate model for vertex showed midrange R squared values. This indicated that about 50% of age could be explained by CVT using the model. The model interpretation plots indicated that the model was a good fit to the data. The variance model data further supported the goodness of fit. The plot illustrating age regressed on CVT with PIs, illustrated narrow PIs at lower CVT measures. The narrowest PI range was 3 years. The PIs increased with increasing CVT, and the widest PI range was 20 years. Results indicated the model at vertex is useful for predicting age.

Vertex Radius

The R squared values for the vertex radius model were low, indicating other factors apart from CVT contributing to age. The model interpretation plots and other summary statistics suggested a poor fit of the model to the data. The variance plot was the best plot for all of the landmarks, and suggested that the model is a good fit for the data. PIs on the plot showing age regressed on CVT widened as CVT increased. The

narrowest range was 9 years and the widest range was 42 years. Therefore, accuracy in age predictions decreased with age. Results suggested that more data would be useful to clarify the predictive ability of the model at vertex radius.

Lambda

The univariate model at lambda had high R squared values, indicating that a large percentage of age could be explained by changes in CVT. The model interpretation plots and variance plot supported a good fit of the model to the data. The plot illustrating age regressed on CVT showed very narrow PIs (5 years >) at small CVT measurements that increased in width as CVT increased. Results suggest that the model at lambda is useful for predicting age.

Opisthocranion

The R squared values were low, meaning that other factors apart from CVT contributed to age. The model interpretation plots and other summary statistics indicated that the model was not a good fit for the data. The variance model supported a poor fit of the model to the data. Overall, results indicated that the model at opisthocranion is uncertain and not useful for predicting age.

All Seven Landmarks

A multivariate model was created using CVT at all seven cranial landmarks. The R squared values were high suggesting that age could be explained by a combination of all CVT measurements. The model interpretation plots suggested that multivariate model was useful for predicting age by CVT; however, summary statistics suggested the model

was not useful for predicting age. More data is needed to accurately address if this model is useful for predicting age using CVT.

Highest Importance

The multivariate highest importance model was created from the highest ranked CVT values, determined using the evimp() function. The R squared value was high, indicating that most of age could be explained by CVT using the model. However, the cross-validated R squared value was negative, meaning that the model did not perform well with the cross-validation sample. The plots showed that the residuals cluster in one spot and the variance models had large confidence limits. The cross-validation line spiked and dropped randomly over the centerline along the entire variance plot, when it should have been straight. This information indicated that the model was not a good fit to the data. Despite their importance in the model using all seven landmarks, the high-ranking combination of CVT values did not produce a useful model for estimating age by CVT.

Vault Set

The R squared values for the vault set were high, indicating that age was explained by CVT using the model; however other data indicated a poor model fit. The RSS value was high and residual points clustered together on the model interpretation plots. The variance model exhibited wide confidence limits, indicating uncertainty in age predictions using the model. Overall, results indicated that the vault set model is not a useful predictor of age using CVT.

Radiographic Test Data

When the models were evaluated against the radiographic test data, they over predicted age at all cranial landmarks. Results from the two test cases indicated that the model over predicted age more in the older juvenile. The CT sample used in model creation contained a larger number of individuals aged between 0 and 3. Therefore, it is possible that the models would more accurately predict age in individuals younger than 3. Results indicated that PIs widened with increasing age, which could also be reflective of the sample used to generate the models.

The fit age estimated by the models at lambda, opisthocranion and nasion was accurate on the younger test sample, but not accurate on the older test sample. With the exception of the model at bregma, each model predicted age consistently for the older test individual when compared to each other. Fit ages produced by each CVT model differed by a maximum of 1 year. However, CVT age estimates were still higher than dental estimates and known age.

The performance of the method on the test radiographs indicated that the method has the potential to accurately predict age at death, but the data needs to be supplemented. More data from older known age samples would need to augment existing models to understand if the model is over predicting age because of sample bias, or because it does not perform well as age increases. Without adding more data, CVT age at death estimates are not very accurate and have large PIs. If skeletal remains have dentition, epiphyseal ends or a complete long bone, this method would not be recommended for age estimation alone. However, if fragmentary cranial remains or cranial remains without dentition were

the only skeletal tissue available, this method could be used cautiously, especially when estimating age in individuals suspected to be older than 3 years old.

Case Studies

Case Study #1 tested the method on radiographic and CT data from an unknown forensic case (MSU2014-02). CVT on the CT scan was measured in TIVMI, which automatically calculated the CVT HMH value. CVT on the radiograph was hand measured in Image J®, and the HMH value was manually calculated. HMH values were similar for bregma, lambda, and opisthocranion on both the CT scan and radiograph. Measurements at nasion, glabella, vertex, and vertex radius were different on the CT scan and radiograph, differing by 1.4 mm to 3.6 mm. This difference was reflected in the predicted fit estimates for those models, except nasion. The fit estimates differed by 0.52 years at nasion, 3.09 years at glabella, 0.35 at bregma, 1.89 years at vertex, 4.42 years at vertex radius, 0.39 years at lambda, and 2.32 years at opisthocranion. The larger measurements and subsequent fit age estimates came from radiographic data, which suggested error in placement and/or measurement on radiographic data. When CVT measurements for the radiograph and CT scan were similar, they produced similar age estimates. Results suggested that manual measurements have the potential to add more error in age predictions than do automatically calculated CVT measurements. More testing is needed to assess the error associated between automatic and hand measured CVT measurements.

In Case Study #2, the aging method was tested on dry bone samples from the Lyon's Bluff collection (n=22). Results were compared with dental age estimates (Moorrees et al., 1963; Shackelford et al., 2012) using a correlation test. Vertex radius

was not used, as it could not be accurately placed on cranial vault fragments. Scatterplots indicated a positive correlation between dental age and CVT age for the following available landmarks: nasion, lambda, vertex, and opisthocranion The plots show that glabella and bregma had weak correlations between the two methods, which was reflected in a correlation value of 0.18 and 0.14. The plot for bregma showed that as age increased using the dental estimation method, it seemed to remain at the same numerical value for the CVT method. Even though the plot for nasion shows a positive correlation, the test produced a value of -0.56, indicating a negative correlation between CVT and age. Points were further from the fit line as age increased in nasion. The same is true of opisthocranion, however the correlation value was 0.41, indicating a moderate relationship between the two methods for predicting age. Vertex produced the largest, correlation of -0.92; indicating a negative correlation between the two methods. Results are unclear as there were only three age estimation values for comparison. CVT and dental development age predictions correlated the best at lambda, with a correlation value of 0.61. A larger number of CVT estimates would clarify results for vertex and opisthocranion.

Case Study #3, the Mitrou archaeological cranium, tested the method on a CT scan of incomplete archaeological material. Univariate models were used to test CVT at each available cranial landmark, and one multivariate model was used to test CVT at all three cranial landmarks. No one model performed well. The models for bregma and nasion severely under predicted fit age, and did not include the dental age estimate. The multivariate model PIs did include the dental age estimate, but the fit age was low. The model for glabella performed the best, as predicted age was closest to the fit dental age.

The PIs, however, were very wide, spanning 13 years. None of the models were useful for predicting a narrow, accurate age estimate. This may have to do with the quality of the CT scan, or the lack of cranial landmarks with better predictive abilities, such as lambda or vertex.

Conclusions of the Method

In this study, the overarching research question was: Can differential CVT of juvenile crania be used as a method to estimate age? Results from this study indicated that MARS models of CVT can be used to estimate age at vertex and lambda. Results indicated that CVT was not useful to estimate age at glabella and bregma. Results also showed that more CVT measurement data is needed to fully clarify the ability of the model at nasion, vertex radius and opisthocranion. Results on each model's ability to predict age are explained in Table 23. In practice, the refined CVT method is less accurate than age predictions made by transition analysis on dental development because the PIs are much wider, as would be expected.

Table 23 Predictive capabilities of the models

Model Name	Useful for predicting age?	Comments:
nasion	Maybe	More data and testing are needed to further clarify the ability of this model.
glabella	No	The age range is too wide to be practical and realistic in age at death estimations.
bregma	No	This model under predicts age.
vertex	Yes	Not useful for fragmentary remains.
vertex radius	Maybe	More data and testing are needed to further clarify the ability of this model. Not useful for fragmentary remains.
lambda	Yes	More data could help refine the model
opisthocranion	Maybe	More data and testing are needed to further clarify the ability of this model.
seven landmarks	Maybe	More data and testing are needed to further clarify the ability of this model.
highest importance	No	The model over predicts age.
vault set	No	The age range is very wide and the model under predicted age during the test.

The table explains which cranial landmarks are useful for predicting age using CVT, and which models could be improved.

Limitations

This study and the refined method were not free from biases that influenced how the models' performance and age estimation results. The discussion is separated into limitations specific to this study and limitations specific to the method.

Limitations of the Study

Sources of error specific to this study were found in the following areas: the limited age range of the sample used to create the method and the small sample size of the test data from *Patricia*.

The CT sample used to create the refined method limited the model's predictive ability because of its composition. As mentioned in Chapter IV, the sample used to create the models contained 74 individuals, of which 35 were younger than 6 years old. This meant that 35 individuals made up the 6 to 18 year old category used to create the middle and upper age range of the model. The lack of middle and older age juveniles (6-18 years old) could be the reason the models were more uncertain as age predictions increased. Since the majority of the sample was younger than 6 years old, the models may be better at predicting individuals younger than 6, because there is more data for those ages used to construct the model and clarify prediction intervals.

The *Patricia* sample is a large data source of known age juvenile radiographs, but it is not the best source for metric data collection on radiographs. The majority of the radiographic images did not include a scale or information on radiograph dimensions, which could be used to create a scale. Because this study required an accurate measurement for CVT, most images from this sample could not be used. The first potential source of error was the lack of results from the radiographic test of the method. Since only two samples were used, there was not enough data to comprehensively test the method. A larger sample size that includes various juvenile ages, especially those older than 6 years old, could be used to remake the models.

Limitations of the Method

Limitations of the CVT method include error in measurement collection. Measurements at nasion and glabella sometimes included a sinus, and there is potential for error when using software and calipers to collect measurement data

During measurement collection, CVT at nasion and glabella was divided into two types measurements. One type of measurement passed through a distinct compact bone-diploe-compact bone boundary. The other type of measurement included a sinus. At these points, sinuses extended or blurred the compact bone-diploe-compact boundary, thus creating inaccurate measurements. The raw CVT scores for these two points were not normal after a normality test, and the models were not well suited for predicting age. Measurements with and without a sinus were included, which could account for unreliability and inaccuracy in both models. To address this issue, measurements could be separated into two categories: those with a sinus present and those without.

A second source of error lies within measurement collection. CVT collection was automated in TIVMI to reduce user error. However, on two separate occasions the software misidentified HMH values for bone, and produced an HMH measure for soft tissue directly above the ectocranial surface. To correct this, the author displayed the mesh and manually placed the ectocranial point above the mesh and the endocranial point below the mesh. This means that measurements should be checked even when they are automated in a software package, otherwise CVT may be a larger or smaller measure than its actual size. If not checked, this could lead to over or under estimations of age in the models. Another source of measurement error can be caused by different measuring equipment. In this study, digital calipers provided the most accurate measurements for

dry bone when compared to sliding calipers. Sliding calipers must be visually read, while digital calipers estimate to the nearest tenth of a millimeter, creating a more exact measurement. Differences in tenths of a millimeter can cause over or under estimation in age by the models. Measurement error could arise when measurements are collected on radiographic images. Radiographic images may be blurred or radiolucent at cranial landmarks, causing the user to over or under estimate thickness. Estimations could lead to over and under prediction of age as measurements differ by millimeter.

Discussion

This study used the MARS modeling methodology put forth in Stull and colleagues' (2014) study estimating subadult age from diaphyseal dimensions of long bones, which used a larger sample size (n=1,310) than employed in the current study. The models performed much better with RSq and CVRSq values greater than 0.93. This indicated that greater than 93% of the age estimations could be explained by diaphyseal dimensions of long bones. As shown in the publication, predicted age intervals adjusted and widened as age increased. Stull and colleagues (2014) found that in individuals older than 10 years of age, age predictions using diaphyseal length underestimated age, and the degree of underestimation increased with increasing age. They noted that the diaphyseal breadth models overestimated age in younger individuals and underestimated age in older individuals. Despite the over and underestimation in the models, chronological age fell within the PIs from 94% to 100%. Stull and colleagues (2014) note that the models lost precision after 10 years of age, reflecting greater variability in growth after 10 years.

Age estimations using CVT are still unclear. More research is needed to address variability in growth and its relationship to overprediction of older ages. Results from this

study show that CVT models can be used to estimate age in juveniles. The estimate from the CVT method is not as narrow and accurate as dental age determinations, but it produces an age range. This adds to the literature of methods available for estimating age in juveniles, specifically using the cranium, which is suitable for forensics and bioarchaeology. In instances where remains are highly fragmented, such as mass disasters where dentition or smaller epiphyses may not be recovered or material for aging using long bones is not available, CVT can suffice. CVT measurements on cranial fragments can be used within the models to differentiate between multiple children, and children and adults. This information contributes to the biological profile and can be used for identification purposes in forensics and to understand health, disease, and populational information in bioarchaeology.

Conclusions

The purpose of this study was to refine and test the CVT method for estimating age at death in juvenile remains. Three hypotheses were used to guide this study: (1) CVT measurements at select cranial landmarks conform to expected growth curves using a locally smoothed (loess) fit; (2) CVT measured on radiographic images of juvenile crania will fit to age estimation models developed on CT scans; and (3) CVT will compare to chronological age and age-at-death estimates using dental development scores of all available teeth developed by Shackelford et al. (2012), however it will not offer as narrow prediction intervals as aging by dental development. The first hypothesis tested whether CVT conformed to expected growth curves for juvenile remains at each of the seven cranial landmarks under study. From there, univariate and multivariate MARS models were created using the seven cranial landmarks. The second hypothesis tested

whether the models would produce an age that correlated to known age from a radiographic test sample. The third hypothesis tested whether age predicted by CVT models would correlate to age predicted by transition analysis on dental development. This study refined the CVT age estimation method and includes measurement tables with error that are easy to use and understand. This method can be used on forensic cases because the samples come from individuals from contemporary populations, but it also applies to bioarchaeological samples.

Overall, 74 individuals from CT scans were used to create the models. Two individuals from the Patricia sample were used to test the model and assess CVT and dental age. Archaeological juvenile samples and an unknown juvenile forensic case (n=24) were used to illustrate this method on various case examples.

In summary, CVT models varied in their predictive ability to estimate age. Aging by CVT produced large confidence intervals that sometimes stretched into adulthood. The CVT models at vertex and lambda were useful predictors of age. Models at glabella, bregma, the highest ranked landmarks and the vault set of landmarks were not useful for predicting age. The models at vertex radius, nasion, opisthocranion and all seven landmarks could be refined with more data. Test cases showed that age estimations for younger individuals produced a more accurate and narrow age range at bregma, lambda and opisthocranion. The CVT models at nasion, glabella, lambda and opisthocranion over predicted age in the older juvenile test case. Aging by CVT has the potential to improve if more known age data are used to create the models, especially juveniles older than 6 years. By adding more data to existing models, the PIs may narrow and produce a more accurate fit

Future Directions

The study is suitable for aging as currently stands, however a larger sample size would improve the method. A larger sample, with a large number of individuals older than 6 years old should be added to the CT data used in model creation. The models were created with data mainly from young juveniles, specifically, individuals younger than 6 years old. This bias affected the models, as they became more unreliable for predicting age as juvenile age increased. CVT measurements would need to be taken at the seven cranial landmarks on CT scans using an automated measurement tool, such as TIVMI. By adding new data to existing models and recreating the models using the Earth package, the models' ability to predict age would be clarified, especially at nasion, bregma, the vertex radius, opisthocranion, and the multivariate models.

In order to finalize the CVT method as useful for a bioarchaeological sample, it must be calibrated by another, more accurate age estimation method, such as dental development. The author plans to examine a large, juvenile archaeological sample, like the collection at the University of Alabama. Such an archaeological sample presents a great opportunity to calibrate the method using dental development and compare CVT to long bone length measurements for growth and development studies.

REFERENCES

Bookstein F. 1991. Morphometric Tools for Landmark Data: Geometry and Biology. Cambridge University Press. Cambridge.

Braga J, Treil J. 2007. Estimation of pediatric skeletal age using geometric morphometrics and three-dimensional cranial size changes. International Journal of Legal Medicine. 121:439-443.

Brown T, Pinkerton SK, Lambert W. 1979. Thickness of the cranial vault in Australian Aboriginals. Archaeology and Physical Anthropology in Oceania. 14:54-71.

Buschang PH, Baume RM, Nass GG. 1983. A Craniofacial Growth Maturity Gradient for Males and Females Between 4 and 16 Years of Age. American Journal of Physical Anthropology. 61:373-381.

Cardoso HFV, Abrantes J, Humphrey LT. 2013. Age estimation of immature human skeletal remains from the diaphyseal length of the long bones in the postnatal period. International Journal of Legal Medicine. 128:809-824.

Cattaneo C. 2007. Forensic anthropology: developments of a classical discipline in the new millennium. Forensic Science International. 165:185-193.

Christiansen AM, Crowder CM. 2009. Evidentiary Standards for Forensic Anthropology. Journal of Forensic Sciences. 54:1211-1216.

Condon K, Charles DK, Cheverud JM, Buikstra JE. 1986. Cementum annulations and age determination in Homo sapiens. II. Estimate and accuracy. American Journal of Physical Anthropology. 71:321-330.

Coquerelle M, Bookstein FL, Braga J, Halazonetis DJ, Weber GW, Mitteroecker P. 2011. Sexual Dimorphism of the Human Mandible and Its Association with Dental Development. American Journal of Physical Anthropology. 145:192-202.

Cunha E, Baccino E, Martrille L, Famsthaler F, Prieto J, Schuliar Y, Lynnerup N, Cattaneo C. 2009. The problem of aging human remains and living individuals: A review. Forensic Science International. 193:1-13.

de la Cova C. 2011. Race, Health, and Disease in the 19th –Century-Born Males. American Journal of Physical Anthropology. 144:526-537.

Demirjian A, Goldstein H, Tanner J. 1973. A New System of Dental Age Assessment. Human Biology. 45:211-227.

Dirkmaat DC, Cabo LL, Ousley SD, Symes SA. 2008. New Perspectives in Forensic Anthropology. Yearbook of Physical Anthropology. 51:33-52.

Dutailly B and Guyomarc'h P. 2012. TIVMI V2.1 User Manual.

Fazekas IG, Kósa F. 1978. Forensic fetal osteology. Budapest: Akademiai Kiadó.

Field A, Miles J, Field Z. 2012. Discovering Statistics Using R. Sage Publications.

Franklin D. 2010. Forensic age estimation in human skeletal remains: Current concepts and future directions. Legal Medicine. 12:1-7.

Franklin D, Cardini A, O'Higgins P, Oxnard C, Dadour I. 2008. Mandibular morphology as an indicator of human subadult age: geometric morphometric approaches. Forensic Science Medicine and Pathology. 4:91-99.

Garofalo E, Zuckerman MK, Ortner DJ. 2008. The incomplete juvenile: Cranial vault thickness as a technique for juvenile skeletal remains. American Journal of Physical Anthropology. 132: 52.

Garvin HM, Passalacqua NV, Uhl NM, Gipson DR, Overbury RS, Cabo LL. 2012. Developments in Forensic Anthropology: Age-at-Death Estimation. In: Dirkmaat D, editor. A Companion to Forensic Anthropology. Vol 10. John Wiley and Sons. p. 202.

Gleiser I, Hunt EE. 1955. The permanent mandibular first molar: its calcification, eruption and decay. American Journal of Physical Anthropology. 13:253-283.

Gordon C, Buikstra J. 1981. Soil pH, Bone Preservation, and Sampling Bias at Mortuary Sites. American Antiquity. 46:566-571.

Guyomarc'h P, Santos F, Dutailly B, Desbarats P, Bou C, Coqueugniot H. 2012. Three-dimensional computer-assisted craniometrics: A comparison of the uncertainty in measurement induced by surface reconstruction performed by two computer programs. Forensic Science International. 219:221-227.

Hansmen CF. 1966. Growth of Interorbital Distance and Skull Thickness as Observed in Roentgenographic Measurements. Radiology. 86:87-96.

Hoffman JM. 1979. Age estimations from diaphyseal lengths: two months to twelve years. Journal of Forensic Science. 24:461-469.

Hoppa RD, Fitzgerald CM. 1999. From head to toe: integrating studies from bones and teeth in biological anthropology. In: Human growth in the past. Studies from bones and teeth. Hoppa RD, FitzGerald CM, editors. Cambridge.

Howell WW. 1973. Cranial Variation in Man. Papers of the Peabody Museum of Archaeology and Ethnology. Harvard University, Cambridge, Mass. Vol. 67.

Hunt DR, Albanese J. 2005. History and Demographic Composition of the Robert J. Terry Anatomical Collection. American Journal of Physical Anthropology. 127:406-417.

Ingervall B, Thilander B. 1972. The human spheno-occipital synchondrosis. I. The time of closure appraised macroscopically. Acta Odontologica Scandinavia. 30:349-356.

Inter-Parliamentary Union. International Committee of the Red Cross. 2009. Missing Persons-A Handbook for Parliamentarians.

Iscan M, Loth S. 1986. Estimation of Age and Determination of Sex from the Sternal Rib. In: Reichs K, editor. Forensic Osteology. Springfield, IL: Thomas. p 68-89.

Jantz RL, Mahfouz M, Shirley NR, Fatah EA. 2008. Improving Sex Estimation from Crania using 3-dimensional CT Scans. US Department of Justice.

Kimmerle E. 2004. Biological and Statistical Variation in Age Estimation from Pubic Symphyseal Morphology with Regard to Individual Identification and Demographic Profiling.

Kimmerle EH, Falsetti A, Ross AH. 2010. Immigrants, Undocumented Workers, Runaways, Transients and the Homeless: Towards Contextual Identification Among Unidentified Decedents. Forensic Science Policy & Management: An International Journal. 1:178-186.

Konigsberg LW, Herrmann NP, Wescott DJ, Kimmerle EH. 2008. Estimation and Evidence in Forensic Anthropology: Age-at-Death. Journal of Forensic Sciences. 53:541-557.

Kranioti E, Paine R. 2011. Forensic Anthropology in Europe: an assessment of current status and application. Journal of Anthropological Science. 89:71-92/

Larsen CS. 1997. Bioarchaeology. Cambridge, New York: Cambridge University Press.

Lewis ME. 2007. The bioarchaeology of children: perspectives from biological anthropology and forensic anthropology. Cambridge University Press: New York.

Lovejoy C, Meindl R, Pryzbeck T, Mensforth R. 1985. Chronological metamorphosis of the auricular surface of the ilium: A new method for the determination of adult skeletal age at death. American Journal of Physical Anthropology. 68:16-28.

Maat GJR. Mastwijk RW. 2005. Fusion status of the jugular growth plate: An aid for age at death determination. International Journal of Osteoarchaeology. 5:163-167.

Manifold B. 2013. Differential preservation of children's bones and teeth recovered from early medieval cemeteries: possible influences for the forensic recovery of non-adult skeletal remains. Anthropological Review. 76:23-49.

Maresh MM. 1955. Linear Growth of Long Bones of Extremities from Infancy Through Adolescence. American Journal of Diseases of Children. 89:725-742.

Martin R. 1928. Lehrbuch der Anthropologie in systematischer Darstellung. Mit besondereer Berücksichtigung der antrhopologischen Methoden für Studierende, Ärzte und Forschungsreisende. Jena: Gustav Fischer.

Mays S. 1998. The Determination of Age and Sex. In: The Archeology of Human Bones. Mays S, editor. London: Taylor & Francis. P 33-73.

McKern T, Stewart T. 1957. Skeletal age changes in young American males, analyzed from the standpoint of identification. Natick, Massachusetts: Headquarters QM Tes and Dev Command.

Melnick RL. 2005. A *Daubert* Motion: A Legal Strategy to Exclude Essential Scientific Evidence in Toxic Tort Litigation. American Journal of Public Health. 95(S1):S30-S34.

Milborrow S. Derived from mda:mars by Hastie T and Tibshirani R. 2011. Earth: Multivariate Adaptive Regression Spline Models. R Software Package.

Milborrow S. 2014. Notes on the earth package. Available online at: www.milbo.org/doc/earth-notes.pdf

Moorrees C, Fanning E. Hunt E. 1963. Age Variation of Formation Stages for Ten Permanent Teeth. Journal of Dental Research. 42:1490-1502.

Morris I. 1989. Burial and Ancient Society: The Rise of the Greek City-State. Cambridge: Cambridge University Press.

Ousley S, Daly S, Frazee K, Stull K. 2013. A Radiographic Database for Estimating Biological Parameters in Modern Subadults. National Institute of Justice.

Ortner DJ. 2003. Identification of Pathological Conditions in Human Skeletal Remains. San Diego: Academic Press.

Peacock E and Hogue SH. 2005. A New Series of Absolute Dates from Lyon's Bluff (22OK520), East-Central Mississippi. Southeastern Archaeology. 24:47-58.

Pedley JG. 2007. Greek Art and Archaeology, 4th Edition. Boston: Prentice Hall.

Plattner D. 1984. Protection of Children in International Humanitarian Law. International Committee of the Red Cross. Available online at https://www.icrc.org/eng/resources/documents/article/other/57jmat.htm

Redfield A. 1970. A New Aid to Aging Immature Skeletons: Development of the Occipital Bone. American Journal of Physical Anthropology. 33:207-220.

Ritz-Timme S, Cattaneo C, Collins M, Waite E, Schutz H, Kaatsch H, Borrman H. 2000. Age estimation: The state of the art in relation to the specific demands of forensic practise. International Journal of Legal Medicine. 113:129-136.

Rogers T. 2009. Skeletal Age Estimation. In: Blau S, Ubelaker D, editors. Handbook of Forensic Anthropology and Archaeology. Walnut Creek: Left Coast Press. p 208-221.

Rutter JB. 1993. Review of Aegean Prehistory II: The Prepalatial Bronze Age of the Southern and Central Greek Mainland. American Journal of Archaeology. 79:745-797.

Scheuer L, Black S. 2000a. Development and Ageing of the Juvenile Skeleton. In: Cox M, Mays S, editors. Human Osteology in Archaeology and Forensic Science. Cambridge: Cambridge University Press. p 9-21.

Scheuer L, Black S. 2000b. Developmental Juvenile Osteology. London: Academic Press.

Scheuer L, Black S. 2004. The Juvenile Skeleton. London: Elsevier Academic Press.

Scheuer L, MacLaughlin-Black S. 1994. Age Estimation from the Pars Basilaris of the Fetal Juvenile Occipital Bone. International Journal of Osteoarchaeology. 4:377-380.

Scheuer JL, Musgrave JH, Evans SP. 1980. The estimation of late fetal and perinatal age from limb bone length by linear and logarithmic regression. Annals of Human Biology. 7:257-265.

Schmeling A, Geserick G, Reisinger W, Olze A. 2007. Age Estimation. Forensic Science International. 165:178-181.

Schultz R, Muhler M, Mutze S, Schmidt S, Reisinger W, Schmeling A. 2005. Studies on the time frame for ossification of the medial epiphysis of the clavicle as revealed by CT scans. International Journal of Legal Medicine. 119:142-145.

Shackelford LL, Stinespring Harris AE, Konigsberg LW. 2012. Estimating the distribution of probable age-at-death from dental remains of immature human fossils. American Journal of Physical Anthropology. 147:227-253.

Spoor CF, Zonneveld FW, Macho GA. 1993. Measurements of Cortical Bone and Dental Enamel by Computed Tomography: Applications and Problems. American Journal of Physical Anthropology. 91:469-484.

Stull KE, L'Abbe EN, Ousley SD. 2014. Using multivariate adaptive regression splines to estimate subadult age from diaphyseal dimensions. American Journal of Physical Anthropology. 154: 376-386.

Suchey JM, Katz D. 1986. Skeletal age standards derived from an extensive multiracial sample of modern Americans. American Journal of Physical Anthropology. 69:269.

Tartaron TF. 2008. Aegean Prehistory as World Archeology: Recent Trends in the Archaeology of Bronze Age Greece. Journal of Archaeological Research.16:83-161.

Todd TW. 1920. Age changes in the pubic bone. I. The male white pubis. American Journal of Physical Anthropology. 3:285-334.

Ubelaker D. 1989. Human Skeletal Remains: Excavation, Analysis, Interpretation. 2nd ed. Washington, D.C.: Taraxacum.

Usher B. 2002. Reference Samples: the first step in linking biology and age in the human skeleton. In: Hoppa R, Vaupel J, editors. Paleodemography: Age distributions from skeletal samples. Cambridge, UK: Cambridge University Press. p 29-47.

White TD, Folkens PA. 2000. Human Osteology, Second Edition. Academic Press.

Zuckerman M, Garofalo E, Frohlich B, Ortner D. 2014. Anemia or scurvy: A pilot study on differential diagnosis of porous and hyperostotic lesions using differential cranial vault thickness in subadult humans. International Journal of Paleopathology. *In press.*

APPENDIX A

CRANIAL LANDMARK DEFINITIONS

Cranial Landmark Definitions

The definitions of the cranial landmarks used in this study are listed in Table 10.

Table 24 Definition and source of cranial landmarks used in this study.

Landmark	Definition	Reference
Infraorbitale	The most inferior point on the orbital rim.	(Dutailly and Guyomarc'h, 2012)
Porion	The most superior point on the external auditory meatus.	(Dutailly and Guyomarc'h, 2012)
Nasion	The intersection of the fronto-nasal suture and the median plane. Consider nasion as on the frontal bone.	(Howell, 1973)
Glabella	The maximum projection of the midline profile between nasion and supraglabellare (or the point at which the convex profile of the frontal bone changes to join the prominence of the glabellar region.	(Howell, 1973)
Bregma	The posterior border of the frontal bone in the median plane. Normally, this point is the meeting point of the coronal and sagittal suture. The sagittal suture may diverge from the midline, but the measurement should stay on the midline and metopic sutures should be disregarded.	(Howell, 1973)
Vertex Radius	The perpendicular to the transmeatal axis from the most distant point on the parietals (including bregma or lambda), wherever found.	(Howell, 1973)
Vertex	The highest point on the ear-eye plane aligned to the median sagittal plane of the skull.	(Martin, 1928)
Lambda	The apex of the occipital bone at its junction with the parietals, in the midline. This is the meeting of the sagittal and lambdoidal sutures and must be placed in the midline.	(Howell, 1973)
Opisthocranion	The most posteriorly protruding point of the occipital bone in the midsagittal plane.	(Jantz et al., 2008)

The cranial landmark definitions and sources are listed in the above table.

APPENDIX B

TABLES FOR AGE ESTIMATION USING CVT

Age Estimation Tables Using CVT

Table 25 Age estimation table for CVT at nasion at the 95% PI

CVT	fit_age	lwr_age	upr_age
<4.25	0.54	0.05	2.03
4.3	0.56	0.05	2.07
4.4	0.66	0.07	2.32
4.5	0.76	0.09	2.58
4.6	0.87	0.12	2.84
4.7	0.99	0.15	3.12
4.8	1.12	0.18	3.42
4.9	1.25	0.22	3.72
5	1.39	0.26	4.03
5.1	1.54	0.31	4.35
5.2	1.69	0.36	4.69
5.3	1.86	0.41	5.03
5.4	2.03	0.47	5.38
5.5	**2.20**	**0.53**	**5.75**
5.6	**2.38**	**0.60**	**6.12**
5.7	**2.53**	**0.65**	**6.41**
5.8	**2.57**	**0.67**	**6.49**
5.9	**2.61**	**0.68**	**6.58**
6	**2.65**	**0.70**	**6.66**
6.1	**2.70**	**0.71**	**6.75**
6.2	**2.74**	**0.73**	**6.83**
6.3	**2.78**	**0.75**	**6.91**
6.4	**2.82**	**0.76**	**7.00**
6.5	**2.86**	**0.78**	**7.08**
6.6	**2.90**	**0.79**	**7.16**
6.7	**2.94**	**0.81**	**7.24**
6.8	**2.98**	**0.82**	**7.32**
6.9	**3.02**	**0.84**	**7.40**
7	**3.06**	**0.86**	**7.48**
7.1	**3.10**	**0.87**	**7.55**
7.2	**3.14**	**0.89**	**7.63**
7.3	**3.18**	**0.90**	**7.71**
7.4	**3.22**	**0.92**	**7.78**
7.5	**3.26**	**0.93**	**7.86**

Table 25 (Continued)

7.6	**3.30**	**0.95**	**7.93**
7.7	**3.34**	**0.96**	**8.01**
7.8	**3.38**	**0.98**	**8.08**
7.9	**3.41**	**0.99**	**8.16**
8	**3.45**	**1.01**	**8.23**
8.1	**3.49**	**1.03**	**8.30**
8.2	**3.53**	**1.04**	**8.37**
8.3	**3.56**	**1.06**	**8.45**
8.4	**3.60**	**1.07**	**8.52**
8.5	**3.64**	**1.09**	**8.59**
8.6	**3.67**	**1.10**	**8.66**
8.7	**3.71**	**1.12**	**8.73**
8.8	**3.75**	**1.13**	**8.80**
8.9	**3.78**	**1.15**	**8.87**
9	**3.82**	**1.16**	**8.94**
9.1	**3.85**	**1.18**	**9.00**
9.2	**3.89**	**1.19**	**9.07**
9.3	**3.93**	**1.21**	**9.14**
9.4	**3.96**	**1.22**	**9.21**
9.5	**4.00**	**1.23**	**9.27**
9.6	**4.03**	**1.25**	**9.34**
9.7	**4.07**	**1.26**	**9.41**
9.8	**4.10**	**1.28**	**9.47**
9.9	**4.13**	**1.29**	**9.54**
10	**4.17**	**1.31**	**9.60**
10.1	**4.20**	**1.32**	**9.67**
10.2	**4.24**	**1.34**	**9.73**
10.3	**4.42**	**1.42**	**10.08**
10.4	**4.62**	**1.50**	**10.44**
10.5	**4.81**	**1.59**	**10.81**
10.6	**5.02**	**1.67**	**11.18**
10.7	**5.22**	**1.77**	**11.56**
10.8	**5.43**	**1.86**	**11.94**
10.9	**5.64**	**1.95**	**12.33**
11	**5.86**	**2.05**	**12.72**
11.1	**6.08**	**2.15**	**13.12**
11.2	**6.30**	**2.25**	**13.52**
11.3	**6.52**	**2.36**	**13.92**
11.4	**6.75**	**2.47**	**14.33**
11.5	**6.98**	**2.57**	**14.75**
11.6	**7.22**	**2.69**	**15.17**
11.7	**7.46**	**2.80**	**15.59**

Table 25 (Continued)

11.8	**7.70**	**2.91**	**16.02**
11.9	**7.94**	**3.03**	**16.45**
12	**8.19**	**3.15**	**16.88**
12.1	**8.44**	**3.27**	**17.32**
12.2	**8.69**	**3.40**	**17.76**
12.3	**8.95**	**3.52**	**18.21**
12.4	**9.21**	**3.65**	**18.66**
12.5	**9.47**	**3.78**	**19.11**
12.6	**9.73**	**3.91**	**19.57**
12.7	**10.00**	**4.05**	**20.03**
12.8	**10.27**	**4.18**	**20.49**
12.9	**10.26**	**4.17**	**20.46**
13	**10.22**	**4.16**	**20.41**
13.1	**10.19**	**4.14**	**20.35**
13.2	**10.16**	**4.13**	**20.30**
13.3	**10.13**	**4.11**	**20.25**
13.4	**10.10**	**4.10**	**20.19**
13.5	**10.07**	**4.08**	**20.14**
13.6	**10.04**	**4.07**	**20.09**
13.7	**10.01**	**4.05**	**20.04**
13.8	**9.98**	**4.04**	**19.99**
13.9	**9.95**	**4.02**	**19.94**
14	**9.92**	**4.01**	**19.89**
14.1	**9.89**	**3.99**	**19.84**
14.2	**9.86**	**3.98**	**19.79**
14.3	**9.84**	**3.96**	**19.74**
14.4	**9.81**	**3.95**	**19.69**
14.5	**9.78**	**3.94**	**19.64**
14.6	**9.75**	**3.92**	**19.60**
14.7	**9.72**	**3.91**	**19.55**
14.8	**9.70**	**3.89**	**19.50**
14.9	**9.67**	**3.88**	**19.46**
15	**9.64**	**3.87**	**19.41**

CVT measurements are in mm. Bolded measurements are generated outside of the model's ability and are more unpredictable; they should be used with caution.

Table 26 Age estimation table for CVT at glabella at the 95% PI

CVT	fit age	lower age	upper age
<3.00	1.41	0.00	9.46
3.25	1.76	0.02	10.05

Table 26 (Continued)

3.50	2.14	0.05	10.63
3.75	2.33	0.08	10.90
4.00	2.33	0.08	10.90
4.25	2.33	0.08	10.90
4.30	2.33	0.08	10.90
4.40	2.33	0.08	10.90
4.50	2.33	0.08	10.90
4.60	2.33	0.08	10.90
4.70	2.33	0.08	10.90
4.80	2.39	0.09	10.98
4.90	2.46	0.10	11.08
5.00	2.53	0.12	11.17
5.10	2.60	0.13	11.26
5.20	2.67	0.15	11.36
5.30	2.74	0.16	11.45
5.40	2.81	0.18	11.54
5.50	2.88	0.20	11.64
5.60	2.95	0.21	11.73
5.70	3.03	0.23	11.82
5.80	3.10	0.25	11.91
5.90	3.18	0.28	12.00
6.00	3.25	0.30	12.09
6.10	3.33	0.32	12.18
6.20	3.40	0.35	12.28
6.30	3.48	0.37	12.37
6.40	3.56	0.40	12.45
6.50	3.63	0.42	12.54
6.60	3.71	0.45	12.63
6.70	3.79	0.48	12.72
6.80	3.87	0.51	12.81
6.90	3.95	0.54	12.90
7.00	4.03	0.58	12.99
7.10	4.11	0.61	13.08
7.20	4.19	0.64	13.16
7.30	4.27	0.68	13.25
7.40	4.36	0.72	13.34
7.50	4.44	0.75	13.43
7.60	4.52	0.79	13.51
7.70	4.61	0.83	13.60
7.80	4.69	0.87	13.69
7.90	4.77	0.91	13.77
8.00	4.86	0.96	13.86

Table 26 (Continued)

8.10	4.94	1.00	13.94
8.20	5.03	1.05	14.03
8.30	5.12	1.09	14.12
8.40	5.20	1.14	14.20
8.50	5.29	1.19	14.29
8.60	5.38	1.23	14.37
8.70	5.47	1.28	14.46
8.80	5.56	1.34	14.54
8.90	5.64	1.39	14.63
9.00	5.73	1.44	14.71
9.10	5.82	1.49	14.79
9.20	5.91	1.55	14.88
9.30	6.00	1.61	14.96
9.40	6.10	1.66	15.05
9.50	6.19	1.72	15.13
9.60	6.28	1.78	15.21
9.70	6.37	1.84	15.30
9.80	6.47	1.90	15.38
9.90	6.56	1.96	15.46
10.00	6.65	2.03	15.55
10.10	6.75	2.09	15.63
10.20	6.84	2.16	15.71
10.30	6.94	2.22	15.80
10.40	7.03	2.29	15.88
10.50	7.13	2.36	15.96
10.60	7.22	2.43	16.04
10.70	7.32	2.50	16.13
10.80	7.42	2.57	16.21
10.90	7.51	2.64	16.29
11.00	7.61	2.72	16.37
11.10	7.71	2.79	16.45
11.20	7.81	2.86	16.54
11.30	7.91	2.94	16.62
11.40	8.01	3.02	16.70
11.50	8.11	3.10	16.78
11.60	8.21	3.18	16.86
11.70	8.31	3.26	16.94
11.80	8.41	3.34	17.03
11.90	8.51	3.42	17.11
12.00	8.61	3.50	17.19
12.10	8.71	3.59	17.27
12.20	8.82	3.67	17.35

Table 26 (Continued)

12.30	8.92	3.76	17.43
12.40	9.02	3.85	17.51
12.50	9.13	3.93	17.59
12.60	9.23	4.02	17.67
12.70	9.33	4.11	17.75
12.80	9.44	4.21	17.83
12.90	9.54	4.30	17.91
13.00	9.65	4.39	18.00
13.10	9.76	4.48	18.08
13.20	9.86	4.58	18.16
13.30	9.97	4.68	18.24
13.40	10.08	4.77	18.32
13.50	10.18	4.87	18.40
13.60	10.29	4.97	18.48
13.70	10.40	5.07	18.56
13.80	10.51	5.17	18.64
13.90	10.61	5.27	18.72
14.00	10.72	5.37	18.80
14.10	10.83	5.48	18.87
14.20	10.94	5.58	18.95
14.30	11.05	5.69	19.03
14.40	11.16	5.79	19.11
14.50	11.27	5.90	19.19
14.60	11.39	6.01	19.27
14.70	11.50	6.12	19.35
14.80	11.61	6.23	19.43
14.90	11.72	6.34	19.51
15.00	11.83	6.45	19.59

CVT measurements are in mm.

Table 27 Age estimation table for CVT at bregma at the 95% PI

CVT	fit age	lower age	upper age
1.20-2.34	1.30	0.90	1.80
2.61	1.35	0.94	1.88
2.78	1.42	1.04	1.98
2.99	1.51	1.10	2.11
3.20	1.60	1.19	2.24
3.50	1.74	1.23	2.44
3.64	1.80	1.24	2.53
3.89	1.82	1.24	2.56

Table 27 (Continued)

4.21	1.85	1.26	2.60
4.35	1.87	1.27	2.62
4.48	1.88	1.28	2.64
4.73	1.90	1.29	2.67
4.82	1.91	1.30	2.68
5.23	1.95	1.32	2.74
5.39	1.96	1.33	2.76
5.69	1.99	1.35	2.80
5.89	2.01	1.37	2.83
6.02	2.02	1.37	2.85
6.21	2.04	1.39	2.88
6.43	2.06	1.40	2.91
6.59	2.08	1.41	2.93
6.94	2.11	1.43	2.98
7.04	2.12	1.44	3.00
7.32	2.15	1.46	3.03
7.46	2.17	1.47	3.06
7.69	2.19	1.48	3.09
7.84	2.21	1.49	3.12
7.99	2.22	1.50	3.14

CVT measurements are in mm. It is not recommended to use this model for age predictions.

Table 28 Age estimation table for CVT at vertex at the 95% PI

CVT	fit age	lower age	upper age
0.25	0.30	0.02	1.16
0.50	0.43	0.04	1.55
0.75	0.58	0.07	2.01
1.00	0.78	0.11	2.56
1.25	1.01	0.15	3.20
1.50	1.29	0.21	3.95
1.75	1.61	0.29	4.80
2.00	1.98	0.37	5.76
2.25	2.41	0.48	6.85
2.50	2.89	0.60	8.06
2.75	3.44	0.75	9.41
3.00	4.04	0.91	10.90
3.25	4.72	1.10	12.54
3.50	5.46	1.31	14.34
3.75	6.28	1.54	16.30
4.00	7.18	1.80	18.43
4.25	**8.16**	**2.09**	**20.74**
4.30	**8.37**	**2.16**	**21.22**
>4.40	**8.52**	**2.20**	**21.57**

CVT measurements are in mm. Bolded measurements are generated outside of the model's ability and are more unpredictable; they should be used with caution.

Table 29 Age estimation table for CVT at vertex radius at the 95% PI

CVT	fit age	lower age	upper age
1.34-3.52	**3.35**	**0.612**	**9.84**
3.76	**3.49**	**0.65**	**10.17**
3.88	**3.83**	**0.74**	**10.98**
4.21	**4.82**	**1.03**	**13.28**
4.27	**5.01**	**1.09**	**13.70**
4.66	**6.27**	**1.48**	**16.55**
4.79	**6.71**	**1.62**	**17.52**
5.10	**7.79**	**1.98**	**19.87**
5.23	**8.25**	**2.13**	**20.88**
5.37	**8.75**	**2.31**	**21.96**
5.86	**10.56**	**2.94**	**25.82**
5.90	**10.71**	**2.99**	**26.14**
6.21	**11.89**	**3.42**	**28.61**
6.30	**12.24**	**3.55**	**29.34**
6.44	**12.78**	**3.75**	**30.47**
6.84	**14.35**	**4.33**	**33.71**
6.92	**14.67**	**4.45**	**34.37**
7.10	**15.39**	**4.72**	**35.84**
7.32	**16.27**	**5.06**	**37.63**
7.48	**16.91**	**5.30**	**38.94**
7.69	**17.76**	**5.63**	**40.66**
7.90	**18.61**	**5.97**	**42.39**
8.03	**19.14**	**6.17**	**43.45**
8.32	**20.33**	**6.64**	**45.83**
8.47	**20.95**	**6.89**	**47.06**
8.69	**21.85**	**7.25**	**48.87**
8.93	**22.84**	**7.65**	**50.84**

CVT measurements are in mm. Bolded measurements are generated outside of the model's ability and are more unpredictable; they should be used with caution.

Table 30 Age estimation table for CVT at lambda at the 95% PI

CVT	fit age	lower age	upper age
<1.25	0.42	0.00	3.31
1.50	0.57	0.00	3.82
1.75	0.75	0.01	4.39
2.00	0.96	0.02	5.00
2.25	1.21	0.04	5.68
2.50	1.50	0.08	6.39
2.75	1.72	0.12	6.93
3.00	1.97	0.17	7.49

Table 30 (Continued)

3.25	2.24	0.23	8.09
3.50	2.53	0.30	8.72
3.75	2.85	0.38	9.39
4.00	3.20	0.49	10.08
4.25	3.57	0.60	10.81
4.30	3.64	0.63	10.96
4.40	3.80	0.68	11.26
4.50	3.96	0.74	11.57
4.60	4.13	0.80	11.89
4.70	4.30	0.86	12.21
4.80	4.48	0.93	12.53
4.90	4.66	0.99	12.86
5.00	4.85	1.07	13.20
5.10	5.04	1.14	13.54
5.20	5.24	1.22	13.89
5.30	5.44	1.30	14.25
5.40	5.64	1.39	14.61
5.50	5.85	1.48	14.98
5.60	6.07	1.57	15.35
5.70	6.29	1.67	15.73
5.80	6.52	1.77	16.12
5.90	6.75	1.88	16.51
6.00	6.99	1.99	16.91
6.10	7.23	2.10	17.31
6.20	7.48	2.22	17.72
6.30	7.74	2.34	18.14
6.40	8.00	2.47	18.57
6.50	**8.26**	**2.60**	**19.00**
6.60	**8.54**	**2.74**	**19.43**
6.70	**8.81**	**2.88**	**19.88**
6.80	**9.10**	**3.02**	**20.33**
6.90	**9.39**	**3.17**	**20.79**
7.00	**9.68**	**3.33**	**21.25**
7.10	**9.99**	**3.49**	**21.72**
7.20	**10.30**	**3.65**	**22.20**
7.30	**10.61**	**3.83**	**22.69**
7.40	**10.93**	**4.00**	**23.18**
7.50	**11.26**	**4.18**	**23.68**
7.60	**11.59**	**4.37**	**24.18**
7.70	**11.93**	**4.56**	**24.70**
7.80	**12.28**	**4.76**	**25.22**
7.90	**12.64**	**4.96**	**25.75**

Table 30 (Continued)

8.00	**13.00**	**5.17**	**26.28**
8.10	**13.36**	**5.38**	**26.82**
8.20	**13.74**	**5.60**	**27.37**
8.30	**14.12**	**5.83**	**27.93**
8.40	**14.51**	**6.06**	**28.50**
8.50	**14.90**	**6.30**	**29.07**
8.60	**15.31**	**6.55**	**29.65**
8.70	**15.71**	**6.80**	**30.24**
8.80	**16.13**	**7.05**	**30.83**
8.90	**16.56**	**7.32**	**31.44**
9.00	**16.99**	**7.59**	**32.05**
9.10	**17.43**	**7.86**	**32.67**
9.20	**17.87**	**8.15**	**33.29**
9.30	**18.33**	**8.44**	**33.93**
9.40	**18.79**	**8.73**	**34.57**
9.50	**19.26**	**9.04**	**35.22**
9.60	**19.74**	**9.35**	**35.88**
9.70	**20.22**	**9.66**	**36.55**
9.80	**20.71**	**9.99**	**37.23**
9.90	**21.21**	**10.32**	**37.91**
10.00	**21.72**	**10.66**	**38.60**

CVT measurements are in mm. Bolded measurements are generated outside of the model's ability and are more unpredictable; they should be used with caution.

Table 31 Age estimation table for CVT at opisthocranion at the 95% PI

CVT	fit age	lower age	upper age
<1.5	0.32	0.00	2.31
1.75	0.51	0.00	3.18
2	0.78	0.01	4.26
2.25	1.13	0.03	5.55
2.5	1.56	0.06	7.08
2.75	2.10	0.12	8.87
3	2.74	0.19	10.94
3.25	3.50	0.30	13.30
3.5-5.4	3.53	0.30	13.39
5.5	3.58	0.31	13.53
5.6	3.73	0.33	13.99
5.7	3.89	0.36	14.46
5.8	4.05	0.38	14.94
5.9	4.21	0.41	15.43

Table 31 (Continued)

6	4.38	0.43	15.93
6.1	4.55	0.46	16.44
6.2	4.73	0.49	16.96
6.3	4.91	0.52	17.49
6.4	5.10	0.55	18.04
6.5	5.29	0.58	18.59
6.6	5.49	0.62	19.16
6.7	5.69	0.65	19.73
6.8	5.89	0.69	20.32
6.9	6.10	0.73	20.92
7	6.32	0.77	21.54
7.1	6.54	0.81	22.16
7.2	6.76	0.85	22.80
7.3	7.00	0.89	23.45
7.4	7.23	0.94	24.11
7.5	7.47	0.98	24.78
7.6	7.72	1.03	25.46
7.7	7.97	1.08	26.16
7.8	8.23	1.13	26.87
7.9	8.49	1.19	27.60
8	8.76	1.24	28.33
8.1	9.03	1.30	29.08
8.2	9.31	1.35	29.84
8.3	9.60	1.41	30.62
8.4	9.89	1.47	31.41
8.5	**10.19**	**1.54**	**32.21**
8.6	**10.49**	**1.60**	**33.02**
8.7	**10.80**	**1.67**	**33.85**
8.8	**11.11**	**1.74**	**34.70**
8.9	**11.44**	**1.81**	**35.55**
9	**11.76**	**1.88**	**36.42**
9.1	**12.10**	**1.95**	**37.31**
9.2	**12.44**	**2.03**	**38.21**
9.3	**12.78**	**2.10**	**39.12**
9.4	**13.13**	**2.18**	**40.05**
9.5	**13.49**	**2.27**	**40.99**
9.6	**13.86**	**2.35**	**41.95**
9.7	**14.23**	**2.43**	**42.92**
9.8	**14.61**	**2.52**	**43.91**
9.9	**14.99**	**2.61**	**44.91**
10	**15.38**	**2.70**	**45.92**
10.1	**15.78**	**2.80**	**46.96**

Table 31 (Continued)

10.2	**16.19**	**2.89**	**48.00**
10.3	**16.60**	**2.99**	**49.07**
10.4	**17.02**	**3.09**	**50.15**
10.5	**17.44**	**3.19**	**51.24**
10.6	**17.87**	**3.30**	**52.35**
10.7	**18.31**	**3.40**	**53.48**
10.8	**18.76**	**3.51**	**54.62**
10.9	**19.22**	**3.63**	**55.78**
11	**19.68**	**3.74**	**56.95**
11.1	**20.15**	**3.86**	**58.14**

CVT measurements are in mm. Bolded measurements are generated outside of the model's ability and are more unpredictable; they should be used with caution.